CRC Report No. A-101

AIR QUALITY MODELING OF THE RELATIONSHIP BETWEEN PROJECTED OZONE AND PM TRENDS AND CHANGES IN PRECURSOR RELATIONSHIPS IN THE SOUTH COAST AIR BASIN IN RESPONSE TO VARYING REDUCTIONS OF PRECURSOR EMISSIONS

Final Report

June 2017

COORDINATING RESEARCH COUNCIL, INC.
5755 NORTH POINT PARKWAY • SUITE 265 • ALPHARETTA, GA 30022

The Coordinating Research Council, Inc. (CRC) is a non-profit corporation supported by the petroleum and automotive equipment industries. CRC operates through the committees made up of technical experts from industry and government who voluntarily participate. The four main areas of research within CRC are: air pollution (atmospheric and engineering studies); aviation fuels, lubricants, and equipment performance, heavy-duty vehicle fuels, lubricants, and equipment performance (e.g., diesel trucks); and light-duty vehicle fuels, lubricants, and equipment performance (e.g., passenger cars). CRC's function is to provide the mechanism for joint research conducted by the two industries that will help in determining the optimum combination of petroleum products and automotive equipment. CRC's work is limited to research that is mutually beneficial to the two industries involved. The final results of the research conducted by, or under the auspices of, CRC are available to the public.

Air Quality Modeling of the Relationship Between Projected Ozone and PM Trends and Changes in Precursor Relationships in the South Coast Air Basin in Response to Varying Reductions of Precursor Emissions

CRC A-101 FINAL REPORT

Prepared for

Coordinating Research Council, Inc.
5755 North Point Parkway, Ste. 265
Alpharetta, GA 30022

Prepared by

William R. Stockwell, Rosa Fitzgerald, Roberto Perea
University of Texas at El Paso
Physics Department
El Paso, TX

David E. Campbell
Desert Research Institute
Division of Atmospheric Sciences
Reno, NV

Devoun Stewart
University of San Diego
Department of Chemistry and Biochemistry
San Diego, CA

Emily Saunders
Howard University
Department of Chemistry
Washington, DC

June 30, 2017

The University of Texas at El Paso
500 West University Avenue
El Paso, TX 79968-0587

(915) 747-5680

DISCLAIMER AND ACKNOWLEDGMENTS

 We gratefully acknowledge the South Coast Air Quality Management District for providing the CMAQ modeling input and output files.

TABLE OF CONTENTS

LIST OF TABLES

LIST OF FIGURES

1. EXECUTIVE SUMMARY

1.1 Scope, Objectives and Limitations of CRC Project A-101

Our hypothesis is that both ozone and secondary $PM_{2.5}$ concentrations in California's South Coast Air Basin (SoCAB) are affected by reductions in the emissions of reactive organic gases (ROG) and nitrogen oxides (NO_x = NO_2 + NO). This CRC Project A-101 is an extension to CRC Project A-91 (Fujita et al., 2015). The South Coast Air Quality Management District (SCAQMD) has set emission reduction goals for ROG and NO_x between 2008 and 2030 with the goal of reaching compliance with respect to ozone in the SoCAB. The SCAQMD Air Quality Management Plan (SCAQMD, 2013) is very focused on NO_x reductions. Fujita et al. (2015) used the Community Multi-scale Air Quality model (CMAQ) to simulate the response of ozone concentrations to the planned emission reductions in the SoCAB between the base-year 2008 and the future-year 2030. In contrast to the SCAQMD plan, Fujita et al. found that reductions in ROG are likely to be more effective than NO_x reductions in reducing ozone concentrations in the SoCAB and they found that reductions in NO_x emissions could cause an ozone dis-benefit unless very large NO_x reductions are achieved.

Near the end of CRC Project A-91 (Fujita et al., 2015) it was recognized that emissions of ROG and NO_x affect the formation of particulate matter (PM) as well as ozone. Investigation of the effect of ROG and NO_x emissions on PM was beyond the scope of Fujita et al., 2015. Thus CRC Project A-91 left open the very serious question of whether or not the NO_x reduction strategy might be beneficial in reducing PM concentrations (even if the NO_x reduction strategy is not particularly effective in reducing ozone concentrations at least until very large NO_x reductions are achieved).

The component of PM formed in the atmosphere and most strongly affected by NO_x and ROG emissions is known as secondary PM. A reasonable expectation was that reductions in NO_x emissions would reduce the formation of secondary ammonium nitrate aerosol. Reductions in ROG and NO_x emissions could affect other secondary PM such as secondary organic aerosol (SOA). Therefore CRC Project A-101 focuses on the relationship between ROG and NO_x emissions and the formation of secondary PM.

CRC Project A-101 does not focus on primary PM and changes in their emissions are largely beyond our scope. Primary PM is directly emitted into the atmosphere by emission sources. Primary PM includes fine particles formed through combustion processes, elemental carbon, soot, coarse PM (with diameters of 10 μm or greater), windblown dust, fugitive dust, etc. Primary PM concentrations are not directly affected by changes in ROG and NO_x emissions although it is very likely that the engineering changes to vehicle engines and other sources required to reduce ROG and NO_x emissions could affect their primary PM emissions. The lack of a direct relationship between primary PM concentrations and the emissions of ROG and NO_x puts detailed analysis of primary PM beyond the scope of this project.

However, changes in PM emissions between the 2008 base-year and the 2030 future-year are expected (SCAQMD, 2013). These changes to primary PM emissions are implemented in the emissions inventory. Therefore the effects of primary PM emissions on the total PM concentrations in the SoCAB are included in the CMAQ modeling for Project A-101. For this project changes in PM concentrations due to changes in primary PM emissions are considered to be a background. Again, Project A-101 focuses on the evaluation of the PM changes due to changes in ROG and NO_x emissions and this requires a focus on their effect on secondary PM concentrations.

Ozone has adverse impacts on human health but PM has even greater adverse impacts on human health (Gurjar et al., 2008; Hodzic et al., 2010a,b; Sicard et al., 2011; Zhang et al., 2013). An optimized air quality improvement strategy needs to consider the health effects of both ozone and PM but this is beyond the scope of CRC Project A-101. Therefore the Truck and Engine Manufacture's Association (EMA) has funded a companion study to CRC Project A-101. The EMA companion study focuses on the estimation of changes in health due to changes in ozone and PM concentrations between the 2008 base-year and the 2030 future-year. The companion study applied the Environmental Benefits Mapping and Analysis Program, Community Edition model (BenMap-CE) to estimate the changes in health affected by different ROG and NO_x emission reduction strategies. The simulations prepared for CRC Project A-101 were used as input for BenMap-CE. A separate report on the companion study has been prepared for EMA. A full understanding of the implications of the different emission-reduction scenarios requires reading this CRC project report and the companion EMA report.

1.2 Major Conclusions and Implications

CRC Project A-91 (Fujita et al., 2015) examined the response of ozone concentrations in California's South Coast Air Basin to planned emission reductions in ROG and NO_x. In this project we examined the response of particulate matter for the Fall – Winter aerosol season to these same emission reductions. It is important to examine the effect of emission reductions on particulate matter because ozone and particulate matter both cause damage to human health.

An approach that was very similar to CRC Project A-91 (Fujita et al., 2015) was followed for CRC Project A-101. A trend analysis of PM measurements was performed for specific SoCAB sites. An analysis of PM measurements was used to select two high PM episodes for 2008 base-year and 2030 future-year modeling. The Community Multi-scale Air Quality model (CMAQ) was used to simulate the selected ozone and PM episodes. The main conclusions are given below and these are presented in greater detail in the report.

- Extremely analogous, consistent methodologies were followed between the Previous CRC Project A-91 Fujita et al. (2015) and the current CRC Project A-101.
- Secondary PM was the focus of this study because changes in NO_x and ROG emissions do not directly affect primary PM concentrations.
- There are limitations in an analysis of PM due to the lower number of measurement sites and the lower frequency of PM measurements compared with ozone. Sites used for Project A-101 with PM measurements were: Anaheim, Azusa, Fontana, downtown Los Angeles (CELA), Rubidoux (RUBI) and Long Beach.
- The trend analysis showed that PM has decreased in the SoCAB. Ambient air monitoring data show there is significant decreasing trend in annual mean nitrate concentration, annual mean sulfate concentration and organic aerosol mass and Diesel Particulate Matter (DPM).
- Daily $PM_{2.5}$ concentrations decreased between 2002 and 2010 at Los Angeles and Rubidoux. The annual mean nitrate concentration decreased by about 50% between 2003 and 2010 at both the Los Angeles and Rubidoux sites.
- The highest daily $PM_{2.5}$ concentrations in the SoCAB occurred during the fall season with October being the month with the highest daily $PM_{2.5}$ concentrations during the years between 2002 and 2015.
- Two high PM episodes during the 2008 base-year were chosen for CMAQ modeling. The episode that occurred during November 19-24, 2008 had the highest $PM_{2.5}$ concentrations and the episode with the second highest was September 12-15, 2008. Composition of the $PM_{2.5}$ was high in nitrate. Nitrate is a secondary inorganic aerosol that is expected to respond to changes in NO_x and ROG emissions and these characteristics made these episodes ideal for this CRC project.
- The Community Multi-scale Air Quality model (CMAQ; (Byun and Ching 1999; Byun and Schere 2006) was used to make the ozone and aerosol simulations for selected high aerosol episodes. New CMAQ sensitivity simulations for the Fall and Winter aerosol seasons for the future 2030 year were made based on meteorological, emission data and modeling protocols obtained from the South Coast Air Quality Management District (SCAQMD).
- A total of eighteen fall days were simulated with CMAQ and used in this analysis of $PM_{2.5}$. In addition, two days were simulated as initialization spin-up days before each simulation.
- Analysis of the two CMAQ simulated episodes gave very similar conclusions regarding the effects of the ROG and NO_x reductions on PM. This increases confidence in the representativeness of the selected episodes.

- CMAQ showed only modest performance in modeling $PM_{2.5}$ concentrations for selected measurement sites in the SoCAB. CMAQ under-predicted $PM_{2.5}$ and its components compared with the measurements.
- There is no generally accepted statistic for acceptable model performance for PM but literature suggests that a NME within 50% is reasonable performance for PM. This metric is met at all the stations except for Azusa and Fontana.
- The coarse mass and the primary organic mass make the greatest contribution to PM mass.
- Ammonium nitrate is the most abundant secondary aerosol component.
- Sulfate and secondary organic aerosols are the lowest secondary aerosol components.
- Coarse aerosol mass particle concentrations decrease slightly due to reductions in the NO_x emissions inventory
- The production of ammonium nitrate is a function of NO_x and ROG.
- The response of $PM_{2.5}$ concentrations to reductions in NO_x emissions is very nonlinear.
- The current NO_x emissions control strategy is the least effective in reducing $PM_{2.5}$ concentrations of the 2030 future-year cases simulated in this project.
- Either a control strategy with a lower level of NO_x emission reductions or one with much greater reductions in NO_x emissions would be more effective than the current NO_x emissions control strategy in reducing $PM_{2.5}$ concentrations.
- Deeper reductions of NO_x emissions than the projected 2030 base emissions inventory will be required to meet the NAAQS for $PM_{2.5}$ concentrations in the SoCAB.
- Secondary organic aerosol increases when NO_x emissions are ***reduced*** for the 2030 future-year cases simulated in this project.
- An important limitation of CMAQ and many other air quality models is that its aerosol chemistry module is not completely coupled with its gas-phase chemistry module. This reduces the reliability of CMAQ for the simulation of the effects of emission reductions on secondary $PM_{2.5}$ concentrations.
- However, the CMAQ simulated response of $PM_{2.5}$ concentrations to NO_x and ROG concentration changes was consistent with a separate chemical modeling analysis.

2. BACKGROUND AND PERSPECTIVE

Both ozone and PM concentrations will be affected by planned air pollution control strategies for the SoCAB. PM causes serious damage to human health (Gurjar et al., 2008; Hodzic et al., 2010a,b; Sicard et al., 2011; Zhang et al., 2013). Therefore this project focuses on the modeling of the planned emission changes to assess the potential effects on both ozone and secondary PM concentrations.

The physical and chemical processes that affect PM concentrations are much more complex than those that affect ozone concentration. There are very significant gaps in scientific knowledge of the processes that affect aerosol compared with the ozone modules (Calvert et al. 2015). Laboratory measurements of the gas-phase production of PM are very difficult; for example, measured aerosol yields of aerosol can depend on experimental conditions. Severe underestimates of secondary organic aerosol concentrations have resulted from models based on simple parameterization of aerosol yields from laboratory studies (Heald et al., 2005; Volkamer et al., 2006

Primary sources of PM include direct emissions such as soot, black carbon and elemental carbon from combustion sources; windblown crustal material; and fugitive dust. Emitted primary organic aerosols are likely to consist of minimally oxygenated organic compounds (Donahue et al., 2006; Zhang et al., 2007; Lee-Taylor et al., 2011). Primary sources are the major contributors to coarse PM. Coarse PM tends to settle out relatively rapidly from the atmosphere and it is less of a health problem than $PM_{2.5}$. The chemical production of PM from precursor emissions produces much smaller particles such as $PM_{2.5}$. Small particles such as $PM_{2.5}$ can travel much deeper within the lungs when inhaled and be transported to the heart and brain where they can cause the formation of plaques (Grahame, et al., 2014). Therefore secondary PM have a much greater deleterious effects on human health.

Secondary aerosol formation is strongly coupled with the gas-phase chemistry of ozone formation because NO_x, SO_2 and ROG compounds produce some products with low equilibrium vapor pressures that can partition these products into the aerosol phase. Formation rates of ozone in an urban atmosphere depend on the highly nonlinear chemistry of NO_x and ROG. The composition of ROG is important because different organic compounds have different reactivity for producing ozone. CRC Project A-91 showed that reductions in ROG or NO_x emissions do not always lead to lower ozone levels in the SoCAB.

Likewise, the formation of secondary PM is a highly nonlinear function of the VOC and NO_x emissions. Nitric acid, sulfuric acid and lower volatility decomposition products from the oxidation of ROG are all PM precursors. These are produced through oxidation reactions involving the hydroxyl radical (HO) that is central also to the chemistry of ozone formation. This chemistry provides strong links between secondary PM and ozone production. Secondary organic aerosol can be more important than inorganic aerosol because of its

greater adverse health effects and its contribution to the total aerosol mass. The measured mass of organic aerosols has been shown to range from less than 1 μg m^{-3} in the remote troposphere to greater than 70 μg m^{-3} in highly polluted regions (Coe et al., 2006; Sun et al., 2010). In some cases the mass of organic aerosols has been measured to be greater than the total aerosol mass of sulfate, nitrate, and soot combined (Zhang et al., 2007; Jimenez et al., 2009; Lee-Taylor et al., 2011).

The relationship between ROG and NO_x and ozone formation was summarized in our previous report on CRC Project A-91 (Fujita et al., 2015). Here we summarize that review and extend it to include the formation of secondary inorganic and secondary organic aerosol.

2.1 Fundamentals of Hydroxyl Radical, Hydroperoxy Radical and Ozone Formation

The overall process of ozone formation under urban conditions is well understood (Stockwell et al. 2012, Calvert et al., 2015). The photolysis of nitrogen dioxide (NO_2) produces a ground state oxygen atom ($O(^3P)$) that reacts very rapidly with molecular oxygen (O_2) to produce ozone, Reactions 2.1-1 and 2.1-2.

$$NO_2 + h\nu \rightarrow NO + O(^3P) \qquad (2.1\text{-}1)$$

$$O(^3P) + O_2 (+ M) \rightarrow O_3 (+ M) \qquad (2.1\text{-}2)$$

Note that in Reaction 2.1-2, M represents a third molecule, such as N_2, O_2 or other atmospheric constituent, that is required to stabilize the formation of ozone molecule by carrying away excess collisional energy.

Nitric oxide reacts with ozone to convert it back to molecular oxygen, Reaction 2.1-3.

$$O_3 + NO \rightarrow NO_2 + O_2 \qquad (2.1\text{-}3)$$

If the rate of ozone formation by Reaction 2.1-1 is nearly equal to the rate of its destruction through Reaction 2.1-3 a near steady-state equilibrium ozone concentration [O_3] is established that is expressed by the "O_3-NO-NO_2-photostationary state equation," Equation 2.1-4,

$$[O_3] = \frac{J_1[NO_2]}{k_3[NO]} \qquad (2.1\text{-}4)$$

where: J_1 is the photolysis frequency of Reaction 2.1-1, k_3 is the rate constant for Reaction 2.1-3, and [NO_2] and [NO] are the concentrations of nitrogen dioxide and nitric oxide, respectively. Equation 2.1-4 suggests that reactions that convert NO to NO_2 produce more O_3. Higher concentrations of NO_2 are associated with increases in the rate of O_3 formation while lower concentrations of NO reduce the rate of O_3 destruction. The conversion of NO to NO_2 involves the hydroxyl radical (HO), the hydroperoxy radical (HO_2) and organic peroxy radicals (RO_2).

The most important sources of HO are the photolysis of ozone, formaldehyde (HCHO) and other aldehydes and the subsequent reactions of their photolysis products. Additionally some HO is produced through the photolysis of nitrous acid (HONO) during the early morning hours and by reactions of ozone with alkenes (Calvert et al. 2015).

Reactions 2.1-5 through 2.1-8 show the production of HO from ozone photolysis.

$$O_3 + h\nu \rightarrow O(^1D) + O_2 \quad (2.1\text{-}5)$$

$$O(^1D) + N_2 \rightarrow O(^3P) + N_2 \quad (2.1\text{-}6)$$

$$O(^1D) + O_2 \rightarrow O(^3P) + O_2 \quad (2.1\text{-}7)$$

$$O(^1D) + H_2O \rightarrow 2\ HO \quad (2.1\text{-}8)$$

Ozone photolysis produces excited oxygen atoms, $O(^1D)$, Reaction 2.1-5. Most of the excited oxygen atoms are quenched of their energy through collisions with other air molecules such as molecular nitrogen and molecular oxygen to reproduce ground state oxygen atoms. The ground state oxygen atoms reproduce ozone through Reaction 2.1-2. A few percent of the $O(^1D)$ react with water vapor to produce HO radicals.

Formaldehyde photolyzes by two reactions in the atmosphere. In Reaction 2.1-9 formaldehyde photolysis produces hydrogen molecule and carbon monoxide. In Reaction 2.1-10, a hydrogen atom and a formyl radical (HCO) are produced.

$$HCHO + h\nu \rightarrow H_2 + CO \quad (2.1\text{-}9)$$

$$HCHO + h\nu \rightarrow H + CHO \quad (2.1\text{-}10)$$

The hydrogen atom and formyl radicals (CHO) react with molecular oxygen to produce hydroperoxy radicals, Reactions 2.1-11 and 2.1-12. Hydroperoxy radicals react with NO to produce NO_2 and HO radicals, Reaction 2.1-13.

$$H + O_2 \rightarrow HO_2 \quad (2.1\text{-}11)$$

$$CHO + O_2 \rightarrow HO_2 + CO \quad (2.1\text{-}12)$$

$$HO_2 + NO \rightarrow HO + NO_2 \quad (2.1\text{-}13)$$

Reaction 2.1-13 is an important reaction for the conversion of NO to NO_2. Additional HO_2 radicals are produced by the reaction of HO with CO, Reaction 2.1-14.

$$HO + CO\ (+ O_2) \rightarrow HO_2 + CO_2 \quad (2.1\text{-}14)$$

Organic peroxy radicals are most important for the conversion of NO to NO_2 and their source is the reaction of HO with ROG. For example, Reactions 2.1-15 and 2.1-16 show the production of the methyl peroxy radical (CH_3O_2) from methane.

$$HO + CH_4 \rightarrow CH_3 + H_2O \quad (2.1\text{-}15)$$

$$CH_3 + O_2 \rightarrow CH_3O_2 \quad (2.1\text{-}16)$$

The methyl peroxy radical reacts with NO to convert it to NO_2, Reaction 2.1-17 and the methoxy radical reacts with molecular oxygen to produce HCHO and HO_2, Reaction 2.1-18.

$$CH_3O_2 + NO \rightarrow CH_3O + NO_2 \quad (2.1\text{-}17)$$

$$CH_3O + O_2 \rightarrow HCHO + HO_2 \quad (2.1\text{-}18)$$

Higher molecular weight VOC compounds (RH) react with HO to produce higher molecular weight organic peroxy radicals (RO_2) that convert NO to NO_2 and produce carbonyl containing compounds (CARBONYL), Reactions 2.1-19 through 2.1-22.

$$HO + RH \rightarrow R + H_2O \quad (2.1\text{-}19)$$

$$R + O_2 \rightarrow RO_2 \quad (2.1\text{-}20)$$

$$RO_2 + NO \rightarrow RO + NO_2 \quad (2.1\text{-}21)$$

$$RO + O_2 \rightarrow CARBONYL + HO_2 \quad (2.1\text{-}22)$$

CARBONYL is either an aldehyde (R'CHO) or a ketone (R'CR''O) that may react further with HO or photolyze. However the chemistry of the RO_2 and RO formed can be much more complicated than the simple chemistry of low molecular weight organic compounds. Rearrangement, fragmentation and reactions to form organic nitrates occur in the oxidation reactions of high molecular weight organic compounds.

Carbonyl compounds include aldehydes and ketones and also hydroxycarbonyls, and dicarbonyls, organic acids, peroxyacyl nitrates. The simplest peroxyacyl nitrate is peroxyacetyl nitrate (PAN). PAN thermally decomposes back to its reactants, NO_2 and acetylperoxy radical. The reactions of high molecular weight organic compounds lead to the production of secondary organic aerosols.

2.2 Fundamentals of Secondary Inorganic Aerosol Formation

Gas-phase chemistry produces low vapor products that are the precursors of secondary PM. For example the reactions of HO with NO_2 and SO_2 produce nitric acid and sulfuric acid, respectively, and these are precursors of secondary inorganic aerosol. Sulfuric acid has a vapor pressure that is sufficiently low that it rapidly condenses to form aerosol particles while nitric acid will react with ammonia vapor to produce ammonium nitrate that may condense depending on the ambient humidity and temperature.

The HO radical reacts directly with NO_2 to produce nitric acid (HNO_3), Reaction 2.2-1. The reaction of HO radical with SO_2 is more complicated and the overall mechanism is a chain mechanism that regenerates HOx (Stockwell

and Calvert, 1983), Reactions 2.2-2 to 2.2-4. The vapor pressure of sulfuric acid is so low it is represented as a liquid, H_2SO_4 (l), in Reaction 2.1-4 and it would form fine aerosol particles.

$$HO + NO_2 \rightarrow HNO_3 \quad (2.2\text{-}1)$$

$$HO + SO_2 \rightarrow HOSO_2 \quad (2.2\text{-}2)$$

$$HOSO_2 + O_2 \rightarrow HO_2 + SO_3 \quad (2.2\text{-}3)$$

$$SO_3 + H_2O \rightarrow H_2SO_4\,(l) \quad (2.2\text{-}4)$$

The gas-phase oxidation rate of SO_2 due to its reaction with HO is not fast, the maximum rate is a few percent per hour (Calvert and Stockwell, 1983). The gas-phase oxidation rate of NO_2 by HO is greater because the rate coefficient for the HO + SO_2 reaction is about 10 times greater than the rate coefficient for the HO + NO_2 reaction (Atkinson et al., 2012; Sander et al., 2011).

Gas-phase chemistry produces new aerosol particles. The HNO_3 and H_2SO_4 produced by gas-phase chemistry may react with available ammonia (NH_3) to produce ammonium bisulfate (NH_4HSO_4), ammonium sulfate ($(NH_4)_2SO_4$) and ammonium nitrate (NH_4NO_3) aerosol particles. The formation of ammonium nitrate particles from gas-phase ammonia and nitric acid is reversible. The extent of these reactions depends on the relative concentrations of HNO_3, H_2SO_4 and NH_3, relative humidity and temperature. The partitioning between gas-phase HNO_3 and NH_3 and aerosol NH_4^-, NO_3^+, HSO_4^- and $SO_4^=$ ions may be estimated through the use of equilibrium models (Kim et al., 1993a,b; Kim and Seinfeld 1995; Kuhns et al., 2003). For example, not much ammonia reacts with nitric acid until after almost all of any sulfuric acid present has reacted. Furthermore the formation of solid ammonium nitrate aerosol is a strong function of temperature and relative humidity. This chemistry is shown in Reactions 2.2-5 to 2.1-8.

$$NH_3\,(g) + H_2SO_4\,(l) \rightarrow NH_4HSO_4\,(s) \quad (2.2\text{-}5)$$

$$NH_3\,(g) + NH_4HSO_4\,(s) \rightarrow (NH_4)_2SO_4\,(s) \quad (2.2\text{-}6)$$

$$NH_3\,(g) + HNO_3\,(g) \Leftrightarrow NH_4NO_3\,(g) \quad (2.2\text{-}7)$$

$$NH_4NO_3\,(g) \Leftrightarrow NH_4NO_3\,(s) \quad (2.2\text{-}8)$$

Aqueous-phase oxidation of SO_2 and N_2O_5 on water coated aerosol particles may increase the mass of existing particles. Reactions 2.2-9 to 2.2-12, show the aqueous-phase reaction mechanism for the reaction of SO_2 with H_2O_2 and this process is extremely fast (Seinfeld and Pandis, 2006). First SO_2 dissolves in the water and subsequently produce bisulfate, $HO(SO)O^-$. Then the bisulfate is oxidized by hydrogen peroxide (Jacobson, 1999).

$$SO_2\,(g) + H_2O\,(aq) \Leftrightarrow SO_2\,(aq) + H_2O\,(aq) \quad (2.2\text{-}9)$$

$$SO_2\,(aq) + H_2O\,(aq) \Leftrightarrow HO(SO)OH\,(aq) \quad (2.2\text{-}10)$$

$$HO(SO)OH\,(aq) \Leftrightarrow HO(SO)O^-\,(aq) + H^+\,(aq) \quad (2.2\text{-}11)$$

$$HO(SO)O^- (aq) + H_2O_2 (aq) + H^+ (aq) \rightarrow SO_4^{2-} (aq) + H_2O (aq) + 2H^+ (aq) \quad (2.2\text{-}12)$$

During the nighttime dinitrogen pentoxide (N_2O_5) may form through the reaction of nitrate radical (NO_3) and NO_2. Dinitrogen pentoxide reacts with H_2O on the surfaces of aerosol particles and water droplets to give HNO_3 through a heterogeneous reaction, Reactions 2.2-13 and 2.2-14.

$$NO_3 (g) + NO_2 (g) \leftrightarrow N_2O_5 (g) \quad (2.2\text{-}13)$$

$$N_2O_5 (g) + H_2O (aq) \rightarrow 2\ HNO_3 (aq) \quad (2.2\text{-}14)$$

2.3 Fundamentals of Secondary Organic Aerosol Formation

Secondary organic aerosols (SOA) consist mostly of highly oxygenated organic compounds (Donahue et al., 2006; Zhang et al., 2007; Lee-Taylor et al., 2011). Measurements made in urban source regions show that organic aerosol consists of a relatively high fraction of highly oxygenated organic compounds relative to the fraction of minimally oxygenated organic compounds. The fraction of highly oxygenated organic compounds increases downwind of source regions and this indicates that chemistry is producing more highly oxygenated organic compounds as air masses age (de Gouw et al., 2008; Zhang et al., 2007; Lee-Taylor et al., 2011).

SOA is produced by the oxidation of organic compounds from anthropogenic and biogenic sources (Heisler and Friedlander, 1977; Pandis et al., 1991; Turpin et al., 1991; Pandis et al., 1992; Griffin et al., 1999; Aumont et al., 2000; Claeys et al., 2004; Goldstein and Galbally, 2007; de Gouw and Jimenez, 2009; Lee-Taylor et al, 2011). This chemistry produces highly oxygenated organic compounds with low equilibrium vapor pressures. The highly oxygenated organic compounds condense to form SOA.

Chemical mechanisms for the formation of the compounds that comprise SOA components are the same as the mechanisms for ozone production (Lee-Taylor et al, 2011). As discussed above higher molecular weight ROG compounds (RH) react with HO; Reactions 2.3-1 through 2.3-4 present a highly schematic ROG reaction mechanism. Overall the net effect is to produce an oxygenated ROG from a hydrocarbon or to add another oxygen to an oxygenated compound. (Note also that oxygen atoms can be added to alkenes through ozonolysis as well.)

$$HO + RH \rightarrow R + H_2O \quad (2.3\text{-}1)$$

$$R + O_2 \rightarrow RO_2 \quad (2.3\text{-}2)$$

$$RO_2 + NO \rightarrow RO + NO_2 \quad (2.3\text{-}3)$$

$$RO + O_2 \rightarrow CARB + HO_2 \quad (2.3\text{-}4)$$

This cycle may repeat many times for a high molecular weight (high carbon number) organic compound. Many studies have found that organic compounds with more that six carbon atoms form a large fraction of measured

SOA (Volkamer et al., 2006; Hallquist et al., 2009; Hodzic et al., 2010a,b; Virtanen et al., 2010; Lee-Taylor et al, 2011; Zhang et al., 2013). SOA consists of a very large number of organic compounds (Ketseridis et al., 1976; Middlebrook et al., 1998; Hamilton et al., 2004; Lee-Taylor et al, 2011).

Organic compounds with greater numbers of carbon atoms (C_{11} to C_{25}) are important precursors for the formation of SOA. More explicit representation of the chemistry of these organic compounds along with consideration of the vapor pressure of their products improves model performance for SOA (Lee-Taylor et al., 2011). There are anthropogenic and biogenic sources of these organic compounds (Fuentes et al., 2000). Many organic compounds emitted from biogenic sources are higher molecular weight alkenes. Anthropogenic and biogenic alkenes react with nitrate radical by addition of NO_3 to double bonds and organic products are formed that may become SOA.

2.4 The Representation of Aerosols in CMAQ

The Community Multi-scale Air Quality model (CMAQ; (Byun and Ching 1999; Byun and Schere 2006) was used to make the ozone and aerosol simulations for this project. The CMAQ aerosol module simulates primary emissions of elemental and organic carbon, dust and unspecified species. It simulates secondary aerosols that include sulfate, nitrate, ammonium, water and organic species that are formed from anthropogenic and biogenic emissions.

CMAQ's aerosol module was developed from the Regional Particulate Model (RPM) (Binkowski and Shankar, 1995) and the RPM was derived from the Regional Acid Deposition Model (RADM; Chang et al., 1990). The aerosol module in CMAQ represents the aerosol size distribution using a mode approach. The mode approach uses a superposition of three lognormal sub-distributions (modes) to represent the aerosol size distribution (Binkowski, 1999).

The module simulates both fine particles ($PM_{2.5}$) and coarse particles (PM_{10}). Fine particles are emitted from combustion sources or they are produced through gas-phase chemistry as discussed above. CMAQ simulates the formation of new particles by nucleation from precursor material and the condensation of precursor material onto existing particles (Binkowski, 1999). The coarse particles simulated by CMAQ include wind-blown dust and marine particles such as sea salt. CMAQ includes important physical processes such as coagulation. Differential equations for the number and species mass conservation are represented by analytical solutions to increase numerical accuracy. A very serious weakness in the CMAQ aerosol module (and most other similar air quality models) is that the aerosol module is not tightly coupled with the CMAQ gas-phase chemistry module.

2.5 Summary of Background and Perspective

The science required to accurately simulate PM formation needs much development. Section 2 shows that the chemistry of ozone formation is deeply coupled with the chemistry of secondary aerosol formation. Changes in NO_x and ROG emission inventories that are designed to reduce ozone formation are likely to have a strong effect on the concentrations of PM. Changes in NO_x and ROG emissions are expected to affect the aerosol components: ammonium nitrate, ammonium sulfate and secondary organic aerosol. The ROG that affects secondary organic aerosol formation in the SoCAB may be anthropogenic and biogenic (Fuentes et al., 2000). These secondary inorganic and organic aerosol PM that are affected by NO_x and ROG emissions are the focus of this CRC project. The concentrations of primary emitted PM such as elemental carbon or coarse PM particles are not affected by NO_x and ROG emissions through the processes and reactions discussed in Section 2.

3. EVALUATION OF TRENDS IN $PM_{2.5}$ CONCENTRATIONS IN THE SoCAB

3.1 Ambient Air Monitoring Sites in the SoCAB

The South Coast Air Basin is shown in Figures 3-1 and 3-2. The SoCAB covers an area of 10,743 square miles and over 17.8 million people live there (2010 U.S. Census). The high level of emissions due to the SoCAB's population, its location at the Eastern Pacific and its local topography due its surrounding mountains make it difficult for the SoCAB to reach attainment of air quality standards (Fujita et al., 2015). Figure 3-1 shows the location of the ozone monitoring stations that were used by Fujita et al. (2015). The response of CMAQ simulated PM concentrations was compared with the response of simulated CMAQ ozone concentrations for these air quality measurement sites for consistency with Fujita et al., 2012.

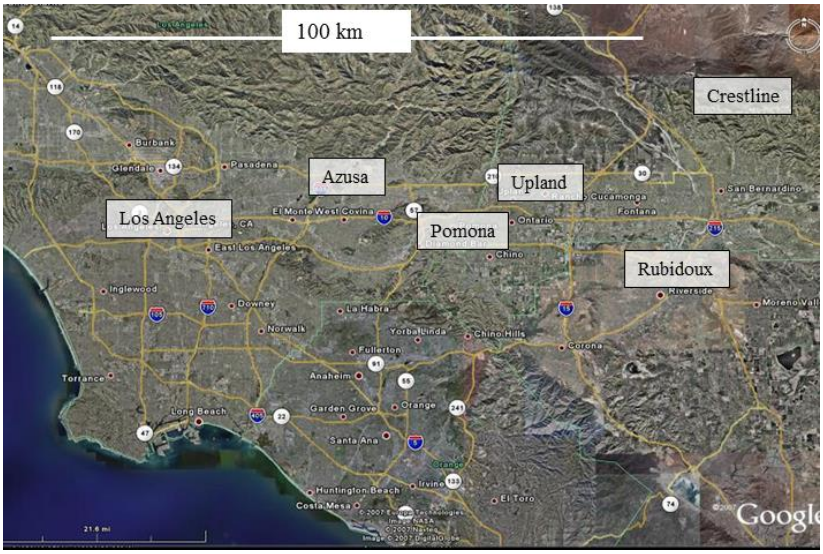

Figure 3-1. Map of the South Coast Air Basin with approximate locations of the air quality monitoring stations that were used in the previous (Fujita et al., 2015) ozone study.

PM measurements made at ambient air monitoring sites operating in the SoCAB were used to update PM trends, to identify high PM episodes for CMAQ modeling and to evaluate CMAQ model performance. These activities required data from sites in addition to the sites used in the previous Fujita et al., 2015 ozone study. Several ambient air monitoring sites operating in the SoCAB reported daily mass concentrations of $PM_{2.5}$ in 2008, Figure 3-2. Four of the stations reported chemical speciation data as well.

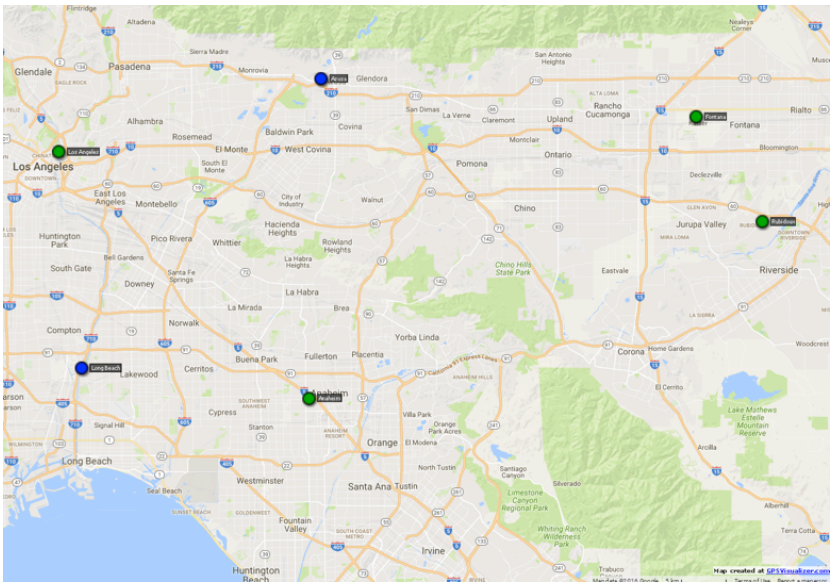

Figure 3-2. Map showing location of $PM_{2.5}$ monitoring sites that reported daily mass concentration in 2008 that were used in this study. Green dots indicate sites that also reported chemical speciation data.

3.2 PM Trends in the South Coast Air Basin

Trends in the annual mean and 98th percentile of daily $PM_{2.5}$ concentrations at the downtown Los Angeles site (CELA) and Rubidoux (RUBI) sites are shown in Figure 3-3. The daily $PM_{2.5}$ concentrations decreased between 2002 and 2010 at Los Angeles and Rubidoux. Following 2010 the $PM_{2.5}$ concentrations level off and may have increased slightly by 2015 at Los Angeles while at Rubidoux the $PM_{2.5}$ concentrations remained almost constant between 2010 and 2015.

Trends in the annual mean and 98th percentile of the organic (OC) and elemental carbon (EC) concentrations at the downtown Los Angeles site (CELA) are shown in Figure 3-4. These measurements show there is significant decreasing trend in organic aerosol mass and diesel particulate matter (DPM) since 2006. The organic carbon concentrations at Los Angeles decreased between 2003 and 2009. Between 2009 and 2015 the organic carbon concentrations at Los Angeles are relatively constant. Elemental carbon was relatively constant between 2003 and 2015 although the 98th percentile may have decreased slightly between 2009 and 2015.

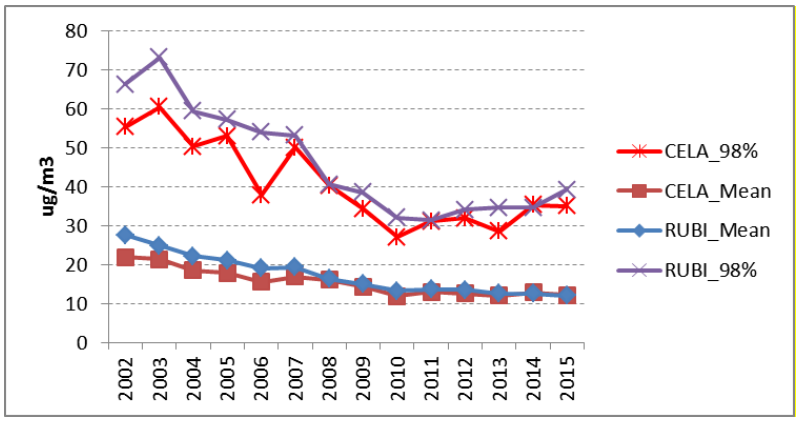

Figure 3-3. Trend in annual mean and 98th percentile of daily $PM_{2.5}$ concentrations at the downtown Los Angeles CELA) and Rubidoux (RUBI) sites.

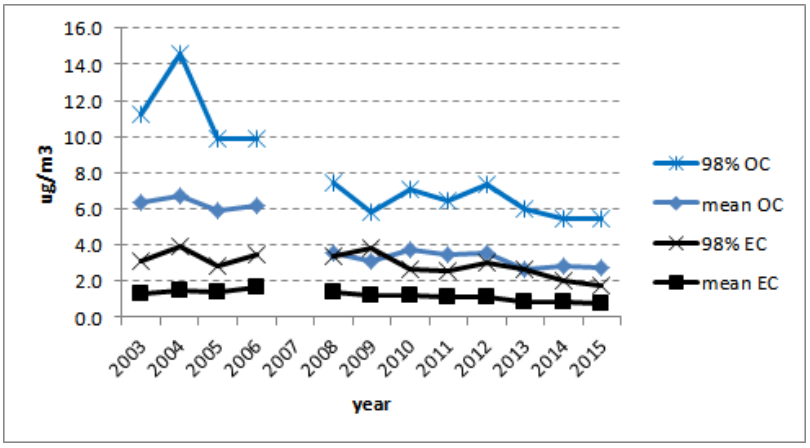

Figure 3-4. Trend in annual mean and 98th percentile of CSN protocol organic and elemental carbon concentrations at the downtown Los Angeles site (CELA). A change in the analysis method for carbon fractions was implemented in 2007, so data collected before and after 2007 may not be fully comparable.

Trend plots for nitrate and sulfate measurements are shown in Figures 3-5 and 3-6, respectively, and the general trend is toward lower concentrations. The annual mean nitrate concentrations at the Rubidoux site were greater than those at the Los Angeles site between 2003 and 2014. The annual mean nitrate concentration decreased by about 50% between 2003 and 2010 at both the Los Angeles and Rubidoux sites but there was little change in concentrations between 2010 and 2014. The nitrate "design values"[1] at the two sites had similar magnitudes. The design value at the Los Angeles site increased initially

[1]Analogous to the design value for ozone, it is the 3-year running average of the annual 98th percentile of daily mean PM concentrations.

and then fell from 2007 to 2014 while at the Rubidoux site the design value fell more steadily during this time. The design value at Los Angeles decreased to 37% of its initial value and the design value at Rubidoux decreased to 50% of its initial value.

The annual mean sulfate concentrations are lower than the annual mean nitrate concentrations at both sites. The annual mean sulfate concentrations were greater at the Los Angeles site than at the Rubidoux site. There was an increase in the annual mean sulfate concentration at Los Angeles during 2005 but there was a decrease to 44% of its initial value between 2002 and 2010. At the Rubidoux site there was a decrease in the annual mean sulfate concentration to 40% of its initial value between 2002 and 2014. There was little change in the sulfate concentrations at both sites between 2010 and 2014. The sulfate design values decreased steadily between 2004 and 2014 at both sites. The decrease was greatest at Los Angeles, decreasing to 27% of its initial value, compared with 39% at Rubidoux. The design values for both stations were almost the same in 2014.

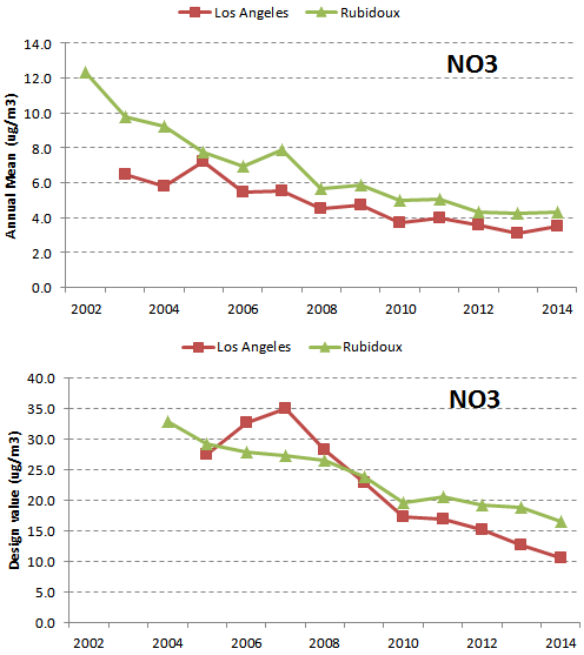

Figure 3-5. Trend in nitrate concentrations at the downtown Los Angeles (CELA) and Rubidoux (RUBI) sites. The top plot shows the trend in the annual mean average while the lower plot shows the trend in the nitrate design value.

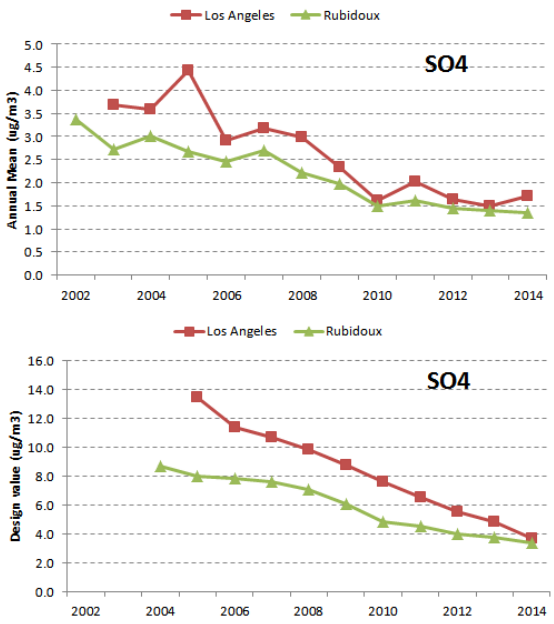

Figure 3-6. Trend in sulfate concentrations at the downtown Los Angeles (CELA) and Rubidoux (RUBI) sites. The top plot shows the trend in the annual mean average while the lower plot shows the trend in the sulfate design value.

3.3 Summary of Trends in PM

The PM trends examined include $PM_{2.5}$, organic carbon, elemental carbon, nitrate and sulfate. PM concentrations have decreased at Los Angeles and Rubidoux since the beginning of the 21st-century. But PM concentrations have been relatively constant during the last few years. The sites, Los Angeles and Rubidoux, show significant decreasing trends in organic carbon and elemental carbon. The general trends for PM nitrate and sulfate are also toward lower concentrations.

4. NO_x EMISSIONS AND DIRECT PM EMISSION INVENTORIES AND DIFFERENCES BETWEEN 2008 AND 2030

4.1 Summary of ROG and NO_x Emission Inventories between 2008 and 2030

As discussed in Fujita et al. (2015) and SCAQMD (2013) The SCAQMD and the California Air Resources Board (CARB) are implementing controls on NO_x emissions designed to reduce ozone and PM. Both agencies used model simulations to estimate that attainment of the National Ambient Air Quality Standards (NAAQS) in the SoCAB will require a 90% reduction in NO_x emissions (SCAQMD, 2013; CARB, 2014). These agencies concluded that meeting the 75 ppb 8-hour ozone standard requires that NO_x emissions must be reduced to 85 tons per day (tpd) in the SoCAB. This 85 tpd is down from 2008 when NO_x emissions were 723 tpd and below the projected baseline NO_x emissions for the year 2030 of 284 tpd. The projected 2030 baseline is based upon control programs that are currently in effect. These programs include the Low Emission Vehicle - III (LEV-III) standards (Fujita et al., 2015).

Fujita et al. (2015) pointed out that the target of 85 tpd in NO_x emissions will be very difficult to meet because on-road vehicles alone are projected to emit 95 tpd in the SoCAB according to the (SCAQMD (2013). Elimination of all NOx emissions from on-road vehicles leaves another 189 tpd to be eliminated in the SoCAB. New technology will be required to meet the ozone NAAQS based on the current NO_x control strategy and this is acknowledged by the (SCAQMD, 2013; Fujita et al., 2015). The current NO_x reduction strategy will cause a period with higher ozone concentrations in the SoCAB, especially in the western SoCAB unless there are ROG emission reductions greater than projected for the 2030 baseline (SCAQMD, 2015; Fujita et al., 2015).

Fujita et al. (2015) performed several air quality model simulations with different multiplying factors for NO_x and ROG, Table 4-1. Table 4-1 also shows a summary of NO_x and ROG emissions in the SoCAB for the 2008 base-year and the projected 2030 future-year. ROG emissions were varied with multiplicative factors of 1.0, 1.5 and 2.0. For the future-year 2030 two levels of the projected ROG emissions were simulated, 1.0 ROG and 1.5 ROG. For each of these ROG emission levels six separate future-year simulations with NO_x emission multipliers of 2.00, 1.75, 1.00, 0.75, 0.5 and 0.3 by Fujita et al. (2015). These emission multipliers correspond to reductions from the 2008 base-year of 2, 31, 61, 70, 81 and 88%, respectively. The 88% reduction in the NO_x emission inventory brings these emissions down to 85 tpd that is below the SCAQMD and CARB estimates of the reduction required to reach ozone attainment of the NAAQS.

However, Fujita et al. (2015) did not examine the consequences of the NO_x and ROG reductions on PM because this was beyond their scope. The purpose of this project was to examine the effects of changes in the emissions inventory for ROG and NO_x on PM concentrations, however ROG and NO_x emissions primarily affect PM formation and therefore the focus is on the simulation of secondary PM concentrations, Table 4-2 shows the variations in

NO_x and ROG emissions inventories that were simulated under the current project. The effect of changes in the ROG emission inventory on secondary PM for the base-year 2008 was investigated. The effect of the six NO_x emission reduction scenarios was simulated for the 2030 future-year.

		ROG				NO_x				
Year	Case	Total ROG (tpd)	Adj Factor	Δ 2008 Base	Δ 2030 Baseline	Total NO_x (tpd)	Adj Factor	Δ2008 Base	Δ2030 Baseline	ROG/NO_x
2008	2R1N	1277	2.0	100%	192%					5.9
	1.5R1N	958	1.5	50%	119%	723	1.0	0%	155%	4.4
	1R1N	639	1.0	0%	46%					2.9
2030	1R'2.5N'	437	1.0	-32% From 1R -54% From1.5R	0%	710	2.5	-2%	150%	2.1
	1R'1.75N'					497	1.75	-31%	75%	2.9
	1R'1N'					284	1.00	-61%	0%	5.1
	1R'.75N'					213	0.75	-70%	-25%	6.8
	1R'.5N'					141	0.50	-81%	-50%	10.4
	1R'.3N'					85	0.30	-88%	-70%	17.1
2030	1.5R'2.5N'	655	1.5	3%	50%	710	2.5	-2%	150%	3.1
	1.5R'1.75N'					497	1.75	-31%	75%	4.4
	1.5R'1N'					284	1.00	-61%	0%	7.7
	1.5R'.75N'					213	0.75	-70%	-25%	10.2
	1.5R'.5N'					141	0.50	-81%	-50%	15.5
	1.5R'.3N'					85	0.30	-88%	-70%	25.7
	.5R2.5N'	218	0.5	-66%	-50%	710	2.5	-2%	150%	1.0
	.5R1N'					284	1.00	-61%	0%	2.6

Table 4-1. 2008 and 2030 model simulations with baseline total ROG and NO_x emissions and sensitivity cases with varying adjustments to baseline emissions used for CRC Project A-91 (Fujita et al., 2015). The ROG/NO_x ratios are given in units of moles carbon / moles nitrogen.

		ROG				NO_x				
Year	Case	Total ROG (tpd)	Adj Factor	Δ2008 Base	Δ2030 Baseline	Total NO_x (tpd)	Adj Factor	Δ2008 Base	Δ2030 Baseline	ROG/NO_x
2008	2R1N	1277	2.0	100%	192%					5.9
	1.5R1N	958	1.5	50%	119%	723	1.0	0%	155%	4.4
	1R1N	639	1.0	0%	46%					2.9
2030	1R'2.5N'	437	1.0	-32% From 1R -54% From1.5R	0%	710	2.5	-2%	150%	2.1
	1R'1.75N'					497	1.75	-31%	75%	2.9
	1R'1N'					284	1.00	-61%	0%	5.1
	1R'.75N'					213	0.75	-70%	-25%	6.8
	1R'.5N'					141	0.50	-81%	-50%	10.4
	1R'.3N'					85	0.30	-88%	-70%	17.1

Table 4-2. 2008 and 2030 model simulations with baseline total ROG and NO_x emissions and sensitivity cases with varying adjustments to baseline emissions used for the current CRC Project A-101, (Stewart, 2017). The ROG/NO_x ratios are given in units of moles carbon / moles nitrogen.

4.2 Differences in Primary PM Concentrations Due to Changes in Emission Inventories between 2008 and 2030

Table 4-3 shows a brief summary of the CMAQ emission inventory and simulation of the origin of $PM_{2.5}$ for the 2008 (ROG = 1.0; NO_x = 1.0) and the 2030 future-year (ROG' = 1.0 and NO_x' = 1.0) sensitivity case. Note that the CMAQ modeling results are shown here only for comparison between the effects of primary and secondary PM emissions. The CMAQ simulations are discussed in detail in subsequent sections of this report.

Table 4-3 shows that the effect of primary $PM_{2.5}$ emissions does not change by a large amount between 2008 and 2030. There is a small decrease in primary organic mass (OM) and elemental carbon (EC). This decrease in OM and EC is presumably due to the large decreases in mobile source (particularly light-duty vehicles).

The decrease in primary $PM_{2.5}$ emission is offset by a large increase in secondary ammonium nitrate production and, to a lesser extent, unspecified anthropogenic mass (UAM). The increase in nitrate follows from the change in ROG/NO_x ratio. The change due to UAM is of concern because it is similar in magnitude to the total of the changes in primary OM and EC.

$PM_{2.5}$ Component	**2008 μgm^{-3}**	**2030 μgm^{-3}**	**2030 - 2008 μgm^{-3}**	**Percent of 2008 $PM_{2.5}$**
Primary Emitted PM				
Primary Organic Mass (OM)	7.52	6.86	-0.66	-2.4%
Elemental Carbon	2.98	1.81	-1.17	-4.2%
PM Weakly Affected by ROG and NO_x Emissions				
Ammonium Sulfate	4.83	4.86	0.03	0.1%
Biogenic SOA	0.13	0.15	0.02	0.1%
PM Strongly Affected by ROG and NO_x Emissions				
Ammonium Nitrate	7.88	15.31	7.43	26.4%
Anthropogenic SOA	0.27	0.31	0.04	0.2%
Unknown PM				
Unspecified Anthropogenic Mass	4.52	6.97	2.45	8.7%
TOTAL	28.14	36.27	8.13	

Table 4-3. Differences between 2008 and 2030 base case predictions of $PM_{2.5}$ mass concentrations at Rubidoux on November 20 for the 2008 (ROG = 1.0; NO_x = 1) and the 2030 future-year (ROG' = 1 and NO_x' = 1) simulations.

4.3 Summary of NO_x Emissions and Direct PM Emission Inventories and Differences Between 2008 and 2030

The projected changes between 2008 and 2030 in primary PM emissions do not have a strong effect on simulated PM concentrations in the SoCAB. Variations in the ROG emissions inventory for 2008 were chosen for simulation to examine the effect of ROG on secondary PM. Variations in the NO_x emissions inventory for 2030 were chosen for simulation to examine the effect of NO_x on secondary PM.

5.0 SELECTION OF HIGH PM EPISODES FOR CMAQ MODELING

5.1 Selection of Episodes

Available project time, good quality data and budget required us to be selective in the number of episodes that were simulated. Selection of episodes considered PM concentration, the availability of speciation data for model evaluation and meteorology. Figure 5-1 shows daily $PM_{2.5}$ concentration data for the years between 2002 and 2015 at the sites Central Los Angeles and Rubidoux. The highest daily $PM_{2.5}$ concentrations occurred during the fall season. October was the month with the highest daily $PM_{2.5}$ concentrations.

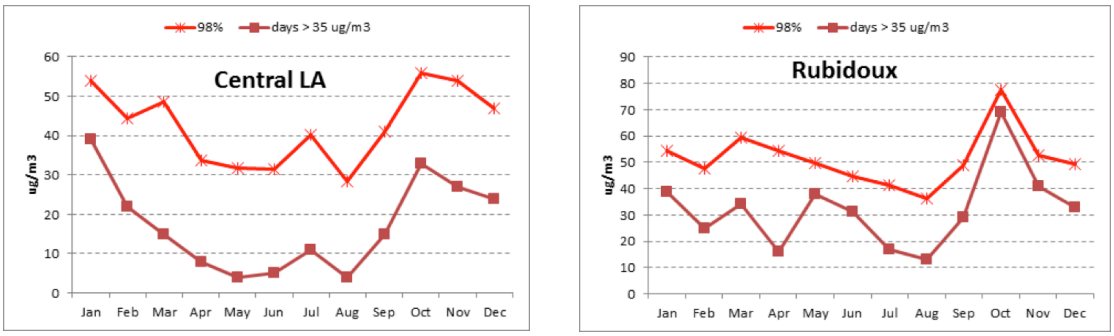

Figure 5-1. Daily $PM_{2.5}$ concentration data by month for the years between 2002 and 2015 are shown for the sites Central Los Angeles and Rubidoux. Plotted are the 98th percentiles of the $PM_{2.5}$ concentrations (upper lines) and the number of days during the time period when the $PM_{2.5}$ concentrations were greater than 35 $\mu g\ m^{-3}$ (lower lines).

A January 2008 episode was eliminated due to the lack of available speciated $PM_{2.5}$ data due to the every-sixth-day PM monitoring schedule used at most measurement sites. Also, southern California typically receives the majority of its annual precipitation during January and February in the form of strong winter storms. Therefore, the meteorology of wintertime episodes might not be representative of typical conditions.

The highest two PM levels during the 2008 base-year were found to occur during the Fall and Winter seasons in the SoCAB, Figure 5-2. The first episode occurred from Friday September 12 to Monday September 15 with the greatest PM concentration on the 13th. The second episode occurred from Wednesday November 19 to Monday November 24. These two episodes were driven by high nitrate (NO_3^-) concentrations based on the available speciation data, Figures 5-3 and 5-4. These two episodes were very appropriate for this modeling study because nitrate is a secondary aerosol pollutant.

Figures 5-3 and 5-4 show two measurements for organic carbon (OC) and two measurements for elemental carbon (EC). Because OC and EC are not distinct chemical compounds they are defined by the analytical method

used to measure them. The urban Chemical Species Network (CSN) protocol was used at Rubidoux in 2008 to measure OC and EC with two variations (Solomon et al., 2014). One of the variations was to use optical transmittance (TOT) and the other variation was to use reflectance (TOR). For each OC and EC pair the first measurement is the TOT value and the second is the TOR value.

There was another high $PM_{2.5}$ episode that occurred during the ozone season, from Friday July 4, 2008 to Monday July 7, 2008. However this episode was unusual because it was driven by high organic carbon (OC). The high $PM_{2.5}$ concentrations were likely caused by atypical holiday weekend activities. Therefore this episode was not considered to be representative enough to be useful for air quality modeling study.

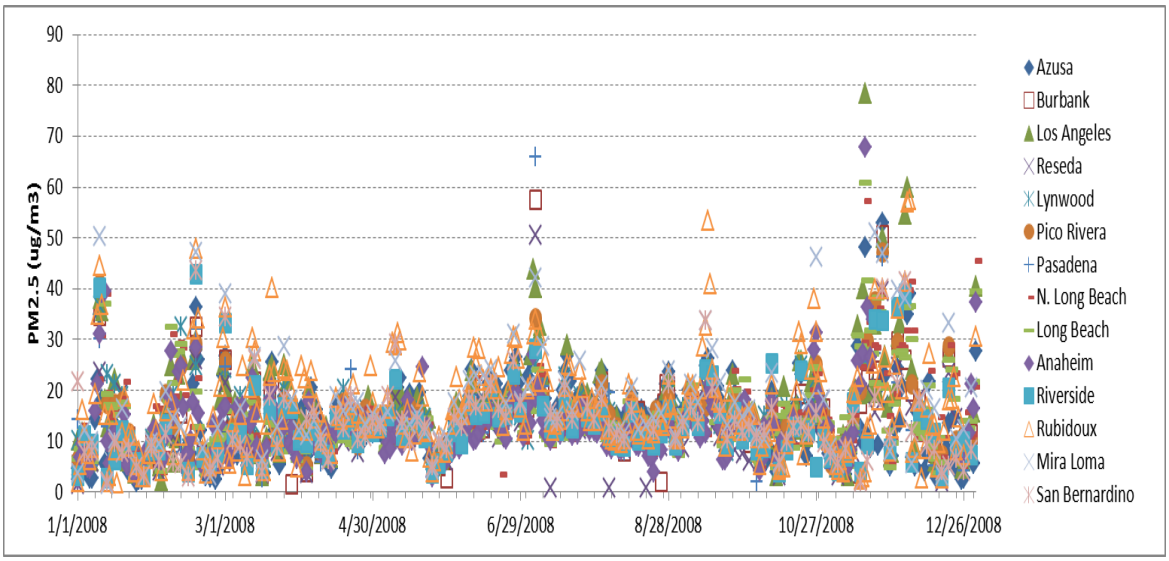

Figure 5-2. Time series plot of daily 24-hr $PM_{2.5}$ concentrations in the SoCAB during 2008 (Stewart, 2017).

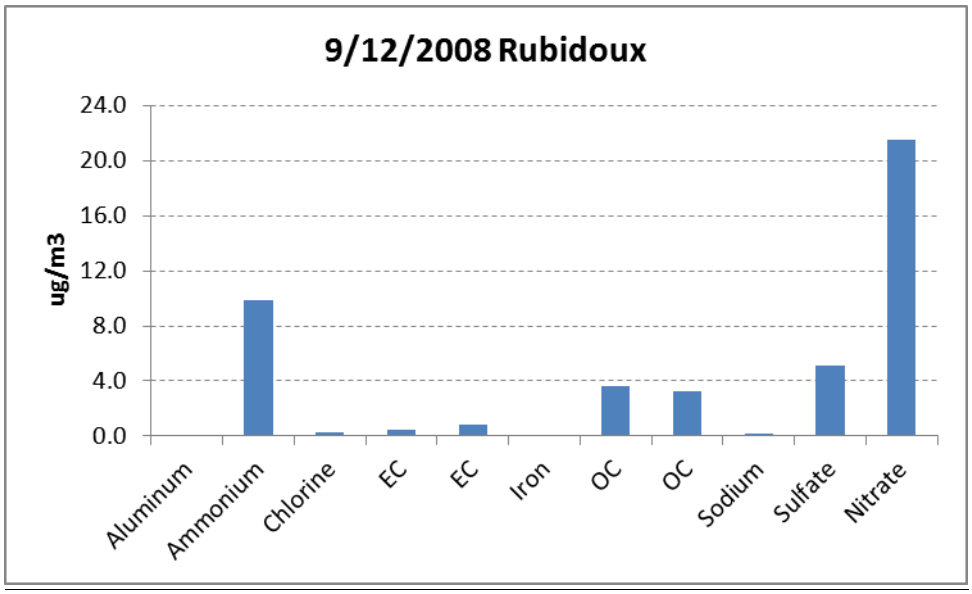

Figure 5-3 Major components of aerosol at Rubidoux (Eastern basin) during the September 2008 $PM_{2.5}$ episode.

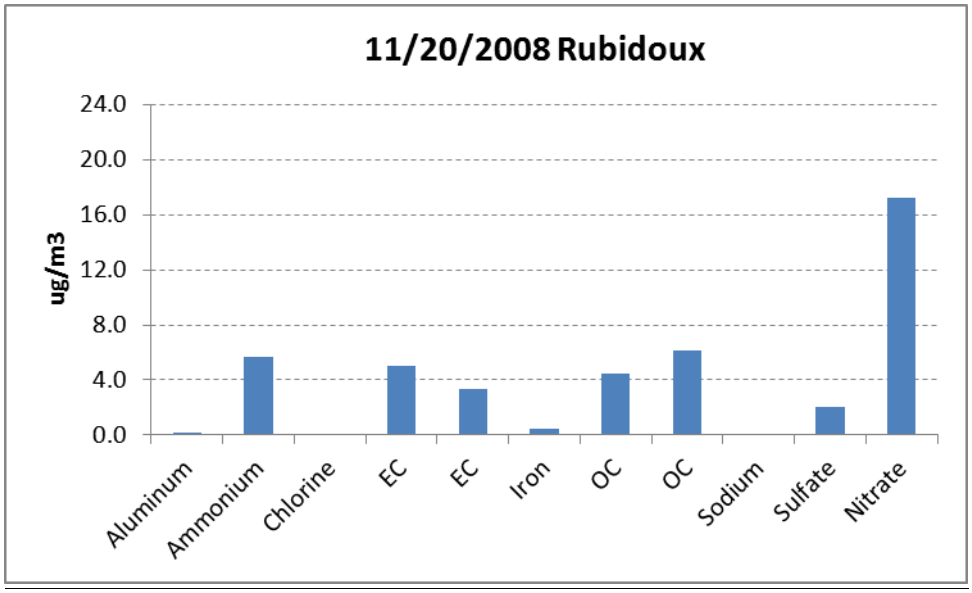

Figure 5-4. Major components of aerosol at Rubidoux (Eastern basin) during the November 2008 $PM_{2.5}$ episode.

Figures 5-5 and 5-6 show $PM_{2.5}$ concentrations for the high aerosol episodes (September, 2008 and November, 2008) that were chosen for modeling. For the September episode Rubidoux had the highest $PM_{2.5}$ concentrations. The $PM_{2.5}$ concentration was over 50 μg / m^3 on September 13, 2008, at that site. At the other stations the $PM_{2.5}$ concentrations were greater than 20 μg m^{-3} during the period chosen for modeling.

The $PM_{2.5}$ concentrations were greater during the November episode chosen for modeling. The $PM_{2.5}$ concentrations reached 80 μg / m^3 at the Los Angeles site and at or above 50 μg / m^3 at the other sites except for Rubidoux on November 16, 2008. Rubidoux became the site with the greatest $PM_{2.5}$ concentrations on November 20, 2008. On November 23, 2008, Azusa became the site with the highest $PM_{2.5}$ concentrations with Los Angeles and Fontana nearly as high.

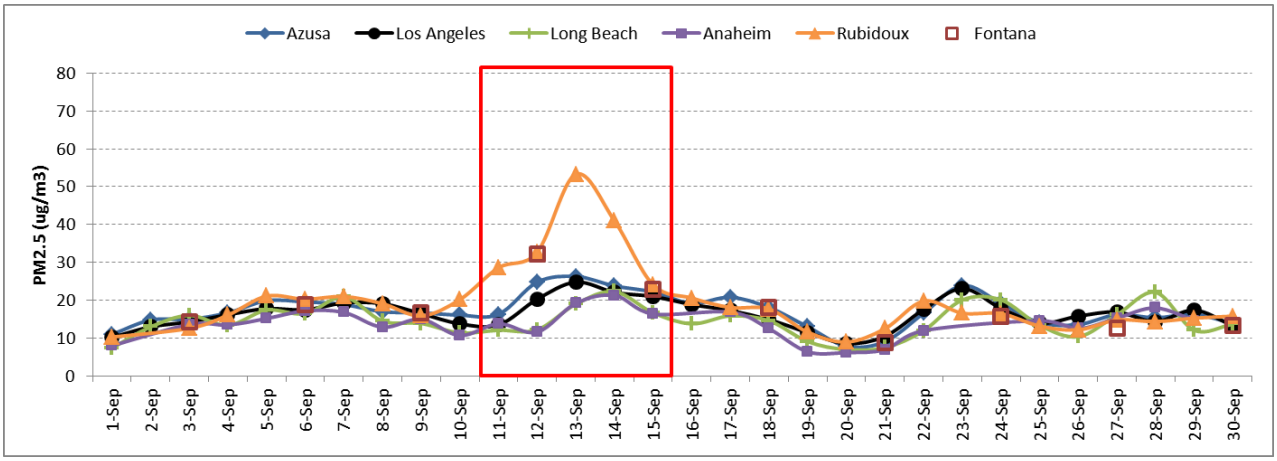

Figure 5-5. Time series plot of daily mean $PM_{2.5}$ concentrations for September 2008. The red box signifies the period selected for modeling (Stewart, 2017).

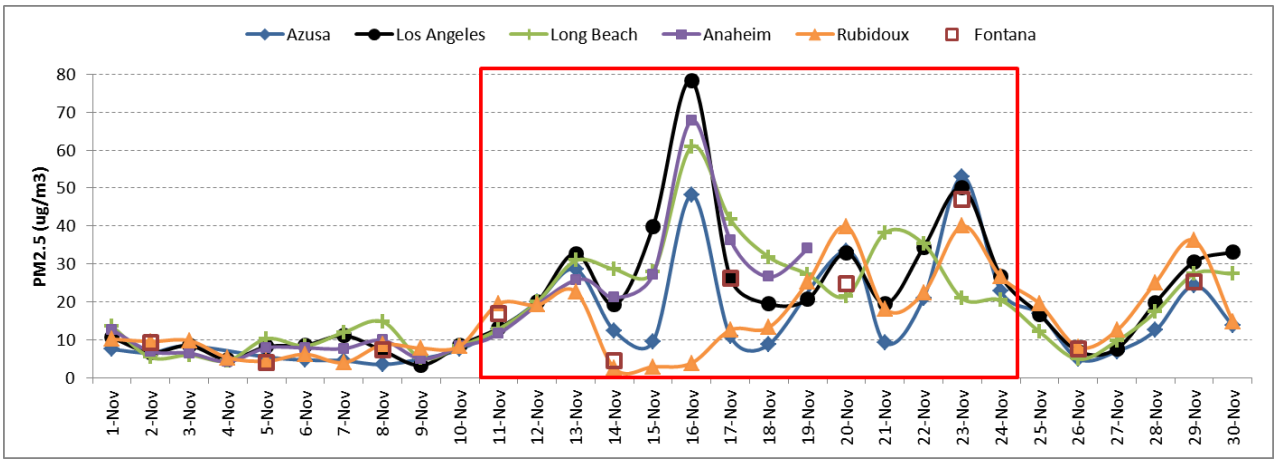

Figure 5-6. Time series plot of daily mean $PM_{2.5}$ concentrations for November 2008. The red box signifies the period selected for modeling (Stewart, 2017).

5.2 Summary of Selection of PM Episodes for Modeling

Two episodes were chosen for CMAQ modeling. The episodes were chosen because they were the two highest PM episodes during the 2008 aerosol season. This choice is analogous with typical EPA-State Implementation Plan (SIP) modeling protocols for ozone. Ozone-SIP modeling is not usually made for average days, instead highly polluted episodes are chosen and we have followed this same strategy. Typically for an ozone-SIP, a field study is conducted and intensive measurements are made during highly polluted events and then these are modeled. However events that are atypical, such as episodes influenced by nearby wildfires are excluded from the process.

Simulations were made for both the September and November episodes. Analysis of the simulations showed that both episodes were leading to similar conclusions. This suggests, but does not prove, that our conclusions based on these two episodes are robust.

6. CMAQ MODELING METHODOLOGY AND ASSUMPTIONS

6.1 Methodology and Assumptions

New CMAQ simulations were made for the Fall and Winter aerosol season for the 2008 base-year. A total of eighteen days were simulated (September 12-15, 2008 and November 11-24, 2008), in addition, two days were simulated as initialization spin-up days before each simulation. Meteorological and emission data were obtained from the SCAQMD to simulate these episodes. We obtained CMAQ input files for the episodes September 12-15, and November 11-24, 2008. The CMAQ simulated PM were compared with available measurements, see Section 7 of this report. New CMAQ sensitivity simulations for the Fall and Winter aerosol seasons for the 2030 future-year were made. The results of the sensitivity of ozone and PM concentrations to the changes in NO_x and ROG emissions are presented in Section 8 of this report.

The Community Multiscale Air Quality (CMAQ) was used to make simulations of the high PM episodes for the base-year 2008 and the 2030 future-year following the same procedures used for the CRC Project A-91 (Fujita et al., 2015). The SCAQMD provided the meteorological simulation data and emissions inventory used in this CRC A-101 Project and their data was used to develop the 2012 Air Quality Management Plan (SCAQMD, 2013). The version of CMAQ used by the SCAQMD and in this project was CMAQ 4.7. Our modeling grid and the spatial resolution (4x4 km) were the same as SCAQMD. The gas-phase chemical mechanism was SAPRC99; the aerosol module was CMAQ 5 with the saprc99_ae5_aq aqueous chemical scheme and all of these choices were the same as used by the SCAQMD. From the previous CRC Project A-91 CMAQ script codes provided by the SCAQMD were modified to allow CMAQ to run in parallel on ninety-six processors at UTEP. For initialization of the multi-day simulations, CMAQ Profile files were used and two days were simulated as initialization spin-up days before each simulation. For successive days CMAQ output files were used to initialize the next day. Appendix V (Modeling and Attainment Demonstrations) of the 2012 AQMP (SCAQMD, 2013) presents more detail of the modeling procedures followed by SCAQMD and by this project.

The UTEP modeling procedures were carefully tested during the previous CRC Project A-91. UTEP CMAQ simulations for the 2008 base-year were compared with those made with the simulations provided by SCAQMD. The comparison made for 91 days in summer 2008 (June 1 to August 30) and the comparison showed that UTEP had successfully reproduced the SCAQMD results.

A new series of simulations were made with adjustments made to the emissions of NO_x and ROG. The adjustments were made by multiplying the 2008 base-year and the 2030 future-year by the factors discussed in Section 4.2 and shown in Tables 4-1 and 4-2 of this report. The adjustments to ROG emissions were made to the 2008 base-year emissions to examine the effects of an underestimate in ROG emissions on PM concentrations. Primary PM

emissions were unchanged from run to run when NO_x and ROG were adjusted so that any changes in the PM concentrations would be due to changes in secondary PM formation alone.

The effect of changes in NO_x emissions on PM concentrations was examined by adjusting the NO_x emission inventory for the 2030 future-year by the multiplicative factors discussed in Section 4.2 and shown in Table 4-3 of this report. This allowed to SCAQMD's NO_x focused reduction strategy to be evaluated. Direct emissions of primary PM are somewhat reduced between the 2008 base-year and the 2030 future-year but the differences had a very small effect on PM concentrations in the SoCAB; see Section 4.2 and Table 4-3.

To illustrate the complex behavior of chemical species related to PM formation, CMAQ simulated distributions of sulfate and nitric acid across the SoCAB for June 13, 2008 are shown in Figure 6-1. These distributions are somewhat different. The sulfate concentrations are highest along the coast while nitric acid concentrations increase further inland for this case. Sulfur dioxide emissions are much lower than NO_x emissions in the SoCAB and therefore the sulfate mixing ratios are much lower than the nitric acid mixing ratios.

CMAQ Simulated Sulfuric Acid

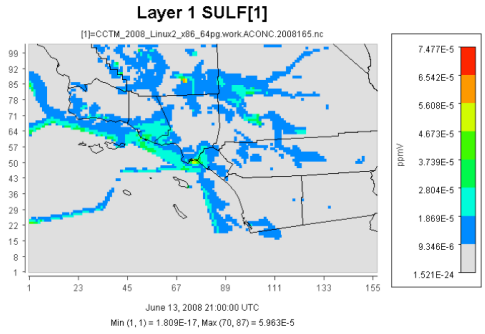

CMAQ Simulated Nitric Acid

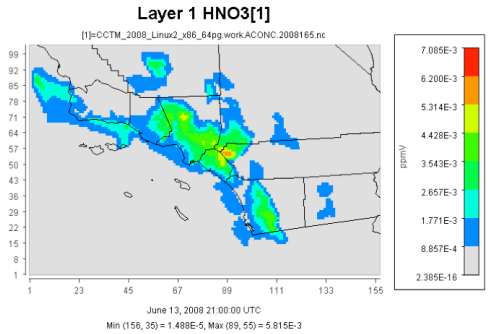

Figure 6-1. Left plot shows gas-phase sulfuric acid and the right plot shows nitric acid across the SoCAB. These CMAQ simulations are for June 13, 2008. The time is 21:00 UTC (2:00 PDT) (Stewart, 2017).

6.2 Summary of CMAQ Modeling Methodology and Assumptions

SCAQMD modeling protocol was followed strictly. This was necessary to keep our results comparable with theirs.

7. CMAQ PERFORMANCE EVALUATION FOR MODELING PM

7.1 CMAQ Model Evaluation for the Fall and Winter Aerosol Season 2008 Base-Year

We expected that CMAQ performance for modeling $PM_{2.5}$ will not be as high as for ozone given the limited current state of the science for measuring and modeling PM. Also, given our project scope to follow SCAQMD protocols we could not make any major changes to the modeling protocol.

In general air quality model performance for simulating PM is not as high as it is for simulating ozone and our PM modeling evaluation is consistent with SCAQMD, (2013). Our analysis showed that CMAQ under-predicted $PM_{2.5}$ mass concentrations and the shared variance between the observed concentrations and the simulated concentrations was not high. Time series plots of $PM_{2.5}$ mass concentrations and its components at a number of sites give at least some confidence that CMAQ preformed well enough for a weight of evidence argument.

CMAQ air quality simulations for the September and November 2008 base-year high PM episodes were evaluated. A number of statistics were calculated for measured and simulated daily average $PM_{2.5}$ mass concentrations. The statistics are commonly used to evaluate air quality models. The statistics were calculated for each of the six stations individually and for all of stations together. These statistics are defined in (Eder and Yu, 2006; Stewart, 2017) and are summarized here. In the equations below N is the number of pairs of simulated points and observations; C_m are the modeled concentrations and C_o are the observed concentrations

The first statistic is mean bias (MB).

$$MB = \frac{1}{N}\sum_{1}^{N}(C_m - C_o)$$

Normalized mean bias (NMB) is defined by:

$$NMB = \frac{\sum_1^N (C_m - C_o)}{\sum_1^N (C_o)} 100\%$$

Root mean square error (RMSE) is defined by:

$$RMSE = \sqrt{\frac{1}{N}\sum_{1}^{N}(C_m - C_o)^2}$$

Normalized mean error (NME) is defined by:

$$NME = \frac{\sum_1^N |(C_m - C_o)|}{\sum_1^N (C_o)} 100\%$$

Unpaired peak ratio (UPRR) is the ratio of model simulated maximum value to the observed maximum value.

$$UPRR = \frac{Maximum\ (C_m)}{Maximum\ (C_o)}$$

The statistic paired mean normalized gross error (PMNGE) is defined by:

$$PMNGE = \frac{1}{N}\sum_{1}^{N}\left(\frac{|C_m - C_o|}{C_o}\right) * 100\%$$

Finally paired mean normalized bias (PMNB) is given by:

$$PMNB = \frac{1}{N}\sum_{1}^{N}\left(\frac{C_m - C_o}{C_o}\right) * 100\%$$

The statistics listed above were calculated to compare the CMAQ simulations with the SoCAB measurement data. Both episodes were used in the calculation of each statistic. It was found that CMAQ under-predicted $PM_{2.5}$ mass concentrations at all six sites, Figure 7-1 (Stewart, 2017).

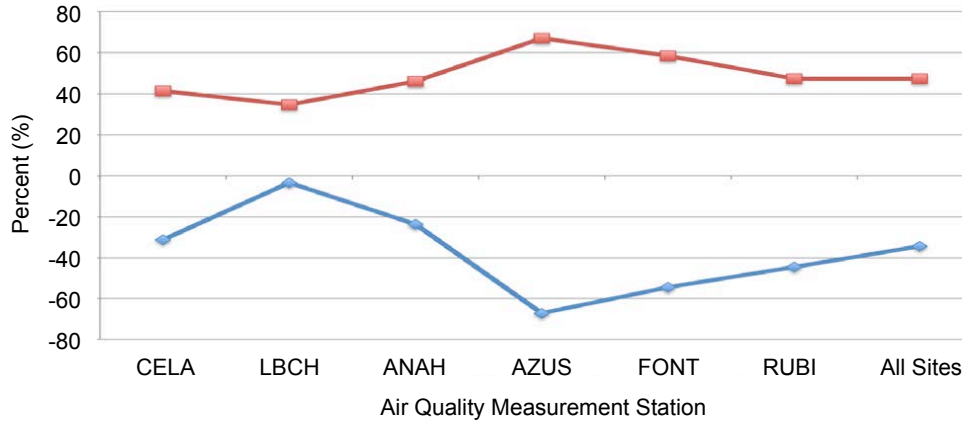

Figure 7-1. The normalized mean error (upper line) and the normalized mean bias (lower line) is shown for the six measurement sites (Los Angeles (CELA), Long Beach (LBCH), Anaheim (ANAH), Azusa (AZUS), Fontana (FONT) and Rubidoux (RUBI)) and all six sites combined.

Overall for the CMAQ simulations of the 2008 base-year the mean bias was -8.87 μg m^{-3}, the normalized mean bias was -34.53% and the normalized mean error was 47.25%. Table 7-1 shows that for all of these statistics CMAQ under-predicted $PM_{2.5}$ mass concentrations at all the sites. The under-prediction was least at Long Beach and the site with the second least under-prediction was Anaheim, (Stewart, 2017). The statistics show that it is difficult to simulate PM and there is no generally accepted statistic for acceptable model performance for PM. Eder and Yu (2006) suggest that a NME within 50% is reasonable performance for PM. This metric is met at Los Angeles, Long Beach, Anaheim, Azusa and Rubidoux but it is not met at Azusa and Fontana.

Station	MB ($\mu g/m^3$)	NMB (%)	RMSE ($\mu g/m^3$)	NME (%)	UPR	PMNGE (%)	MPNB (%)
Los Angeles	-9.08	-31.32	19.63	41.28	0.15	35.33	-18.79
Long Beach	-0.93	-3.42	12.92	34.62	0.73	34.57	9.28
Anaheim	-6.28	-23.62	17.35	45.90	0.66	44.15	-8.70
Azusa	-15.31	-67.10	19.31	67.14	0.30	63.59	-63.51
Fontana	-13.63	-54.53	17.79	58.51	0.43	58.24	-52.39
Rubidoux	-10.40	-44.58	13.29	47.29	0.59	44.77	-41.53
All Stations	-8.87	-34.53	16.76	47.25	0.57	45.36	-27.44

Table 7-1. Table shows the following statistics for the CMAQ simulated $PM_{2.5}$ mass concentrations: Mean Bias (MB), Normalized Mean Bias (NMB), Root Mean Square Error (RMSE), Normalized Mean Error (NME), Unpaired Peak Ratio (UPR), Paired Mean Normalized Gross Error (PMNGE) and Mean Paired Normalized Bias (MPNB) (Stewart, 2017).

Figure 7-2 shows the correlation between CMAQ modeled and measured concentrations $PM_{2.5}$ during the two high $PM_{2.5}$ episodes and Table 7-2 summarizes the shared variance between the model and measurements. The model performed well for the Rubidoux site with a shared variance of 0.65 between the measured and modeled concentrations. The performance was low at Fontana and Azusa with a shared variance of 0.16 and 0.11, respectively. The performance at Long Beach, Anaheim and Los Angeles was poor with low correlation between the measured and modeled concentrations.

Figures 7-3 through 7-8 show comparisons of time series of observed and modeled aerosol for the two high $PM_{2.5}$ episodes; September 12-15 and November 11-24, 2008. For some of the sites and species the observations do not have high temporal-resolution. Elemental carbonaceous mass (EC) is shown in Figure 7-3. EC mass concentrations are expected to be due to direct PM emissions. The CMAQ model showed the best performance at Rubidoux. The simulated mass concentrations were lower than many of the measurements at Rubidoux but the simulated time series appeared to follow the measurements and it correctly simulated the OC mass concentration for November 23, 2008. The other stations, Los Angeles, Anaheim and Fontana provided only three, two and two measurement data points, respectively. The simulations were generally low at these stations but at Los Angeles CMAQ correctly simulated OC for November 20, 2008 and correctly at Anaheim for September 15; both were near the end of the simulated episode.

Measurement Site	Shared Variance for $PM_{2.5}$ Mass Concentrations
Rubidoux	0.65
Fontana	0.16
Azusa	0.11
Long Beach	0.01
Anaheim	0.01
Los Angeles	0.01

Table 7-2. Table shows the correlation between measured $PM_{2.5}$ mass concentrations and CMAQ model simulations during two high $PM_{2.5}$ episodes, September 12-15, 2008 and November 11-24, 2008.

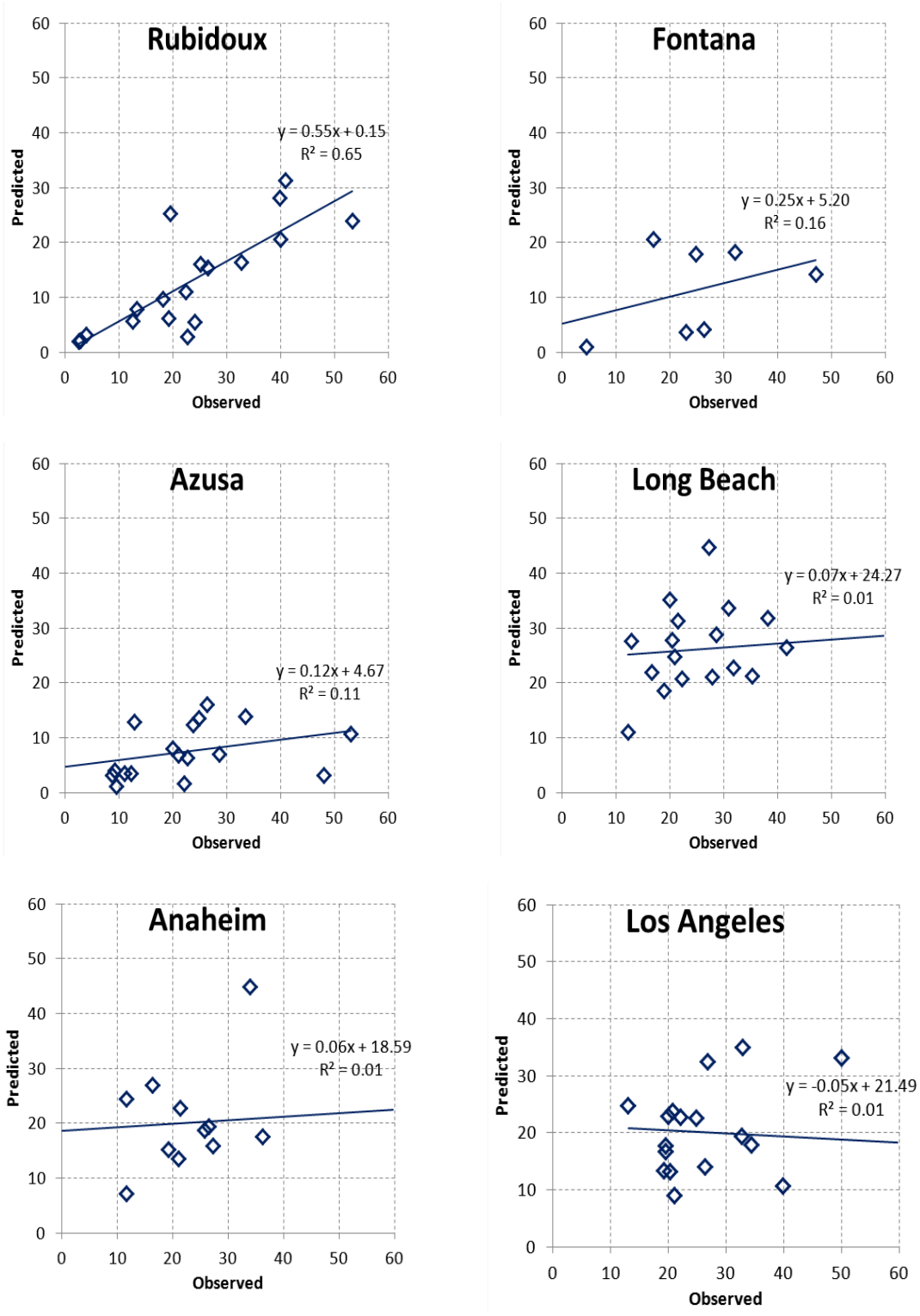

Figure 7-2. Plots show the correlation between CMAQ model results and measured concentrations during two high $PM_{2.5}$ episodes, September 12-15 and November 11-24, 2008.

Measured and modeled organic aerosol mass concentrations are shown in Figure 7-4. The measured organic mass was estimated as a factor of 1.4 times the measured organic carbon (OC). The CMAQ model performance in simulating OC was best at Los Angeles with the measured data and the simulations nearly agreeing on September 15, 2008. For the November case the measurements and model agreed on November 13, 2008 but the simulation was low by 50% on November 20. CMAQ accurately simulated OC for two of the measured points for the November episode at Rubidoux. But overall CMAQ was generally low for the September episode and the remainder of the November episode at Rubidoux. The apparent greater underestimation of organic mass at the Anaheim and Fontana sites may be, in part, related to differences in the analytical protocols used to measure OC.

Figure 7-5 shows a comparison of the CMAQ model results to the measured ammonium sulfate concentrations. The comparison is difficult for ammonium sulfate and for ammonium nitrate because of the scarcity of the observations. The comparison is more difficult for sulfate because its concentrations were lower than the nitrate. The ammonium sulfate was estimated as 1.375 times the total sulfate (1.375 is the ratio of the molecular weight of ammonium sulfate to the molecular weight of sulfate). Within these limitations the performance of the CMAQ model in simulating the ammonium sulfate concentrations appeared to be a bit better than its performance for nitrate.

Figure 7-6 shows a comparison of CMAQ model results to measured ammonium nitrate concentrations. The ammonium nitrate concentrations were estimate as *1.29 times the total nitrate concentrations (1.29 is the ratio of the molecular weight of* ammonium nitrate to the *molecular weight of* nitrate). The comparison is difficult because of the relatively few observations. The CMAQ model ammonium nitrate is generally low but it appears to capture some of the temporal behavior of the observations during both the September and November episodes.

Figure 7-7 shows a comparison of observed and modeled $PM_{2.5}$ concentrations. During the September 12-15 episode $PM_{2.5}$ was relatively well modeled for the Los Angeles, Long Beach and Anaheim sites but the modeled $PM_{2.5}$ was low at the other sites. During the November 11-24 episode the CMAQ modeled $PM_{2.5}$ was usually lower that the measurements and several maxima were missed.

Examination of Figures 7-7 and 7-8 shows that the performance of CMAQ in modeling PM_{10} was not as good as it was for $PM_{2.5}$. The model seriously under-predicted the observed PM_{10} at all the sites. A possible explanation of the low performance is that a greater component of the PM_{10} would be expected to be due to primary emissions than $PM_{2.5}$ that is secondary, produced by atmospheric chemical processes.

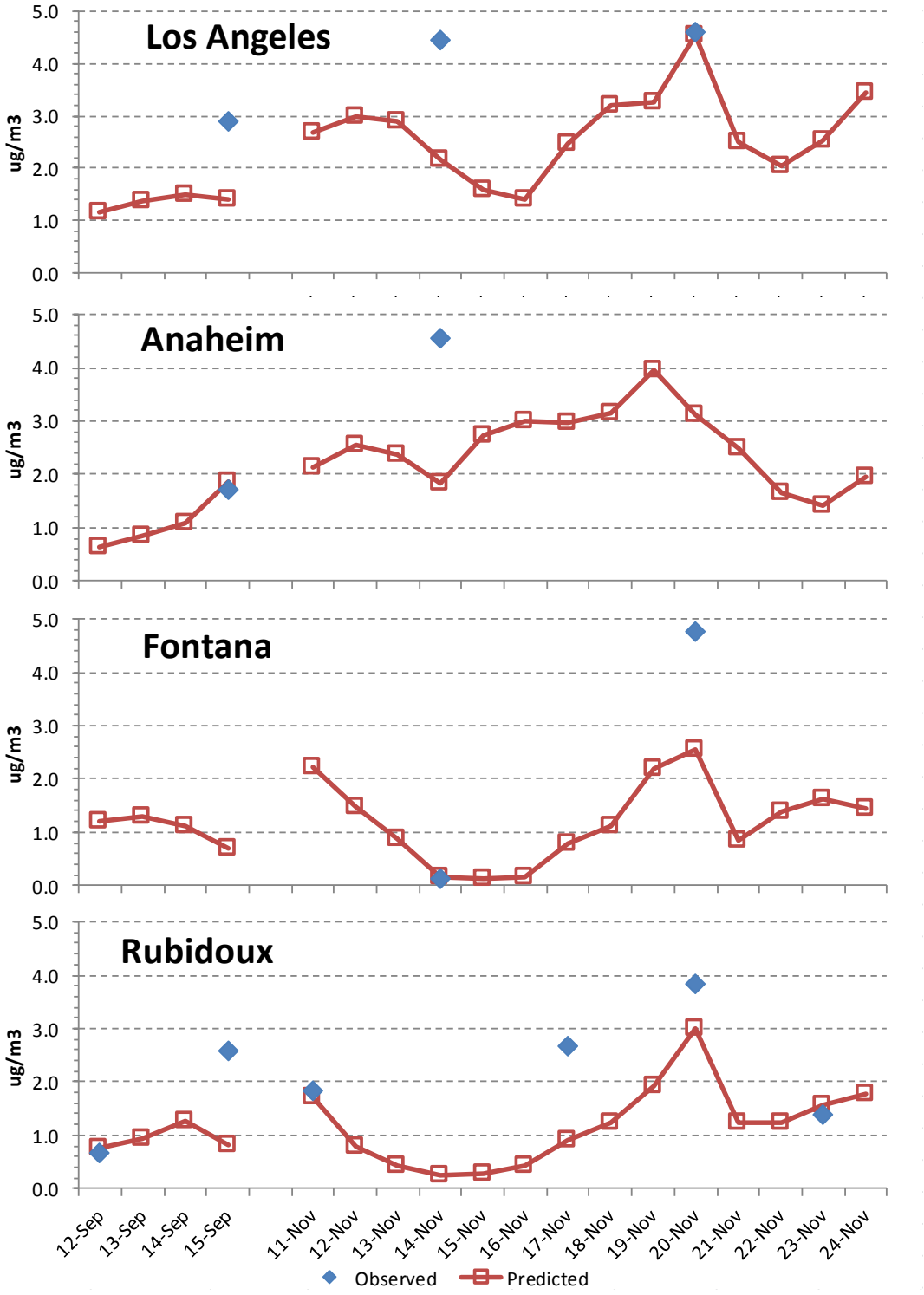

Figure 7-3. Comparison of CMAQ model results to measured elemental carbon concentrations during two high $PM_{2.5}$ episodes, September 12-15 and November 11-24, 2008. *Los Angeles and Rubidoux data are CSN protocol, Anaheim and Fontana are IMPROVE protocol TOR.*

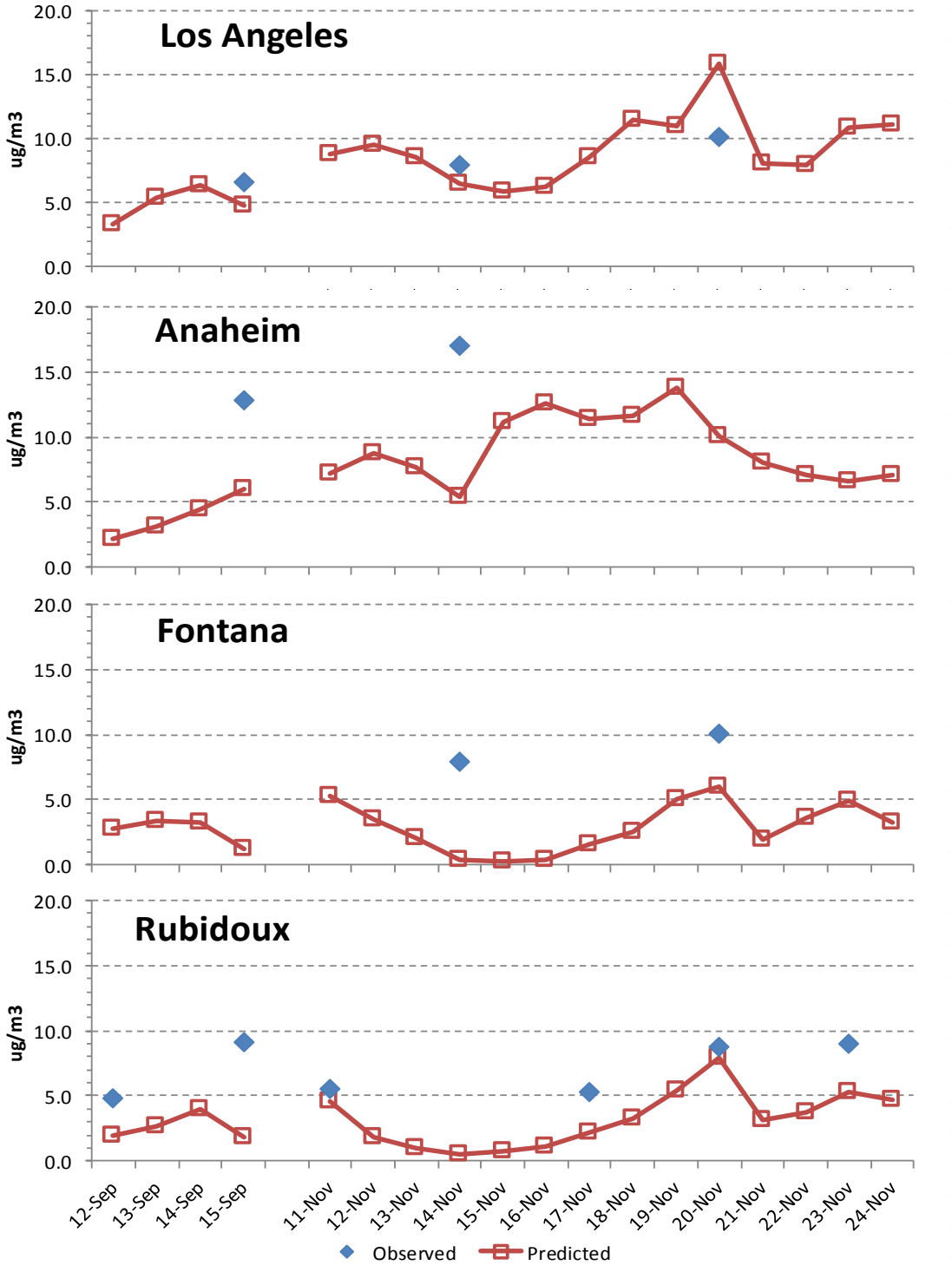

Figure 7-4. Comparison of CMAQ model results to measured organic aerosol mass concentrations during two high $PM_{2.5}$ episodes; September 12-15 and November 11-24, 2008. *Measured organic mass is estimated as 1.4*OC. Los Angeles and Rubidoux data are CSN protocol, Anaheim and Fontana are IMPROVE protocol TOR.*

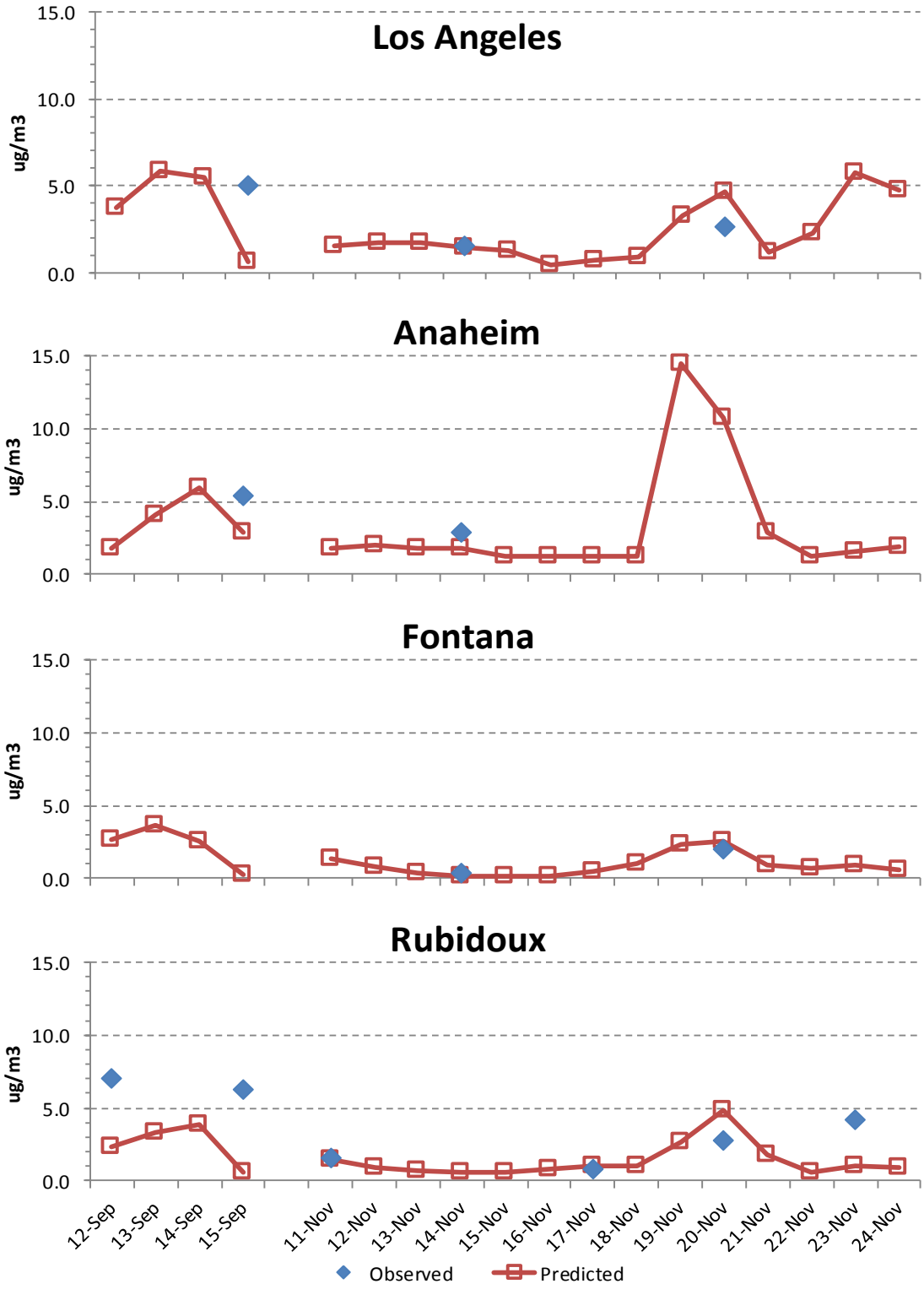

Figure 7-5. Comparison of CMAQ model results to measured ammonium sulfate concentrations during two high $PM_{2.5}$ episodes; September 12-15 and November 11-24, 2008. *Ammonium sulfate is estimated as 1.375*total sulfate.*

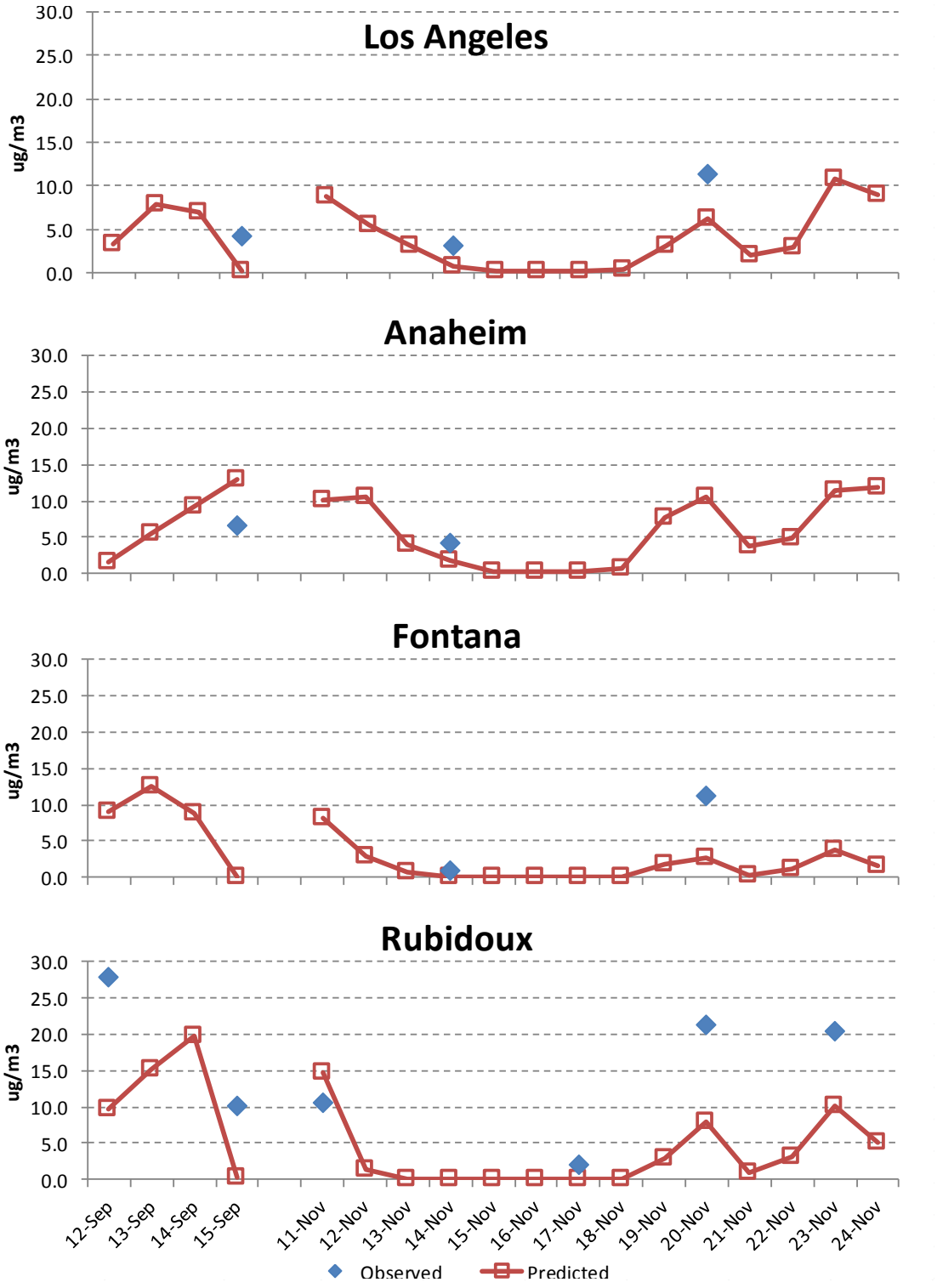

Figure 7-6. Comparison of CMAQ model results to measured ammonium nitrate concentrations during two high $PM_{2.5}$ episodes; September 12-15 and November 11-24, 2008. *Ammonium nitrate is estimated as 1.29*total nitrate.*

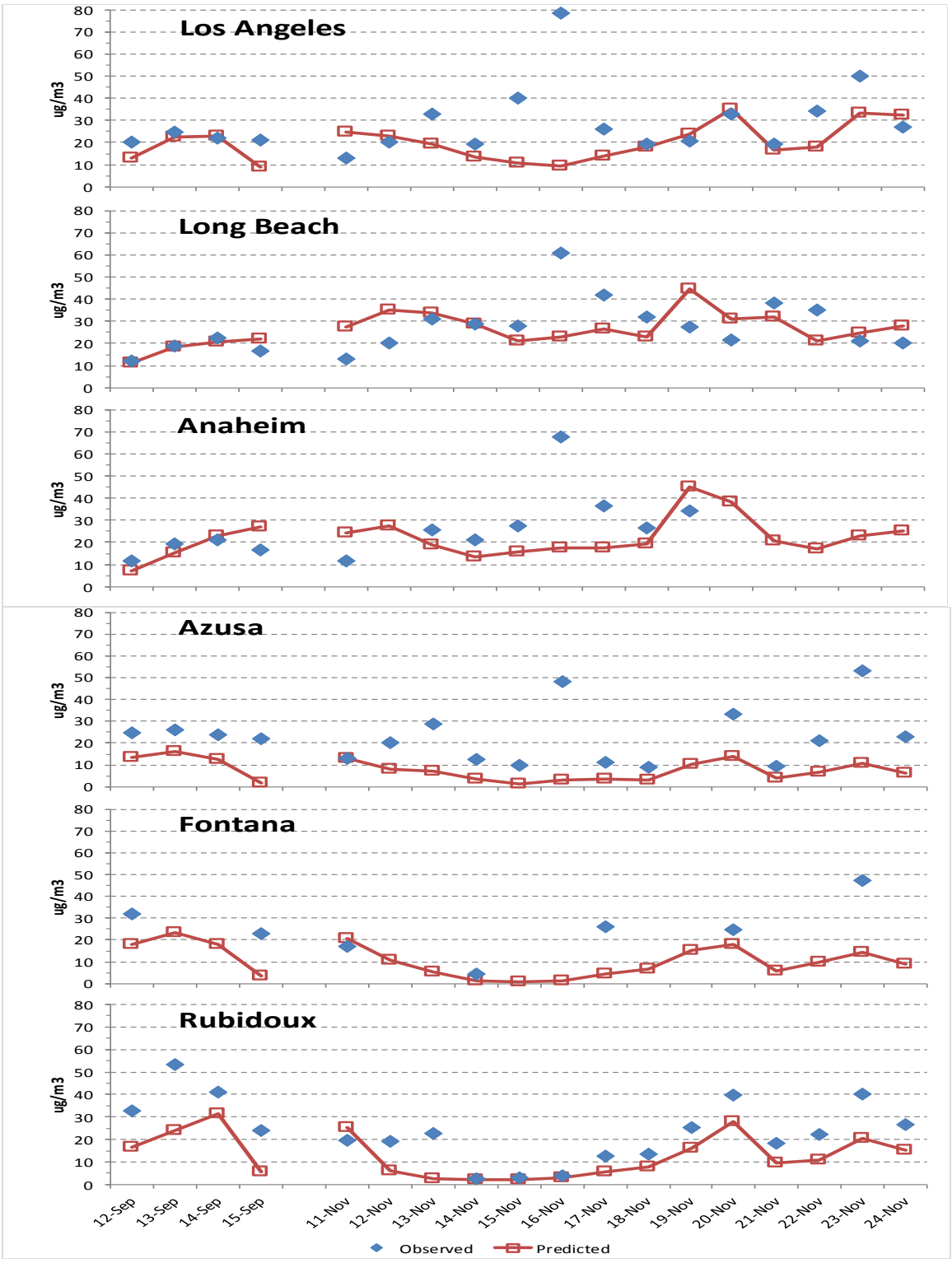

Figure 7-7. Comparison of CMAQ model results to measured $PM_{2.5}$ concentrations during two high $PM_{2.5}$ episodes; September 12-15 and November 11-24, 2008.

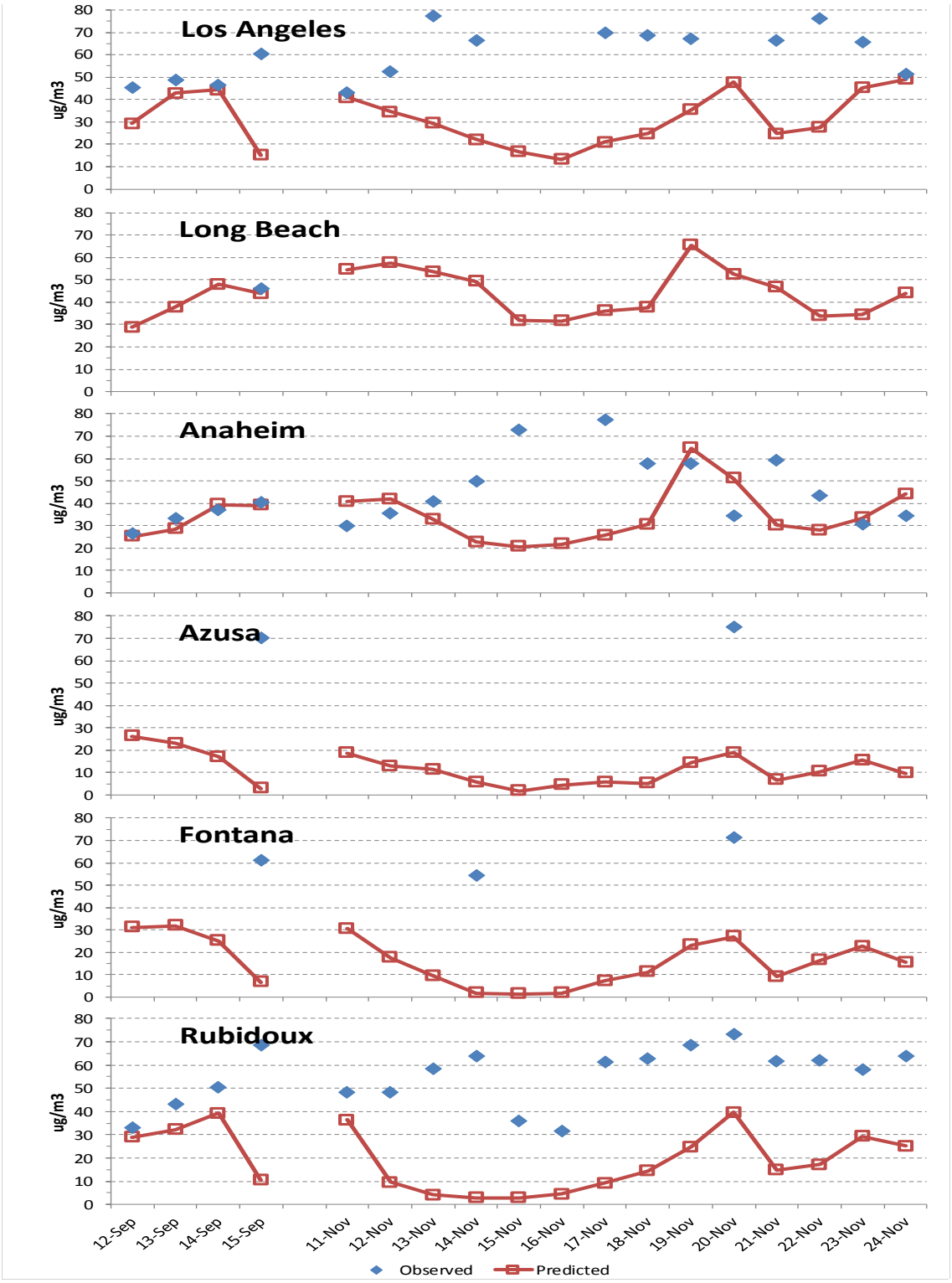

Figure 7-8. Comparison of CMAQ model results to measured PM_{10} concentrations during two high $PM_{2.5}$ episodes; September 12-15 and November 11-24, 2008.

7.2 CMAQ Model Evaluation for the Summer 2008 Base-Year

CMAQ results for the ozone season, June through early September, for the 2008 base-year were taken from simulations made for CRC Project A-91 and compared with measurements and our shown here for reference. During the ozone season the measurements had greater temporal resolution than the measurements for the Fall and Winter seasons compared in Section 7.1. The July episode was examined because of the greater availability of speciation measurements and because this episode was modeled for our previous CRC project. However this episode may not be the most representative for PM because of the July 4th holiday.

Figure 7-9 and 7-10 show a comparison of measured and modeled 24-hr average sulfate $PM_{2.5}$ and nitrate $PM_{2.5}$ concentrations, respectively, at Central LA and Rubidoux (Eastern basin) measurement sites. CMAQ showed a significant bias toward under-prediction of sulfate $PM_{2.5}$ at both sites, Figure 7-9. However CMAQ performed a bit better for nitrate $PM_{2.5}$ concentrations with less under-prediction bias at both sites, Figure 7-10.

Figure 7-11 shows the results of an evaluation of the mean bias caluculated over using data from all six measurement sites for the components sulfate, nitrate organic matter (OM) and elemental carbon (EC) (Stewart, 2017). There is a negative bias for all four components. The mean bias was the most negative for nitrate and most of the nitrate concentrations are expected to be due to its formation in the atmosphere (a secondary pollutant). The organic matter was the next most negative but most of the organic matter concentrations are expected to be due to primary emissions.

Figure 7-12 shows a comparison of measured and modeled daily average $PM_{2.5}$ concentrations at Azusa, Rubidoux and Los Angeles for the summer 2008 ozone season. Overall the shapes of the CMAQ simulated $PM_{2.5}$ concentrations are similar to the measurements but the magnitude of the simulated and measured concentrations can be significantly different. CMAQ tends to under-predict $PM_{2.5}$ at Azusa especially during the first half of the ozone season. During the last half of this period the CMAQ simulations and measurements come together at Azusa. There is better agreement at Rubidoux with the CMAQ simulated concentrations too low during the first half of the ozone season and too high during the second half. CMAQ misses three spikes during the first half of the season.

CMAQ performed the best for the Los Angeles site but it missed a spike in $PM_{2.5}$ concentrations near July 4, 2008. The influence of fireworks on the speciation data should not be a significant factor because no speciation database was collected on July 4. But fireworks may explain the peaks in measured $PM_{2.5}$ mass on July 4 that the model does not predict, Figure 7-12.

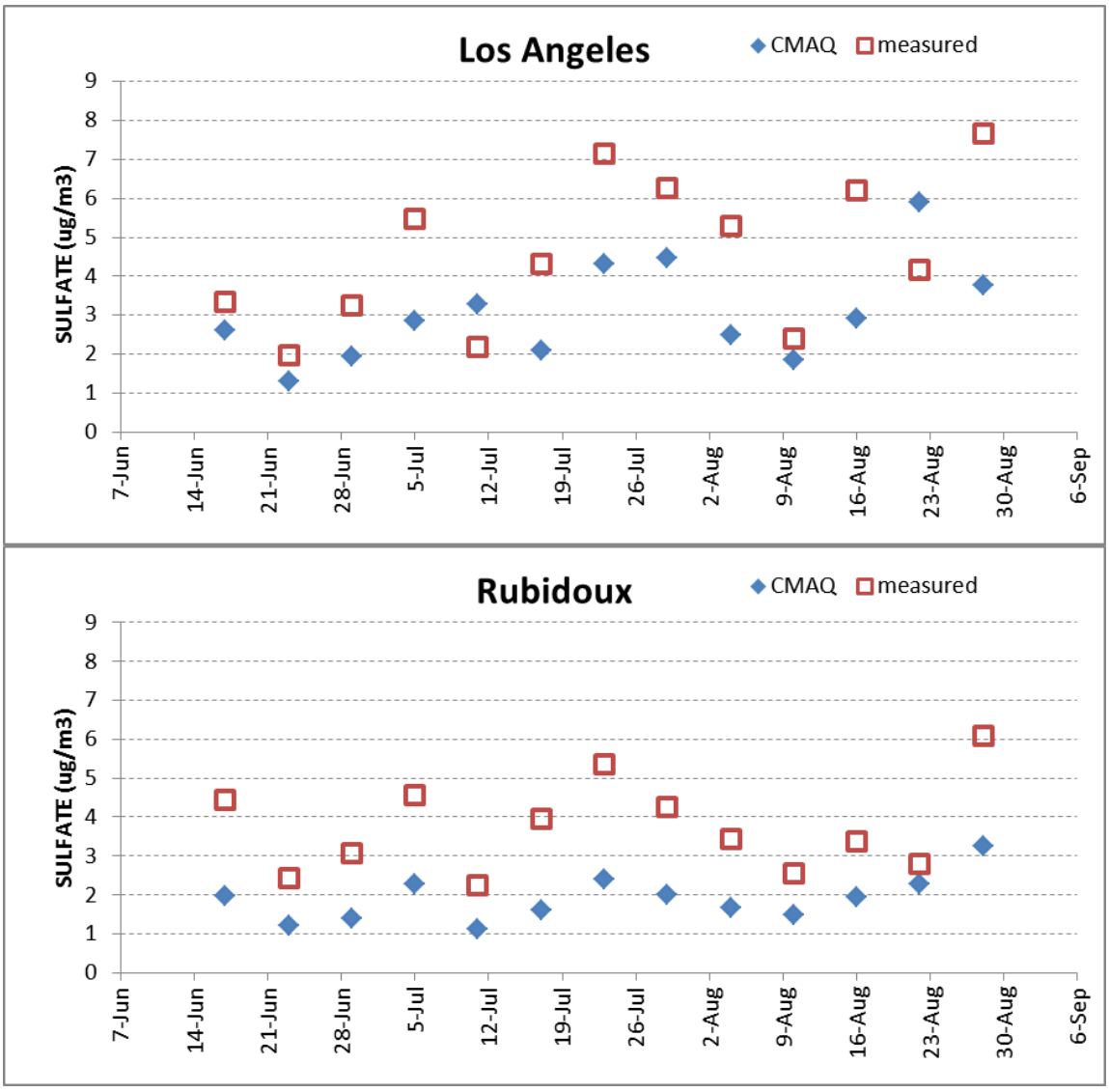

Figure 7-9. Comparison of measured and modeled 24-hr average $PM_{2.5}$ sulfate concentrations at the Central LA and Rubidoux (Eastern basin) monitoring sites during the 2008 ozone season.

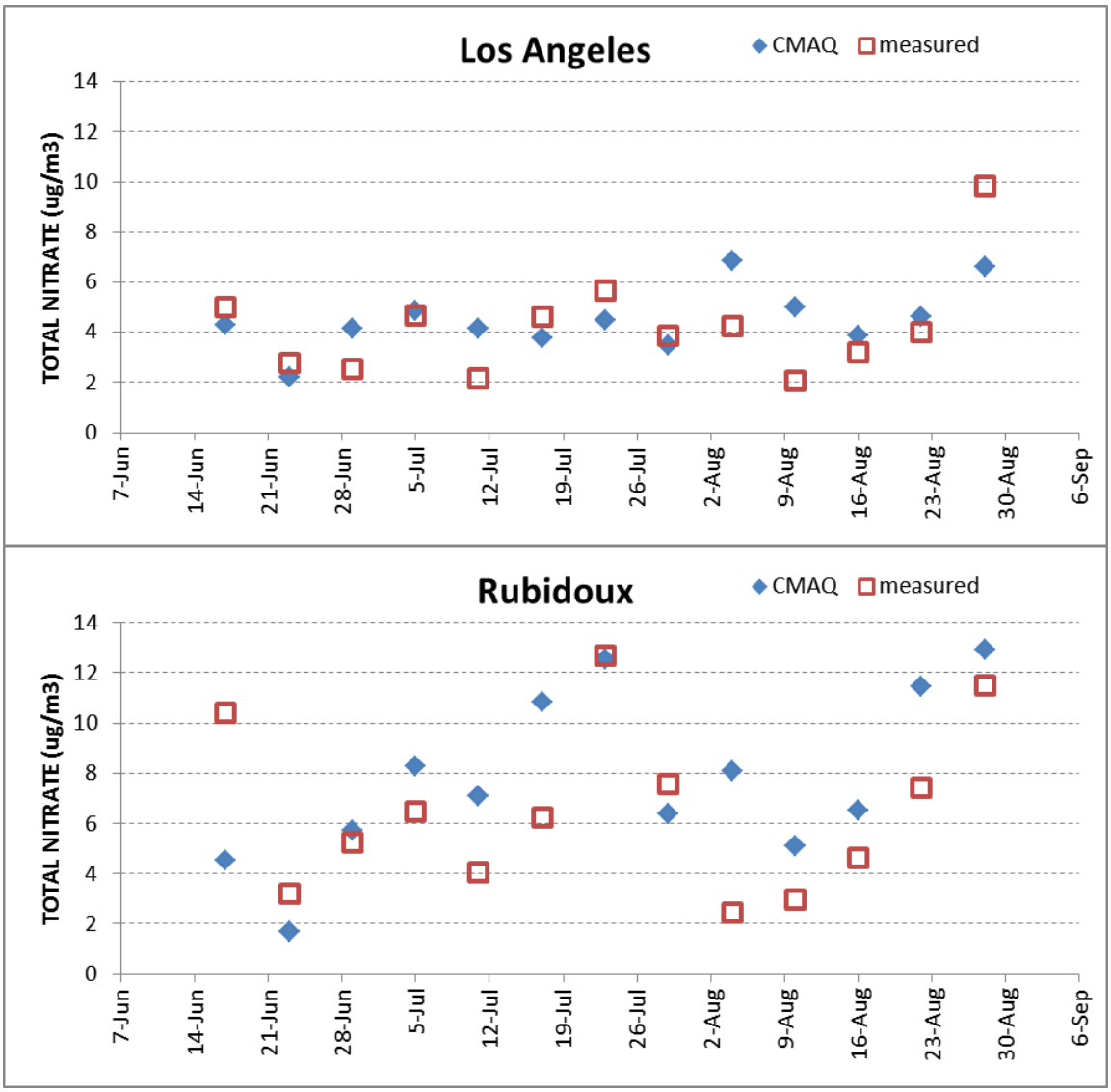

Figure 7-10. Comparison of measured and modeled 24-hr average $PM_{2.5}$ nitrate concentrations at the Central LA and Rubidoux (Eastern basin) monitoring sites during the 2008 ozone season.

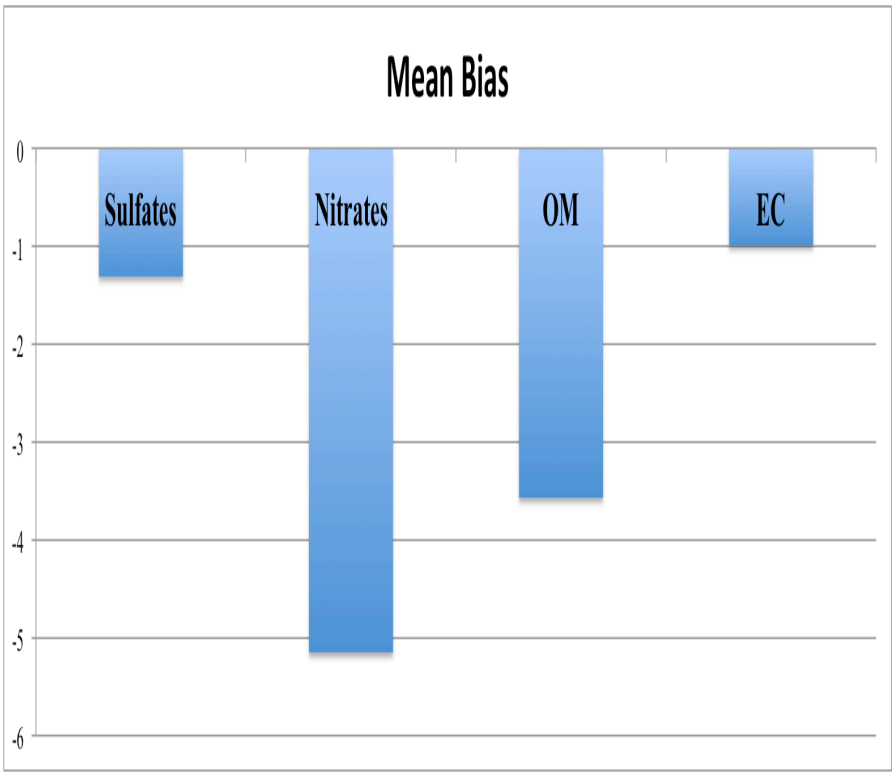

Figure 7-11. This plot shows the mean bias in μg m^{-3} across all sites for sulfate, nitrate organic matter (OM) and elemental carbon (EC) (Stewart, 2017).

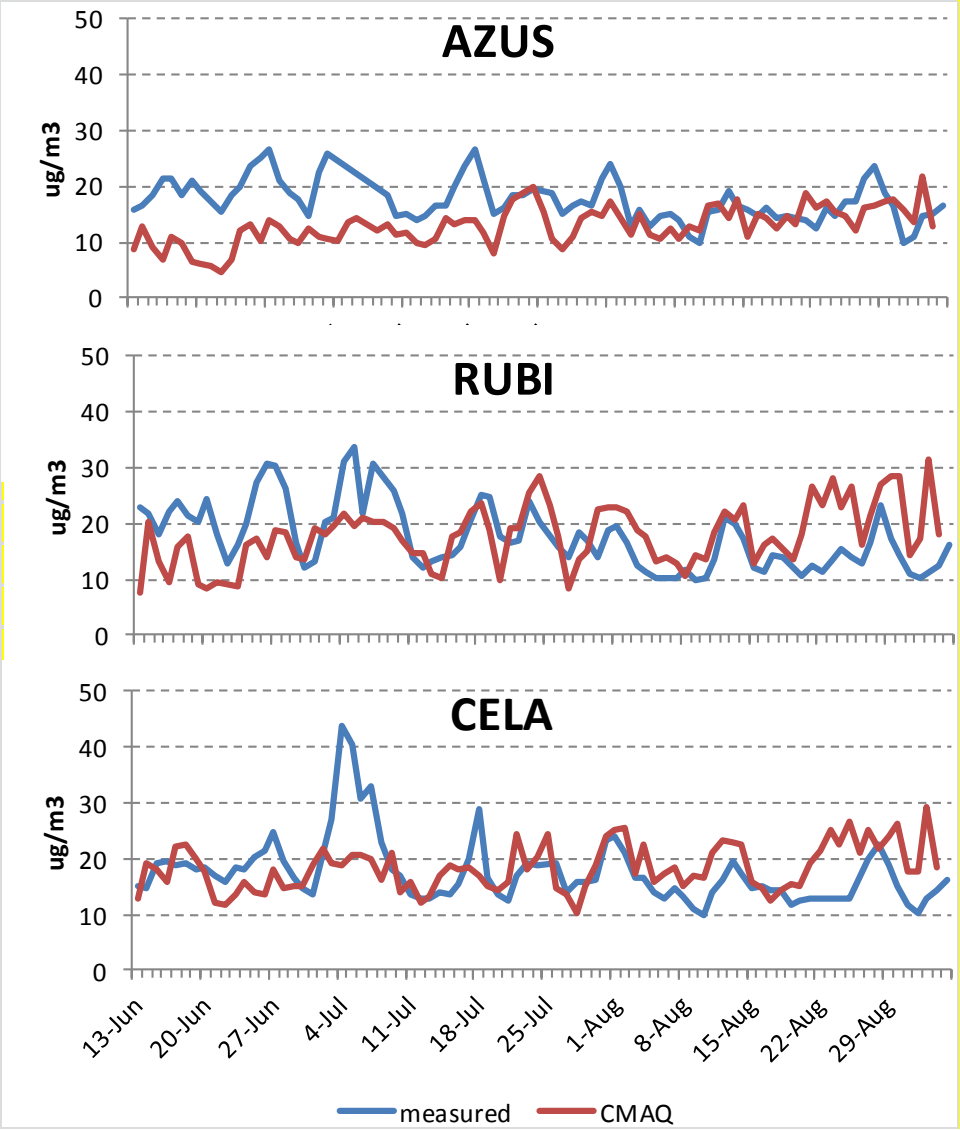

Figure 7-12. Comparison of measured and modeled daily average $PM_{2.5}$ concentrations at Azusa (AZUS), Rubidoux (RUBI) and Los Angeles (CELA) for the summer 2008 ozone season.

7.3 Summary of CMAQ Modeling Performance Evaluation

In general air quality model performance for simulating PM is not as high as it is for simulating ozone and our PM modeling evaluation is consistent with SCAQMD, (2013). This is because the simulation of PM is a much more difficult problem than ozone. For the simulated episodes made for this project the modeled PM concentrations were significantly lower than the measurements. Correlation showed that CMAQ performed best in simulating PM measurements made at Rubidoux. However examination of time series plots showed that CMAQ often replicated the measurements reasonably well.

8. EVALUATION OF THE RESPONSE OF OZONE AND $PM_{2.5}$ TO EMISSIONS CHANGES USING CMAQ

8.1 Changes in Ozone Concentrations Due to Changes in NO_x and ROG Emissions for Base and Future-Years During the Summer Ozone Season

The sensitivity of ozone concentrations to changes in NO_x and ROG emissions was the focus of the CRC Project A-91. Figure 8-1 shows the effect of varying the basin-wide emissions of ROG on 8-hour ozone in the SoCAB at selected stations within the SoCAB. Figure 8-1 suggests strongly that the 2008 ROG emissions are underestimated by a factor of 1.5.

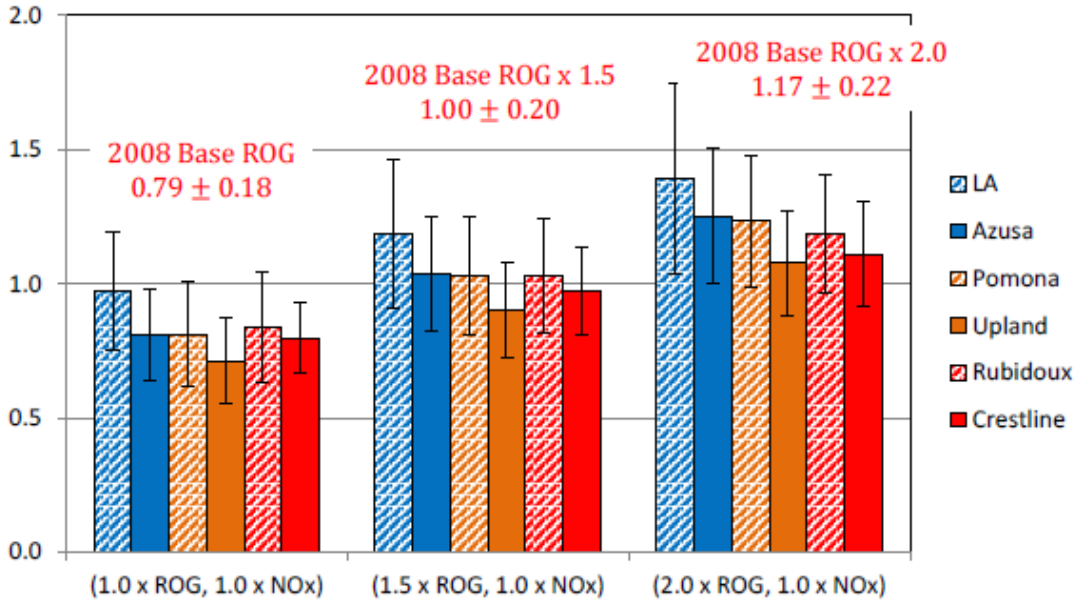

Figure 8-1. Ratios (mean ± standard deviation of simulated/observed) of daily maximum 8-hour ozone for June 15-20 and July 2-8, 2008 episodes with 1.0, 1.5 and 2.0 times 2000 base ROG. Values are for the nine cells (12 × 12 km) containing the SoCAB air quality monitoring stations. (Figure from CRC Project A-91, Fujita et al., 2015).

CMAQ 8-hr ozone concentrations over the SoCAB domain are shown in Figure 8-2 for June 19, during the summertime episode. The purpose of these plots is to show the spatial response of ozone concentrations to changes in ROG emissions. Figure 8-2 shows that the spatial pattern of the ozone concentrations shifts in response to changes in ROG emissions as expected. However it is striking that the ozone concentrations remain high and relatively unaffected by changes in ROG emissions over much of the basin. The effect of varying ROG emissions on ozone concentrations has the appearance of being much greater in Figure 8-1 than it is in Figure 8-2 that shows the spatial patterns over the entire SoCAB.

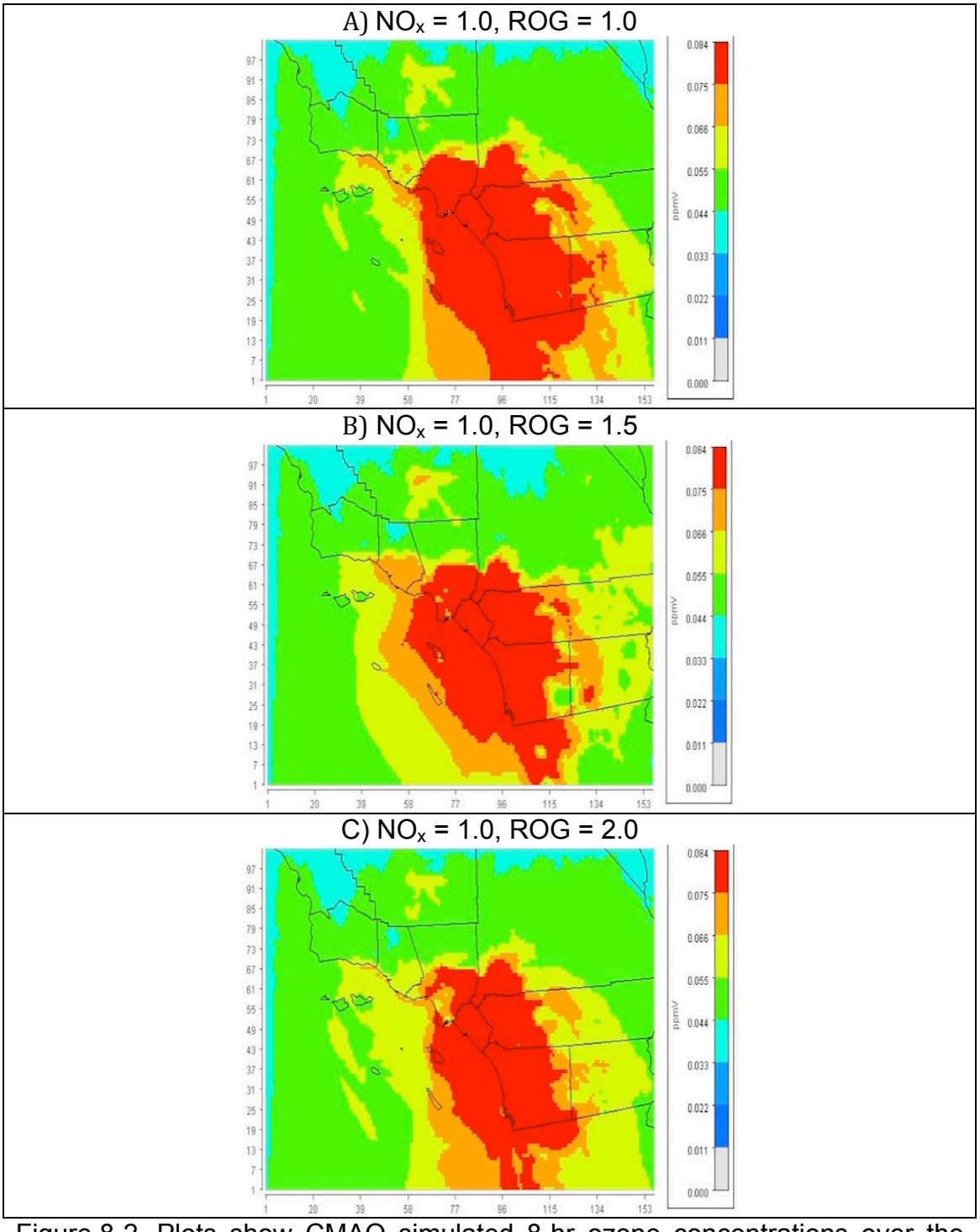

Figure 8-2. Plots show CMAQ simulated 8-hr ozone concentrations over the SoCAB for the base-year on June 19, 2008. The ROG emissions were multiplied by the factors given about the plots while the NO_x emissions were not varied. (Stewart, 2017; Data from CRC Project A-91, Fujita et al., 2015).

Figure 8-3 shows the simulated 2008 base-year and the 2030 future-year daily maximum 8-hour ozone concentrations (ppb) for the June 15-21 and July 2-8 episodes at several stations. Figure 8-3 also shows the basin-wide NO_x and ROG emissions (figure from CRC-91 project; Fujita et al., 2015). Case N'1 is the simulation made with the 2030 future-year projected emissions inventory. The figure suggests that the projected emissions inventory is not optimal for reducing ozone concentrations. Higher NO_x emissions, greater than the projected emissions inventory, would reduce ozone more, provided that the planned reductions in ROG are met. On the other hand, very large NO_x reductions would be required for the 2030 future-year to meet the National Ambient Air Quality Standards (NAAQS).

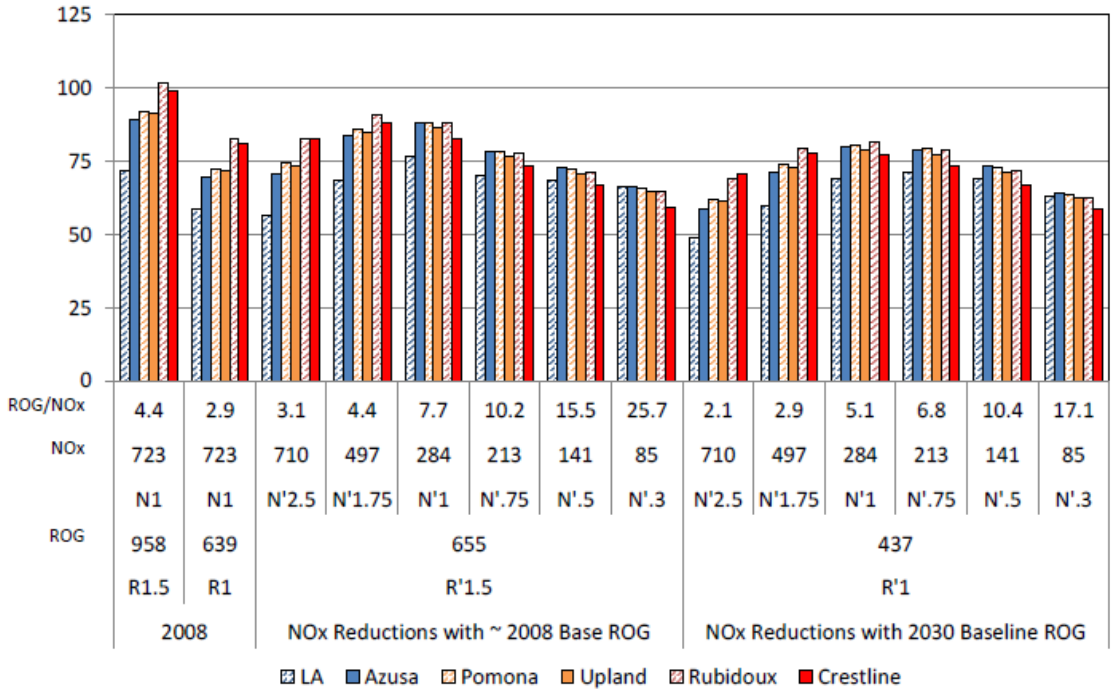

Figure 8-3. Simulated 2008 base-year and 2030 future-year daily max 8-hour ozone concentrations (ppb) for the June 15-21 and July 2-8 episodes. Basin-wide NO_x and ROG emissions (tons per day) are shown above the adjustment factors applied to the 2008 base-year ROG (R) and NO_x (N) emissions and 2030 baseline ROG (R) and NO_x (N) emissions. (From CRC-91 Project, Fujita et al., 2015).

Although Figure 8-3 and the arguments made by Fujita et al. (2015) are correct, they do not give the complete picture of the response of ozone to NO_x emission changes. Figure 8-4 shows that the 8-hr average ozone decreases with decreases in NO_x emissions across the SoCAB. The highest 8-hr average ozone concentration region, the area in red, decreases as the NO_x emissions decrease. This figure does not show any major ozone dis-benefit in the SoCAB due to reducing NO_x emissions. The difference in this major conclusion is due probably to differences between a station-by-station analysis and an examination of the spatial plots shown here.

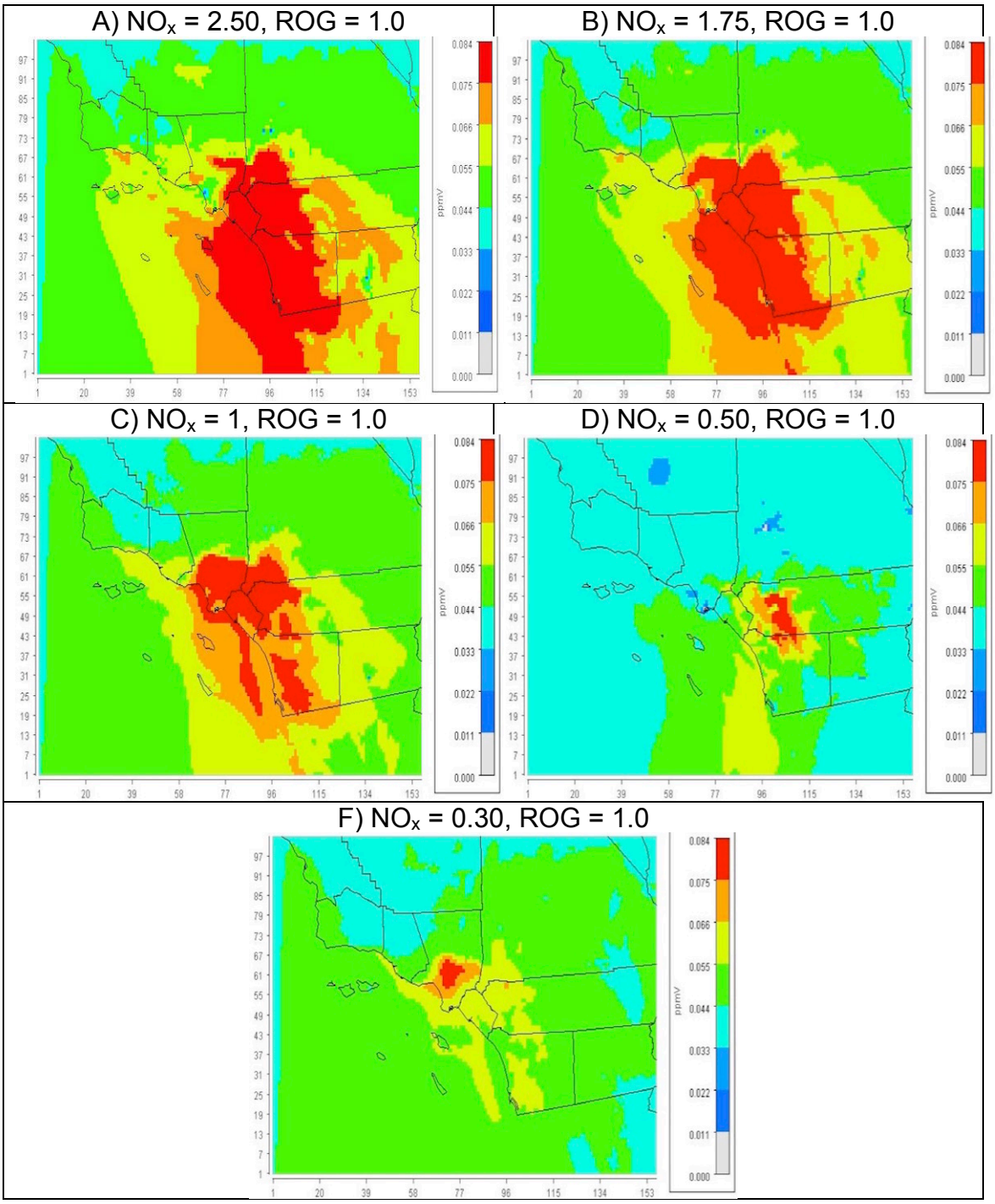

Figure 8-4. Plots show CMAQ simulated 8-hr ozone concentrations over the SoCAB for the future-year on June 19, 2030. The NO_x emissions were multiplied by the factors given about the plots while the ROG emissions were not varied. (Stewart, 2017; Data from CRC Project A-91, Fujita et al., 2015).

8.2 Changes in Ozone Concentrations Due to Changes in NO_x and ROG Emissions for Base and Future-Years During the Aerosol Season

Although ozone is not a problem during the Fall-Winter aerosol episode we believe that ozone production may have some relevance for aerosol productions. Therefore we present the response of ozone concentrations to ROG and NO_x emission inventory variations during the November episode

CMAQ 8-hr ozone concentrations over the SoCAB domain are shown in Figure 8-5 for November 20, 2008, during the Fall-Winter aerosol episode. The spatial pattern for ozone during this time is very different than it is during the summertime. The highest ozone concentrations occur over the ocean while the lowest ozone concentrations are found over central section of the SoCAB. As the ROG emissions are increased the ozone concentrations increase along the coast and a few inland sites experience higher levels of ozone. However, throughout the SoCAB the ozone concentrations remain below the NAAQS in Figure 8-5.

Figure 8-6 shows 8-hr average ozone in the SoCAB for differing NO_x emissions during the November aerosol episode for the year 2030. Plots A and B show that NO titration has a strong effect on ozone concentrations. An increase in NO_x emissions from the projected 2030 inventory leads to very low 8-hr ozone concentrations over the core Los Angeles area. Greater reductions in NO_x emissions from the projected 2030 inventory lead to somewhat increased 8-hr ozone concentrations from the central to the southern region of the coast as can be seen in plots D, E and F.

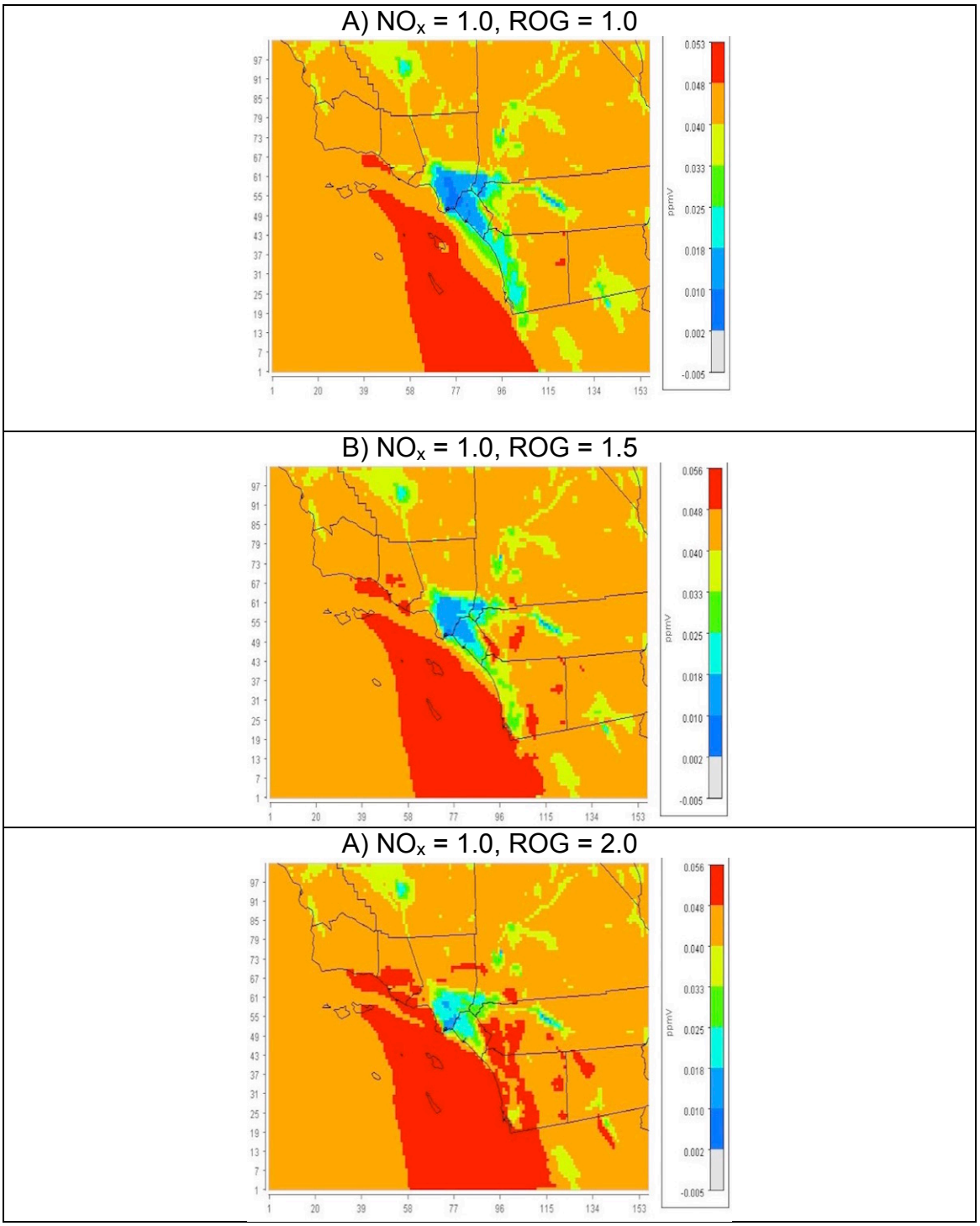

Figure 8-5. Plots show CMAQ simulated 8-hr ozone average concentrations over the SoCAB for the base-year on November 20, 2008 during the Fall-Winter Aerosol Season. The ROG emissions were multiplied by the factors given about the plots while the NO_x emissions were not varied (Stewart, 2017).

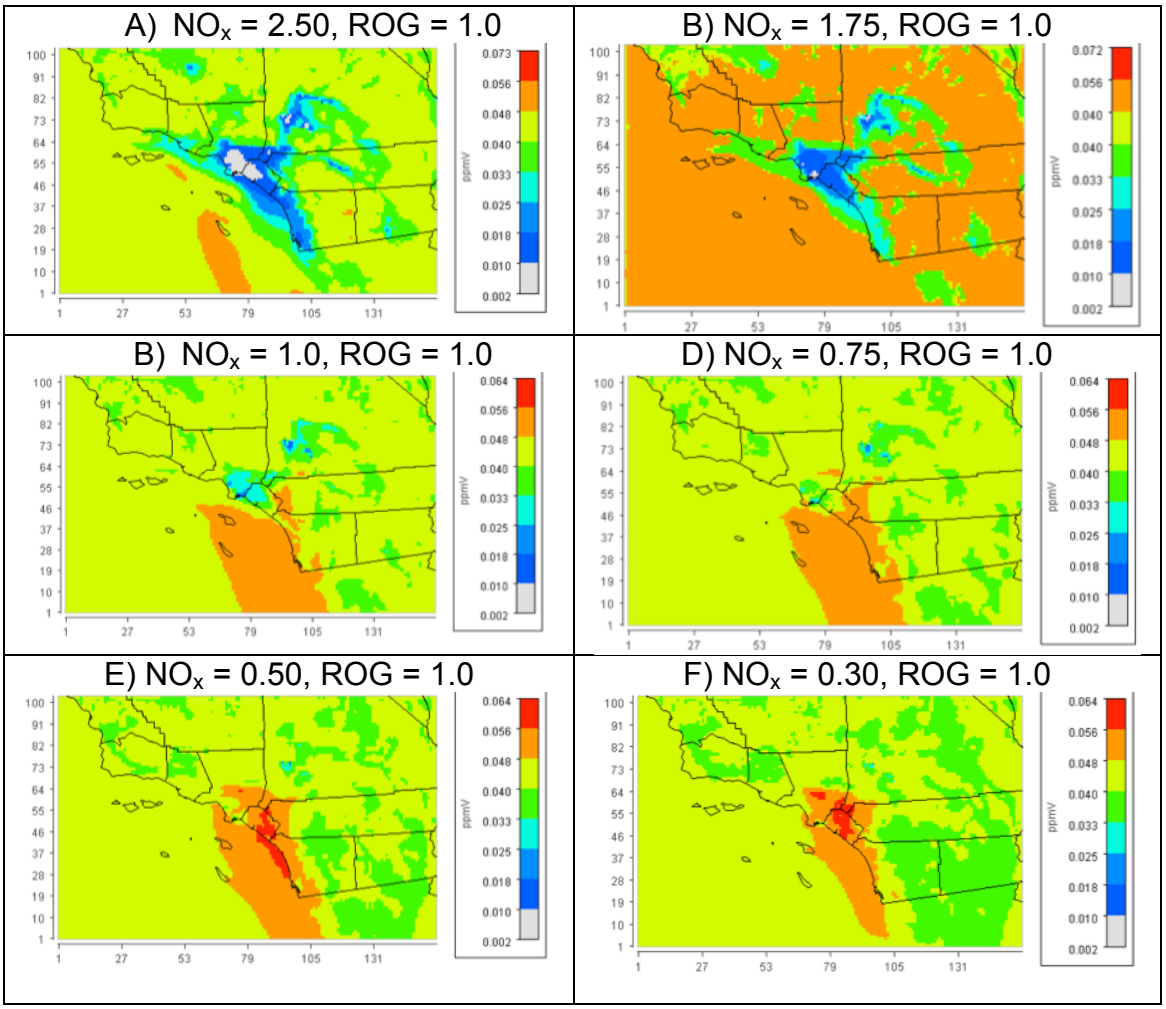

Figure 8-6. Plots show CMAQ simulated 8-hr average ozone concentrations over the SoCAB for the base-year on November 20, 2030 during the Fall-Winter Aerosol Season. The NO_x emissions were multiplied by the factors given about the plots while the ROG emissions were not varied (Stewart, 2017). Note that the scales of plots A and B are slightly different than the other plots.

8.3 Changes in Aerosol Concentration Due to Changes in NO_x and ROG Emissions for Base and Future-Years

Increasing the ROG emissions leads to a marginal improvement in model performance for 24-hour $PM_{2.5}$, Figure 8-7 (Stewart, 2017). However the effect of increasing the ROG on CMAQ performance for 24-hour $PM_{2.5}$ is not as striking as it was for ozone (Fujita et al., 2015b).

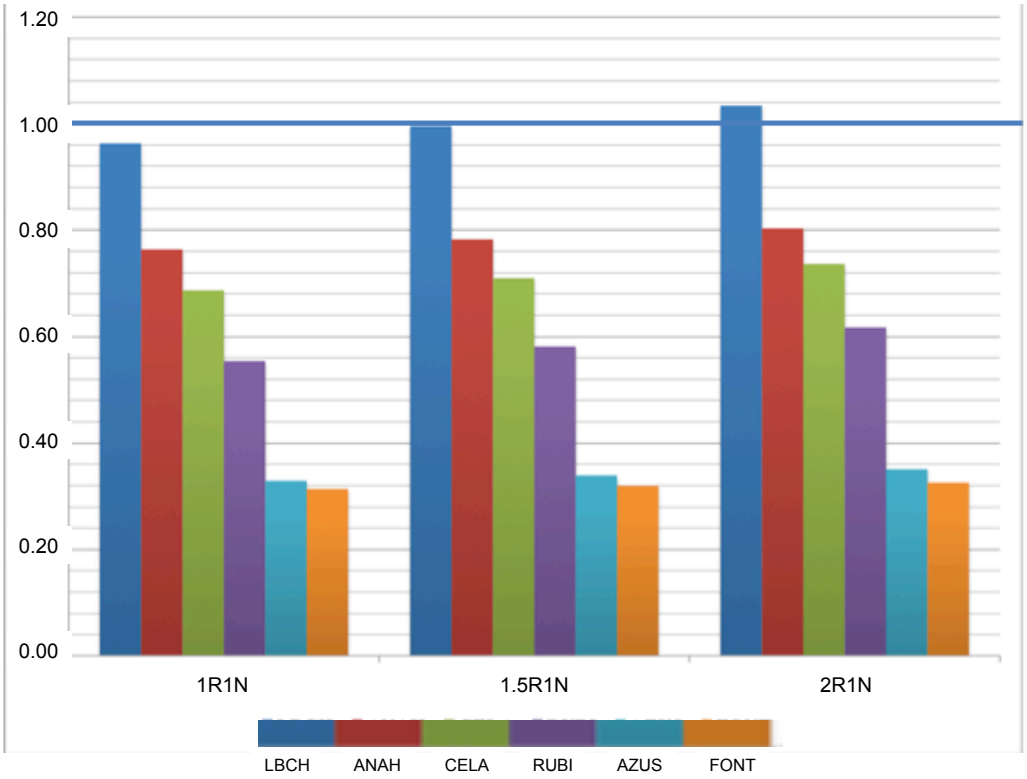

Figure 8-7. Plots show ratio of simulated to measured 24-hour $PM_{2.5}$ at the six measurement sites (Los Angeles (CELA), Long Beach (LBCH), Anaheim (ANAH), Azusa (AZUS), Fontana (FONT) and Rubidoux (RUBI)). The cases are defined in Table 4-2: case 1R1N is the base ROG emissions, case 1.5R1N has the base ROG emissions multiplied by a factor of 1.5 and case 2R1N has the base emissions multiplied by a factor of 2.0 (Stewart, 2017).

Figure 8-8 shows basin-wide plots of 24-hr average $PM_{2.5}$ for November 20, 2008, a day with the highest measured $PM_{2.5}$ mass concentrations for which chemical speciation measurements were available. This figure shows plots made from simulations of the 2008 base case where the ROG emission inventory was varied. The 24-hr average $PM_{2.5}$ increases with increasing ROG emission levels in the central western coast of the SoCAB.

The projected 2030 NO_x emission inventory is the least effective in reducing 24-hr average $PM_{2.5}$ concentrations than the other NO_x emission inventory scenarios simulated. Figure 8-9 shows basin-wide plots of 24-hr

average $PM_{2.5}$ for November 20, 2030. Plot A shows the basin-wide plots of 24-hr average $PM_{2.5}$ for a simulation made with the projected 2030 emissions inventory (N'1) multiplied by a factor of 2.5 (N'2.5). The resulting NO_x emissions for case N'2.5 are about equal to the 2008 NO_x emissions inventory. Plot B shows that when the NO_x emissions inventory is reduced to 1.75 times the projected 2030 inventory (N'1.75) the basin-wide 24-hr average $PM_{2.5}$ are greater than those simulated for case N'2.5, especially in the central western coast of the SoCAB. Plot C shows the effects of further reductions in the NO_x emissions inventory to lower it to the projected 2030 NO_x emissions inventory, case N'1. There is an increase in the basin-wide 24-hr average $PM_{2.5}$ (relative to the N'2.5 and N'1.75 cases).

Plots D, E and F show the effects of greater reductions in the NO_x emissions inventory beyond the projected 2030 NO_x emissions inventory. Plot D corresponds to the projected 2030 NO_x emissions being multiplied by 0.75, Plot E corresponds to the projected 2030 NO_x emissions being multiplied by 0.50 and Plot F corresponds to the projected 2030t NO_x emissions being multiplied by 0.50. The 24-hr average $PM_{2.5}$ decreases with decreasing NO_x emissions in this range of NO_x emission inventories.

A) NO_x = 1.0, ROG = 1.0

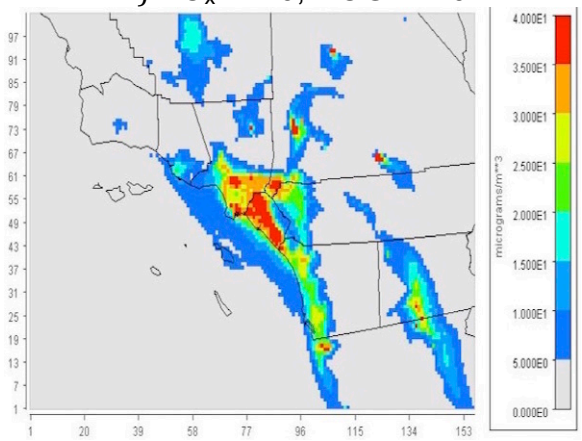

B) NO_x = 1.0, ROG = 1.5

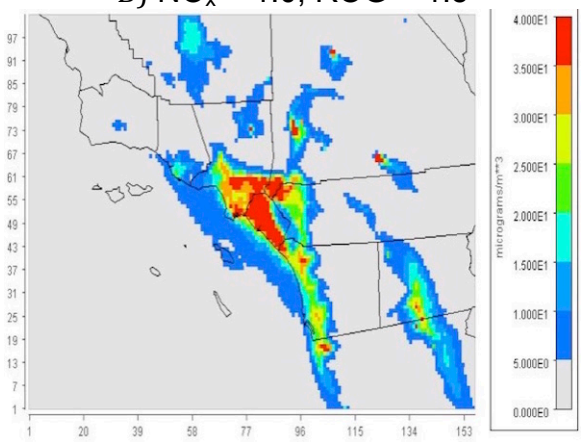

C) NO_x = 1.0, ROG = 2.0

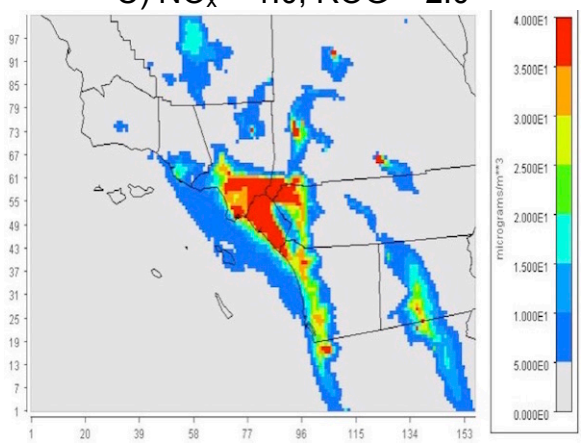

Figure 8-8. Plots show CMAQ simulated 24-hr average $PM_{2.5}$ concentrations over the SoCAB for the base-year on November 20, 2008 during the Fall-Winter Aerosol Season. The ROG emissions were multiplied by the factors given about the plots while the NO_x emissions were not varied (Stewart, 2017).

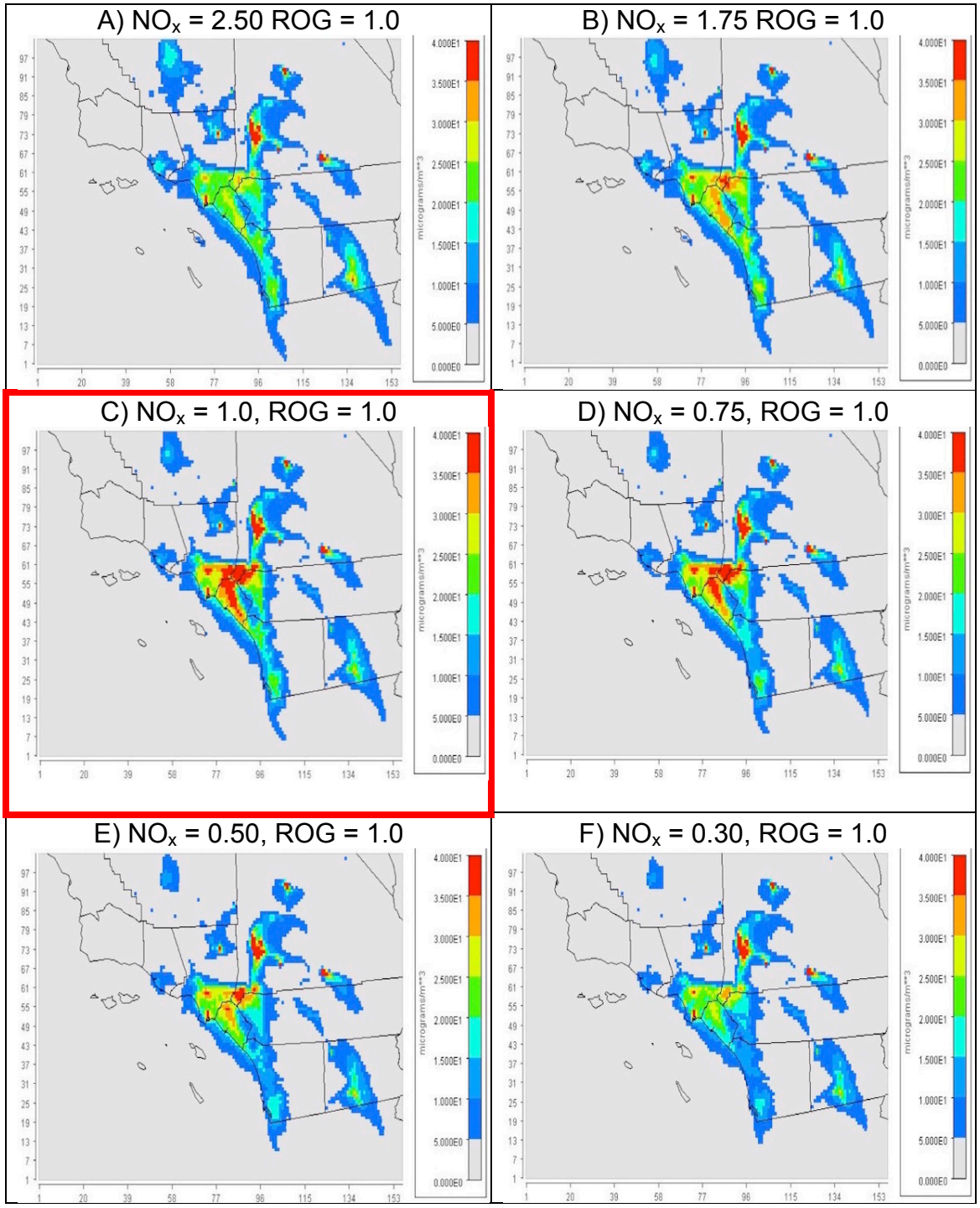

Figure 8-9. Plots show CMAQ simulated 24-hr average $PM_{2.5}$ concentrations over the SoCAB for the future-year on November 20, 2030 during the Fall-Winter aerosol season. The plot outlined in red shows the plot associated with the emission reductions in ROG and NO_x planned for the year 2030. The NO_x emissions were multiplied by the factors given about the plots while the ROG emissions were not varied (Stewart, 2017).

Figure 8-10 shows plots of the range of simulated daily mean mass concentrations of $PM_{2.5}$ at the six monitoring SoCAB sites (Stockwell et al., 2017; Stewart, 2017). Between the 2008 base-year and the 2030 future-year the $PM_{2.5}$ mass concentrations are reduced. The 2030 future-year maxima and the average $PM_{2.5}$ daily mean mass concentrations are greatest at the six stations for the projected 2030 future-year NO_x emission inventory (N'1). For the stations at Long Beach, Anaheim and Rubidoux, the maximum $PM_{2.5}$ daily mean mass concentrations remain above the NAAQS standard. Increasing the NO_x emissions to be near those in 2008 (case N'2.5) decreases $PM_{2.5}$ daily mean mass concentration in the 2030 future-year relative to the N'1 case. Reductions in the NO_x emissions from the N'1 case also reduce the average and maximum $PM_{2.5}$ daily mean mass concentrations until they are reduced to levels near the concentration that was found for the N'2.5 case at most stations.

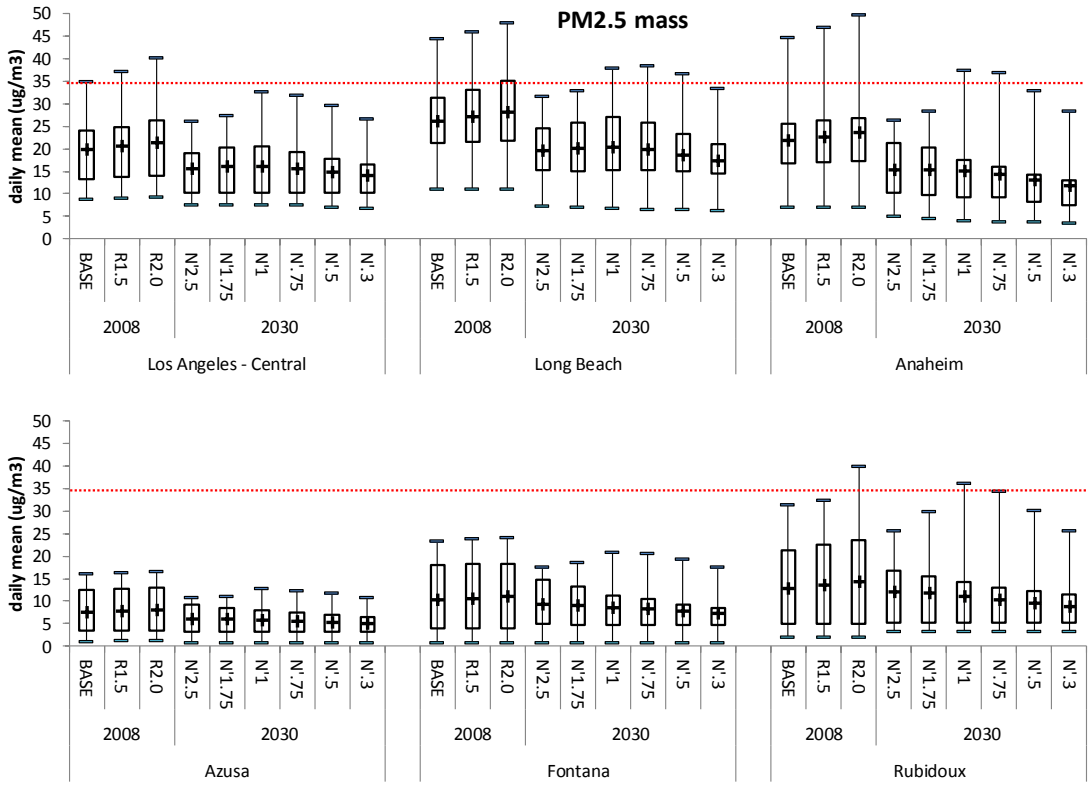

Figure 8-10. Range of simulated daily mean mass of $PM_{2.5}$ at six monitoring sites in the SoCAB. The adjustments to ROG emissions were made for 2008 and the adjustments to NO_x emissions were made for 2030. The box & whisker plots indicate the minimum, 1st and 3rd quantile, maximum, and mean (+) values during two high $PM_{2.5}$ episodes, September 12-15, 2008 and November 11-24, 2008. The red line shows the 35 $\mu g\ m^{-3}$ NAAQS standard.

8.4 Changes in Aerosol Composition During a High Pollution Episode Day Due to Changes in NO_x and ROG Emissions for Base and Future-Years

The mass concentrations of ammonium nitrate show the greatest sensitivity to changes in ROG and NO_x emissions. Figure 8-11 shows an example plot for Anaheim. Ammonium nitrate mass concentrations increase as ROG emissions are increased for the 2008 base-year. For the 2030 future-year the ammonium nitrate mass concentration is greatest for the target 2030 NO_x emission case N'1. For cases N'2.5 and N'1.75 the ammonium nitrate mass concentrations are less than the N'1 case and the ammonium nitrate mass concentrations decrease with increasing NO_x emissions. Cases N'.75, N'.50 and N'.3 all have lower NO_x emissions than N'1 and for these cases there are lower ammonium nitrate concentrations as NO_x emissions are reduced. This behavior is similar to what is seen in Figures 8-8 and 8-9 above.

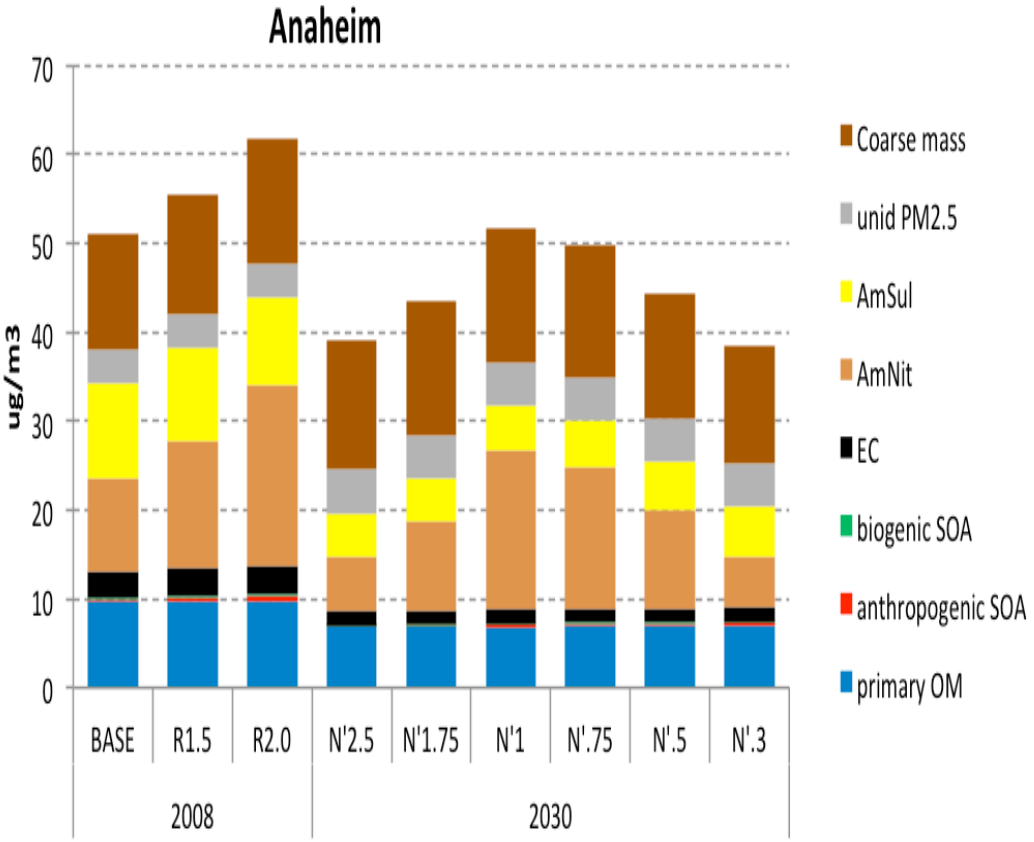

Figure 8-11. Stack plot of simulated daily-average particulate matter mass concentrations by component on November 20 for the 2008 base-year and the 2030 future-year at Anaheim. The components are primary organic matter (primary OM), anthropogenic secondary organic aerosol (anthropogenic SOA), biogenic secondary organic aerosol (biogenic SOA), elemental carbon (EC), ammonium nitrate (AmNit), ammonium sulfate (AmSul), unidentified PM2.5 (unid PM2.5) and course mass (Stewart, 2017).

Figures 8-12 and 8-13 show plots of the composition of CMAQ simulated PM for November 20, 2008, a day with high measured $PM_{2.5}$ mass concentrations. These plots are made from simulations of the 2008 base case where the ROG emissions were varied and simulations of the 2030 future-year cases where the NO_x emissions were varied. Figure 8-12 shows the simulated PM composition at three sites in the Western basin and Figure 8-13 shows the simulated PM composition at three sites in the Eastern basin. Note that the axis for the composition is logarithmic in base ten. The particulate ammonium nitrate (AmNit) concentration was estimated from the sum of CMAQ Aitken and accumulation mode aerosol nitrate, assuming it had all converted to NH_4NO_3 for the sensitivity simulations. Particulate ammonium sulfate (AmSul) was estimated from the sum of CMAQ simulated Aitken and accumulation mode aerosol sulfate, assuming it had all converted to $(NH_4)_2SO_4$.

At the Western Los Angeles site the two largest components of PM are organic mass (OM) and coarse mass, Figure 8-12. OM and coarse mass are due to primary emissions. Other primary emissions with high concentrations at this site include unidentified (unid) $PM_{2.5}$ and elemental carbon (EC). It is not expected that NO_x and ROG emission inventories greatly affect the concentrations of primary emitted species. Figure 8-12 confirms that the concentrations of these primary species are not strong functions of the NO_x and ROG emissions.

NO_x and ROG emissions should affect the concentrations of the secondary PM that is formed in the atmosphere and these PM components are the focus of this project. At the Western Los Angeles site the largest component of secondary PM is ammonium nitrate (AmNit), Figure 8-12. The ammonium nitrate concentration is directly related to the ROG emissions inventory, increasing with increasing ROG emissions at Los Angeles.

The ammonium nitrate concentration's relationship to NO_x emissions is more complicated, Figure 8-12. For the 2030 future-year at Los Angeles the ammonium nitrate concentrations are greatest for the projected NO_x emission inventory (N'1). Increasing the NO_x emissions to near those in 2008 (case N'2.5 with the projected 2030 NO_x emissions inventory multiplied by a factor of 2.50) decrease ammonium nitrate concentrations relative to the N'1 case. Further reductions in the NO_x emissions from the N'1 case reduce the ammonium nitrate concentration until it returns to a level near the concentration that was found for the N'2.5 case.

The simulated concentrations of ammonium sulfate (AmSul) are lower than ammonium nitrate at the Los Angeles site. Although ammonium sulfate is secondary PM, its concentration shows almost no relationship to the differences between NO_x and ROG emission inventories, Figure 8-12. It appears that the production of sulfate is not affected strongly by the concentrations of NO_x and ROG in the SoCAB and apparently the available ammonia does not limit the production of ammonium sulfate from sulfate.

The concentrations of anthropogenic secondary organic aerosol (SOA) and biogenic SOA are lower than the concentrations of ammonium nitrate by at least a factor of ten. The concentrations of anthropogenic SOA and biogenic SOA both increase with increases in the ROG emissions. Anthropogenic SOA and biogenic SOA concentrations ***increase*** with ***decreasing NO_x emissions*** at Los Angeles, Figure 8-12.

The behavior of these aerosol components in the western basin is very similar at the other sites with minor variations. The primary aerosol species, primary OM, coarse mass, unid $PM_{2.5}$ and EC have higher concentrations than anthropogenic SOA and biogenic SOA. The relative concentrations of primary OM, coarse mass, unid $PM_{2.5}$ and EC vary somewhat between the sites but they are not affected by the NO_x and ROG emissions inventory.

At the other sites, ammonium nitrate PM may have comparable or greater (at Anaheim) concentrations when compared to the primary emitted PM species. At the other sites the ammonium nitrate concentrations show the same relationship to the NO_x and ROG emissions as found for Los Angeles. Increased ROG emissions increase the concentrations of ammonium nitrate. Decreasing NO_x emissions from near 2008 levels (N'2.5) increase ammonium nitrate concentrations until the projected NO_x emissions inventory for the 2030 future-year is reached (N'1). Additional decreases in the NO_x emissions inventory reduce ammonium concentrations but they remain higher for the N'.75 and N'.5 cases. For the N'.3 case ammonium nitrate concentrations become similar to those obtained for the N'2.5 case with near 2008 NO_x emission levels.

The concentrations of AmSul, anthropogenic SOA and biogenic SOA and the concentrations of these secondary PM species showed similar behavior to changes in the NO_x and ROG emissions as was found for the Los Angeles sites.

There are no major concentration differences between the Western and Eastern basins, Figures 8-12 and 8-13. In both the Western and Eastern basins the primary emissions of coarse mass and the primary organic mass have the greatest total contribution to PM. The most important secondary contributing species to PM is ammonium nitrate and the second most important secondary contributing species to PM is ammonium sulfate. Ammonium nitrate has a strong and complicated and non-intuitive relationship to NO_x and ROG emissions. Ammonium sulfate concentrations were found to be independent of the NO_x and ROG emissions. Anthropogenic secondary organic aerosol and the biogenic secondary aerosol concentrations are the lowest across the six stations but the concentrations of SOA increase with increased ROG emissions and the concentrations of SOA increase with decreasing NO_x emissions at all the sites, Figures 8-12 and 8-13.

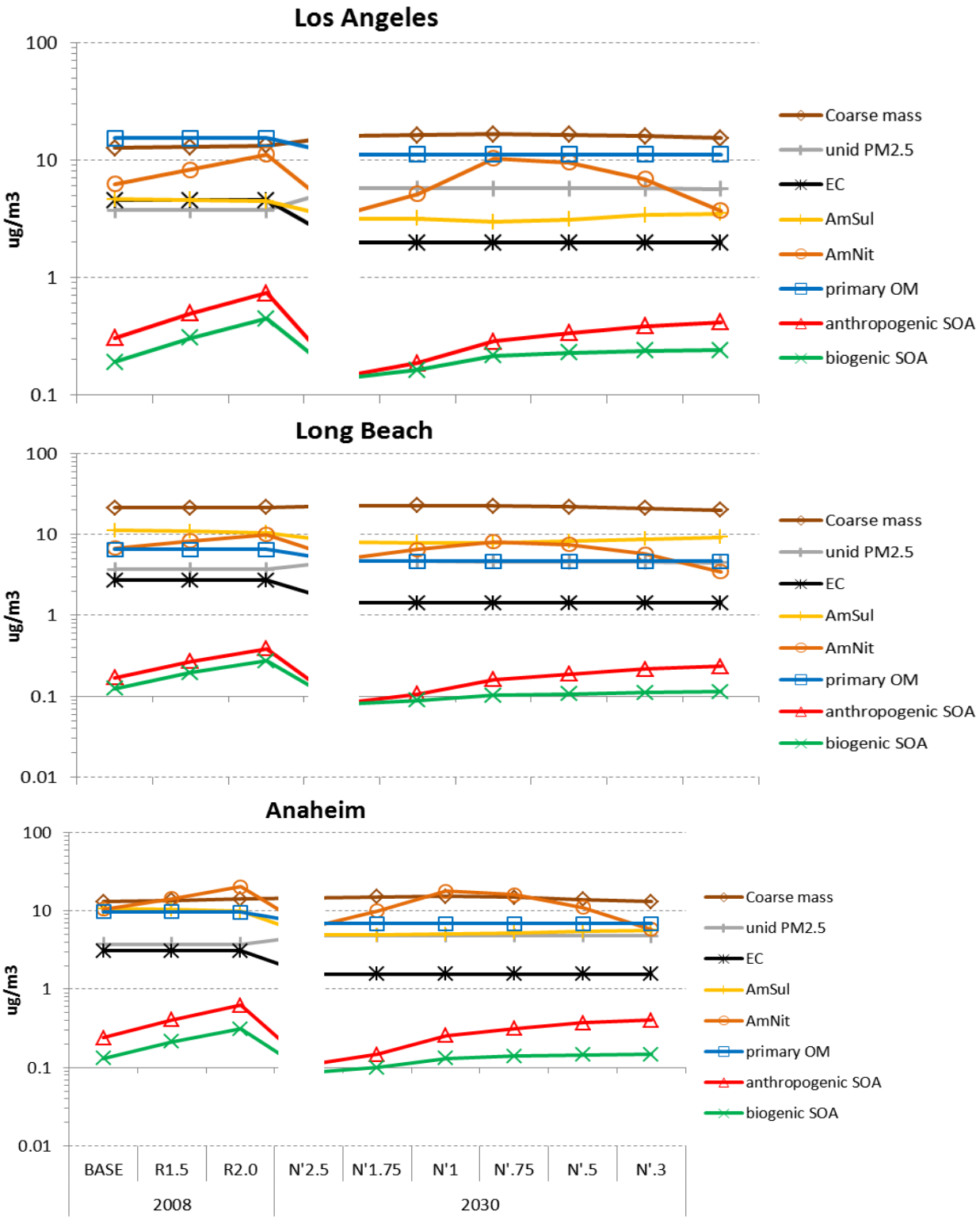

Figure 8-12. Simulated PM composition at 3 sites in the Western basin under varying emissions scenarios on a day with high measured $PM_{2.5}$ mass concentration (November 20, 2008).

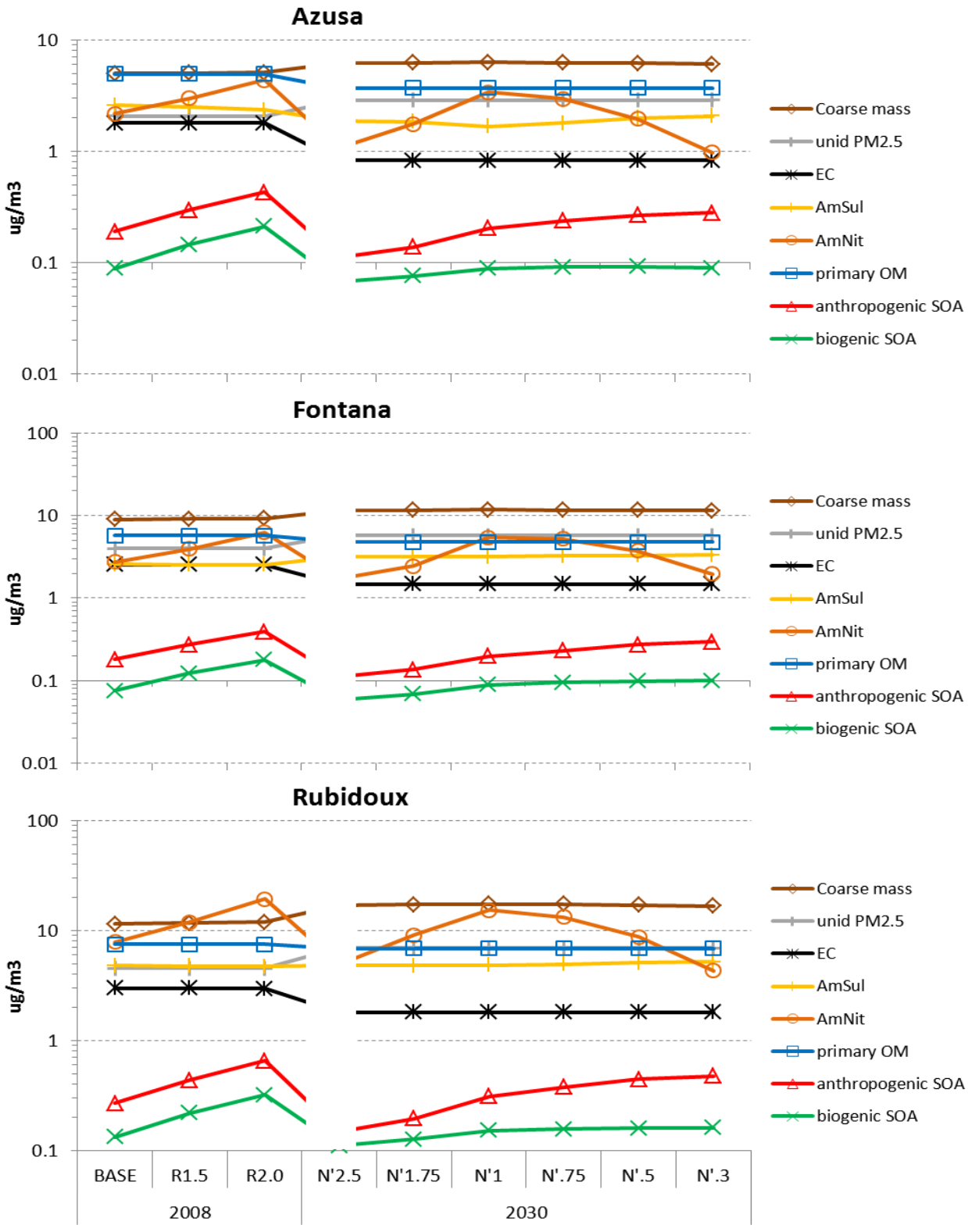

Figure 8-13. Simulated PM composition at 3 sites in the Eastern basin under varying emissions scenarios on a day with high measured $PM_{2.5}$ mass concentration (November 20, 2008).

8.5 Changes in Primary PM Emitted Species: Organic Mass, Coarse Mass, Unidentified $PM_{2.5}$ and Elemental Carbon Due to Changes in NO_x and ROG Emissions for Base and Future-Years

Figure 8-14 shows a comparison of measured, simulated 2008 base-year and simulated 2030 future-year 24-hr average organic mass concentration at two sites during the ozone season. Measurements were available for only a few of those days. CMAQ under-predicts the 24-hr average organic mass concentration for the 2008 base-year at both Rubidoux and Los Angeles. Some of this difference is likely to be due to the 4th of July holiday and the emissions inventory and not CMAQ performance. Rubidoux is predicted to have an increase and Los Angeles is predicted to have a decrease in the 24-hr average organic mass concentration with the 2030 future-year inventory.

Observed CMAQ simulated concentrations of 24-hr average elemental carbon mass concentrations are shown in Figure 8-15. CMAQ performance appears to be better for 4-hr average elemental carbon mass concentrations than it was for 24-hr average organic mass concentration. The elemental carbon mass concentrations are forecasted to be lower in the 2030 future-year at both sites.

The maximum and average 24-hour primary organic mass concentrations for the 2008 base-year and the 2030 future-year are shown in Figure 8-16. As expected, variations in NO_x and ROG emissions do not affect the primary organic mass concentrations.

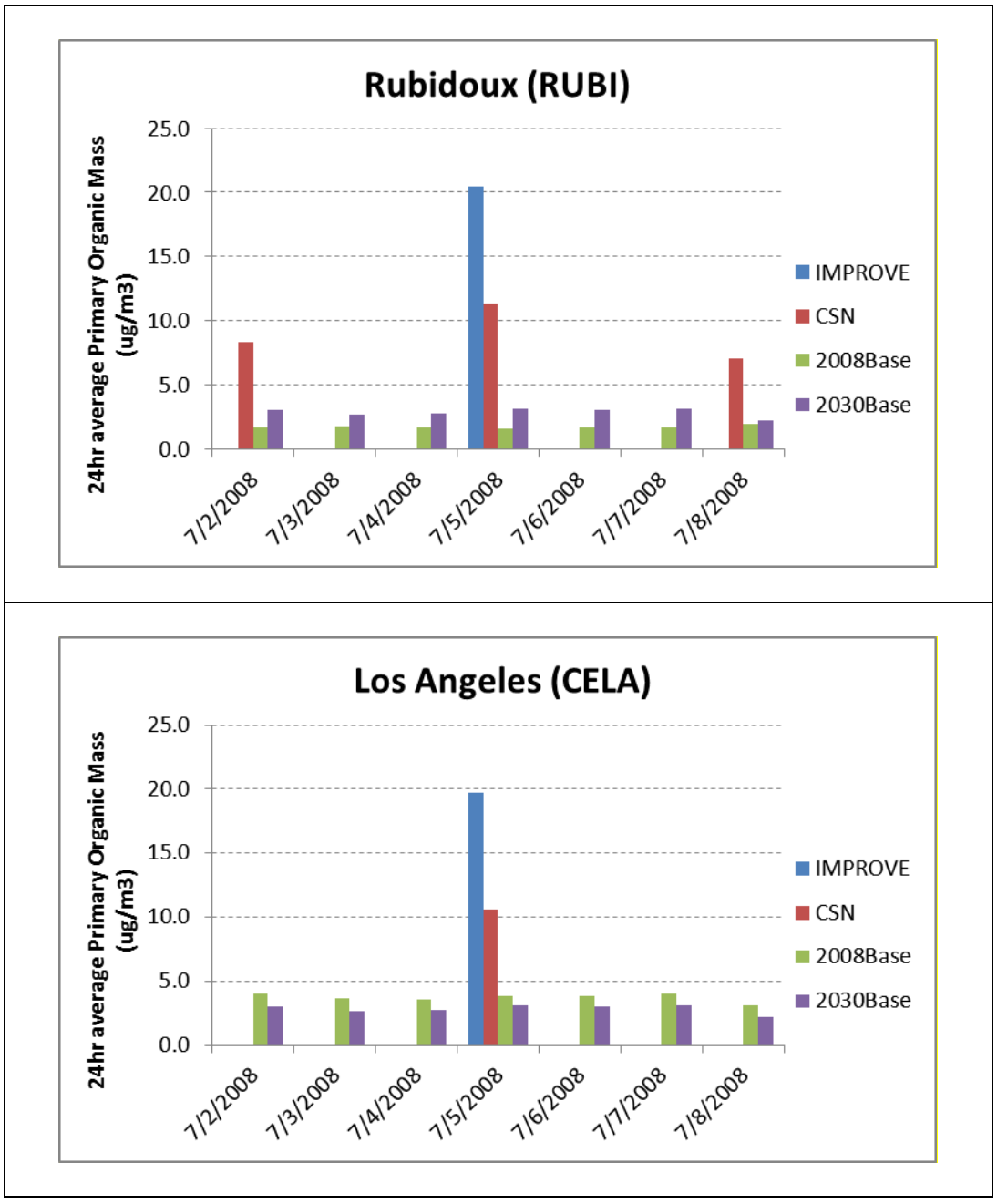

Figure 8-14. Comparison of measured (July 2, 2008, July 5, 2008 and July 8, 2008 only for RUBI and July 5, 2008 only for CELA), and simulated 2008 base-year and simulated 2030 future-year 24-hr average primary organic mass concentrations at two sites. Measurements made using both the IMPROVE and CSN protocols are shown, and measured OC has been multiplied by 1.4 to convert to organic mass. CMAQ estimates are the average of primary organic particle mass concentrations for the 9 grid cells surrounding the indicated sites.

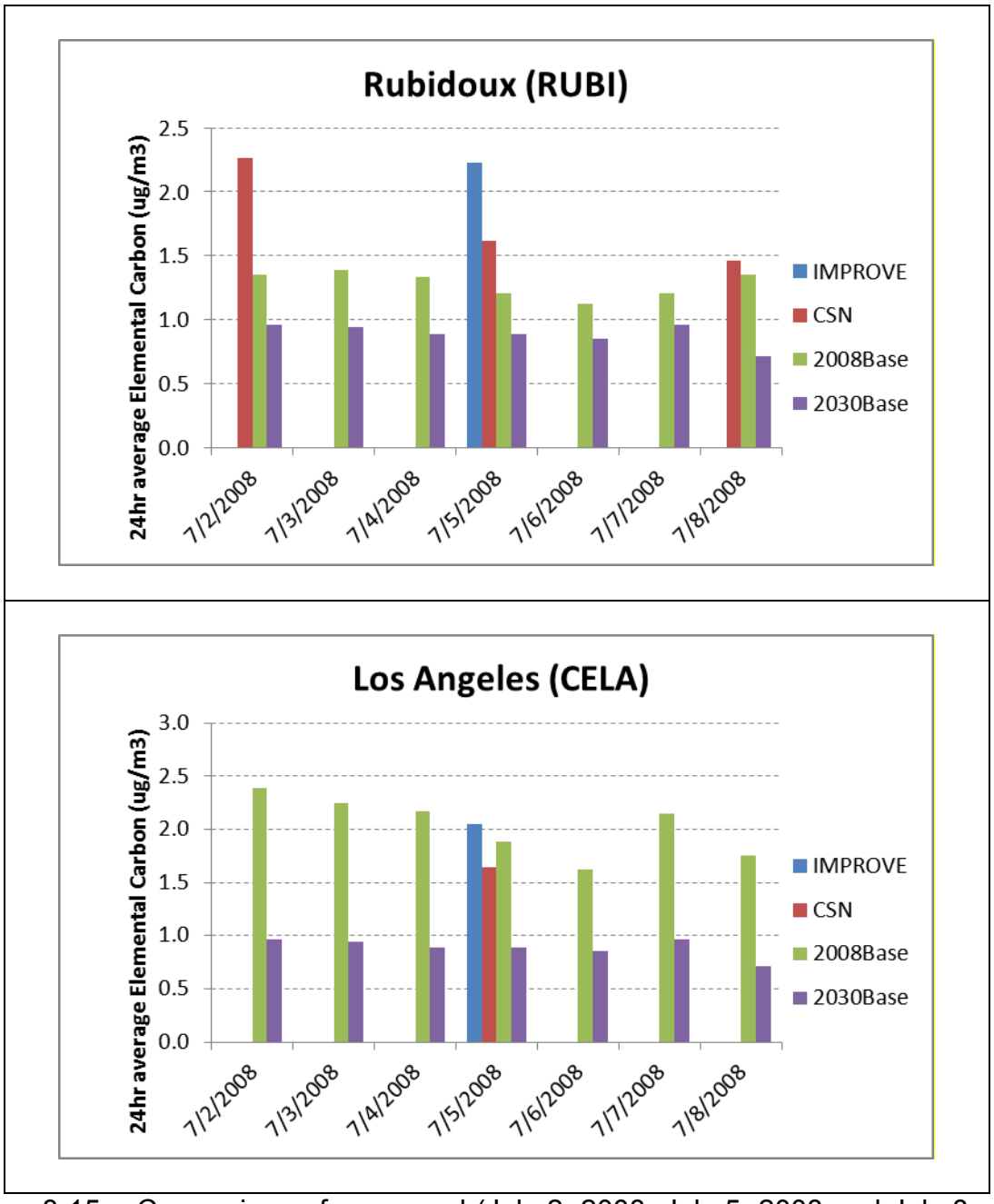

Figure 8-15. Comparison of measured (July 2, 2008, July 5, 2008 and July 8, 2008 only for RUBI and July 5, 2008 only for CELA), 2008 base-year simulated and simulated 2030 future-year 24-hr average elemental carbon mass concentrations at two sites. Measurements made using both the IMPROVE and CSN protocols are shown. CMAQ estimates are the average elemental carbon mass concentrations for the 9 grid cells surrounding the indicated sites.

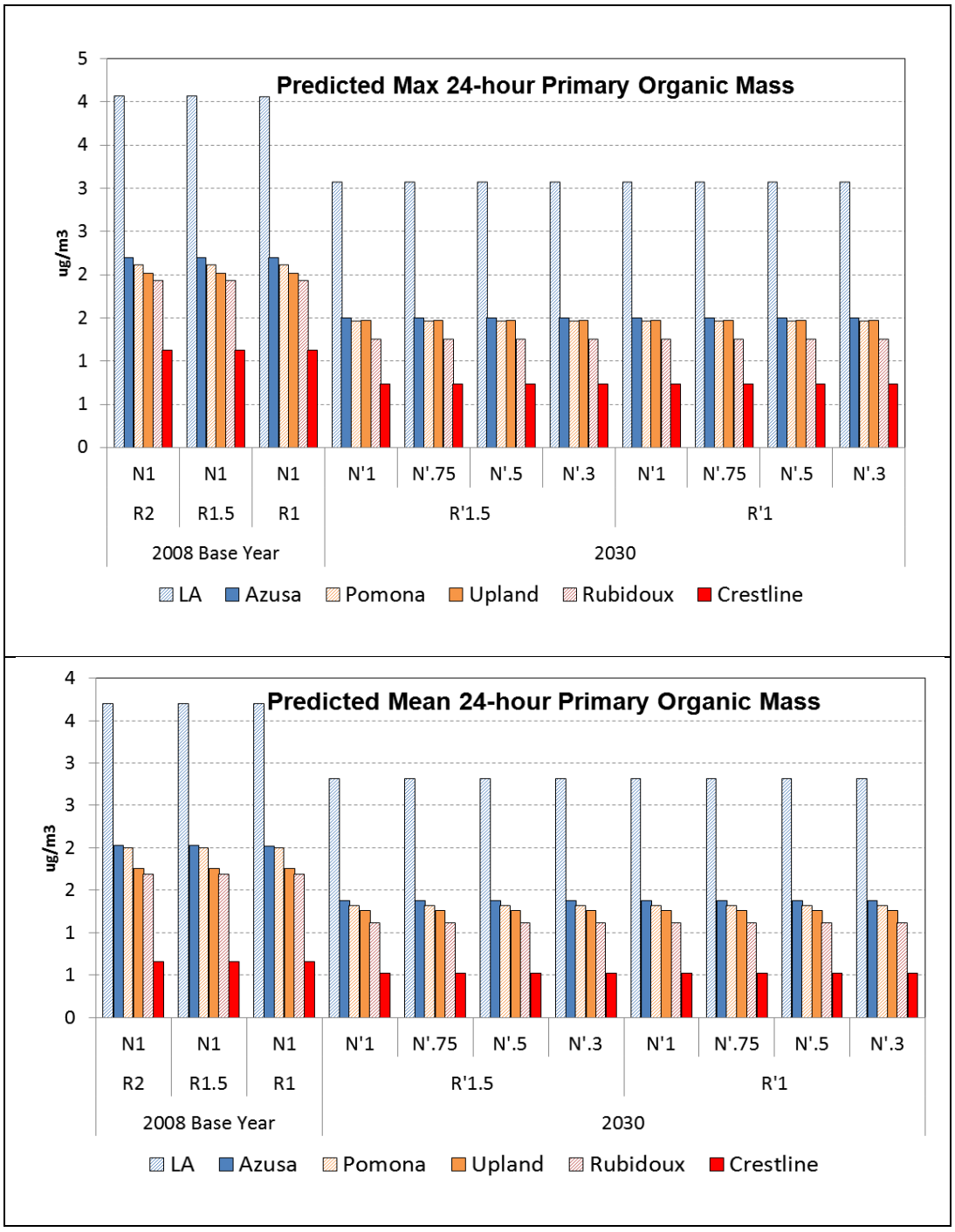

Figure 8-16. Simulated 2008 base-year and 2030 future-year maximum and average 24-hour primary organic mass concentrations ($\mu g\ m^{-3}$) for the July 2-8 episode. Basin-wide NO_x and ROG emissions (tons per day) are shown above the adjustment factors applied to the 2008 base-year ROG (R) and NO_x (N) emissions and 2030 baseline ROG (R) and NO_x (N) emissions.

The daily average coarse aerosol mass concentrations are only slightly affected by changes in ROG emissions for the base-year, Figure 8-17. For the future-year the daily average coarse aerosol mass concentrations are higher at Rubidoux. At the other sites the daily average coarse aerosol mass concentrations show a slight dependence on the NO_x emissions and tend to decrease with lower NO_x emissions.

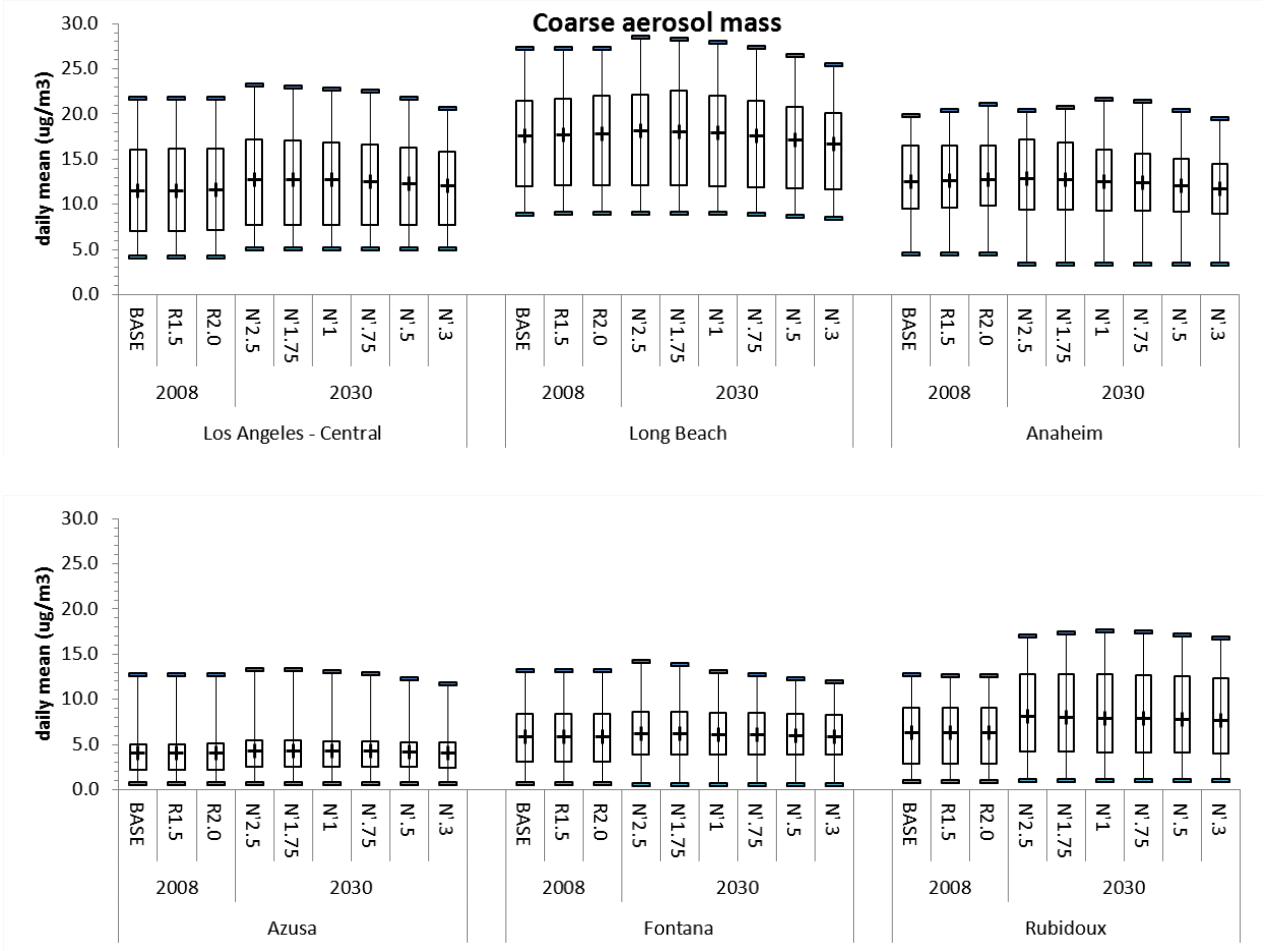

Figure 8-17. Range of simulated daily average coarse aerosol mass concentrations at six monitoring sites in the SoCAB. The adjustments to ROG emissions were made for 2008 and the adjustments to NO_x emissions were made for 2030. The box & whisker plots indicate the minimum, 1st and 3rd quantile, maximum, and mean (+) values during two high $PM_{2.5}$ episodes, September 12-15 and November 11-24.

The daily average total $PM_{2.5}$ organic mass concentrations showed a slight increase with increases in basin-wide ROG emissions for the base-year, Figure 8-18. The projected reductions in emissions reduce the total $PM_{2.5}$ organic mass concentrations for the 2030 future-year but variations in the future-year NO_x emissions have little effect on these concentrations. Figure 8-19 shows that the behavior of the daily average total elemental carbon concentrations is similar to the behavior of the daily average total $PM_{2.5}$ organic mass concentrations There is much more of a simple step function between the base-year and future-year daily average total elemental carbon concentrations.

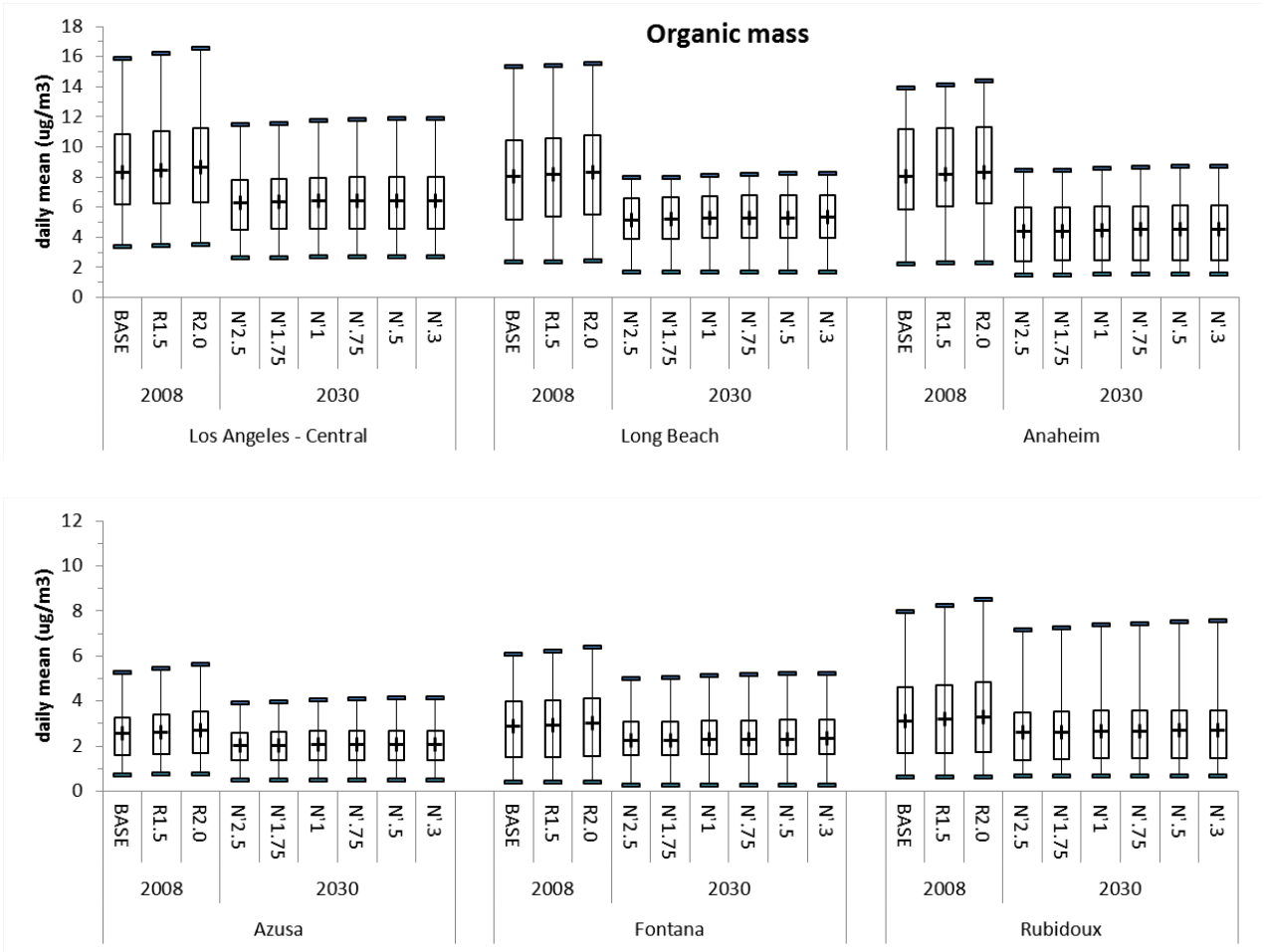

Figure 8-18. Range of simulated daily average total $PM_{2.5}$ organic mass concentrations at six monitoring sites in the SoCAB. The adjustments to ROG emissions were made for 2008 and the adjustments to NO_x emissions were made for 2030. The box & whisker plots indicate the minimum, 1st and 3rd quantile, maximum, and mean (+) values during two high $PM_{2.5}$ episodes, September 12-15 and November 11-24.

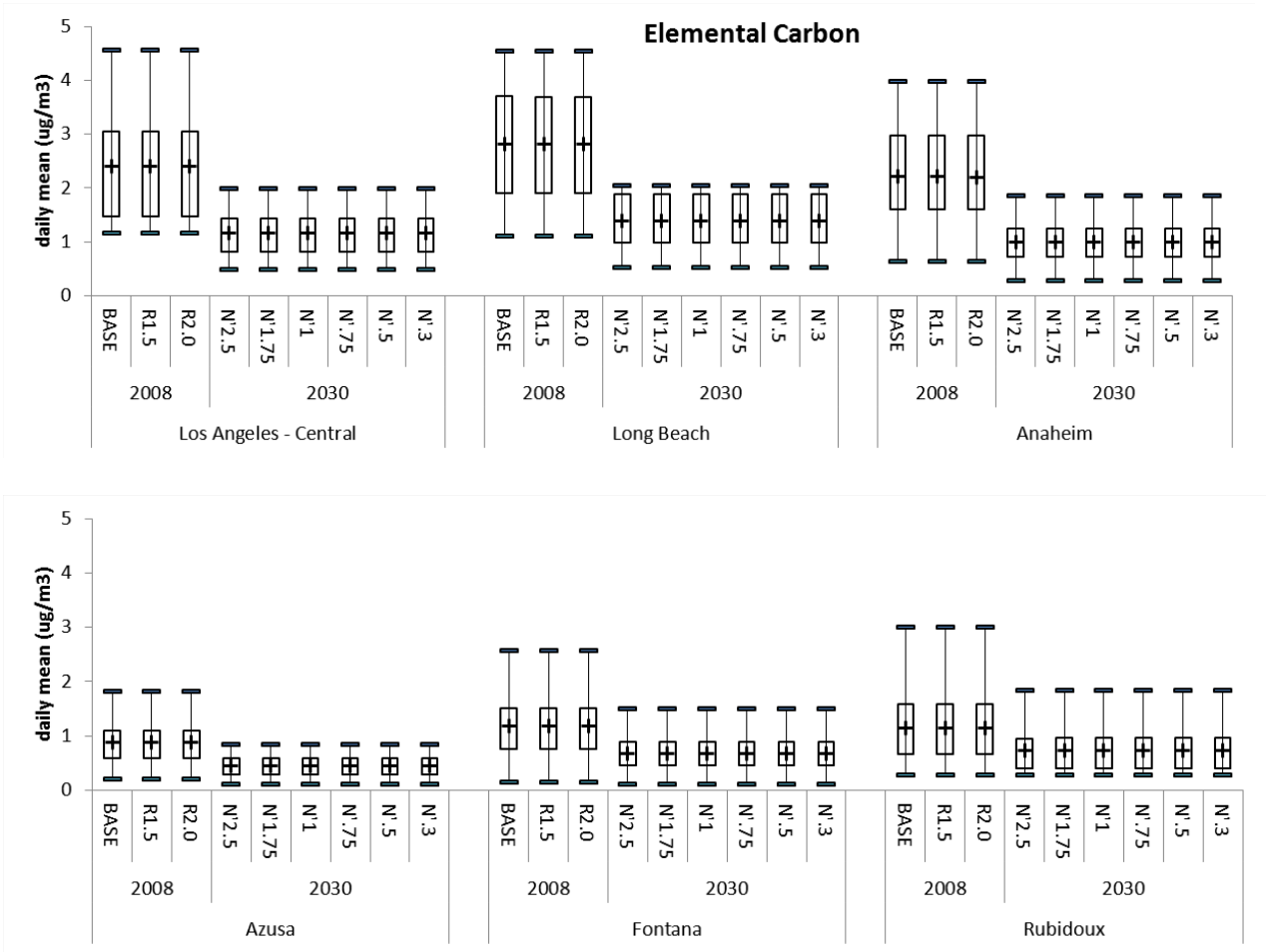

Figure 8-19. Range of simulated daily average total elemental carbon concentrations at six monitoring sites in the SoCAB. The adjustments to ROG emissions were made for 2008 and the adjustments to NO_x emissions were made for 2030. The box & whisker plots indicate the minimum, 1st and 3rd quantile, maximum, and mean (+) values during two high $PM_{2.5}$ episodes, September 12-15 and November 11-24.

8.6 Changes in Secondary PM Species: Ammonium Nitrate and Ammonium Sulfate Due to Changes in NO_x and ROG Emissions for Base and Future-Years

Particulate nitrate was extracted from the base and sensitivity simulations made for the CRC-91 project. Figure 8-20 shows the mean of observed and simulated aerosol nitrate for the June 15-20 episode. There are particulate nitrate measurements for LA and Rubidoux, only. The response of the simulated particulate nitrate aerosol concentrations to changes in the ROG concentrations is not strong. The measured particulate nitrate at the LA site is

greater than the simulated while at the measured particulate nitrate at Rubidoux are lower for all three levels of ROG emission.

Figures 8-21 through 8-25 show the simulated 2008 base-year and 2030 future-year, maximum 24-hour, mean 1-hour, mean 8-hour, maximum 1-hour and maximum 8-hour particulate nitrate concentrations. These five figures are very similar. With current NO_x emissions (N1; 723 tons per day) changes in ROG emissions have little effect on particulate nitrate concentrations at all sites. With the NO_x reduced (N'1, 284 tons per day) there is a strong effect on particulate nitrate concentrations at all sites. Further reductions in NO_x emissions reduce particulate nitrate concentrations while reductions in ROG emissions do not.

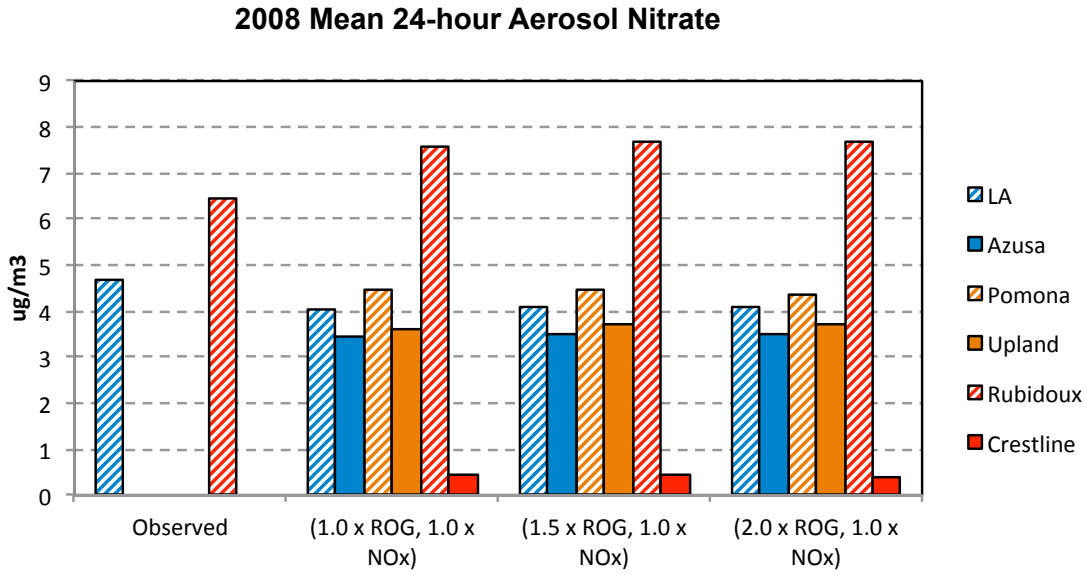

Figure 8-20. Mean of observed and simulated mean 24-hr maximum aerosol nitrate for the June 15-20 episode with 1.0, 1.5 and 2.0 times 2008 base ROG. Values are for the nine cells (12 × 12 km) containing the SoCAB air quality monitoring stations.

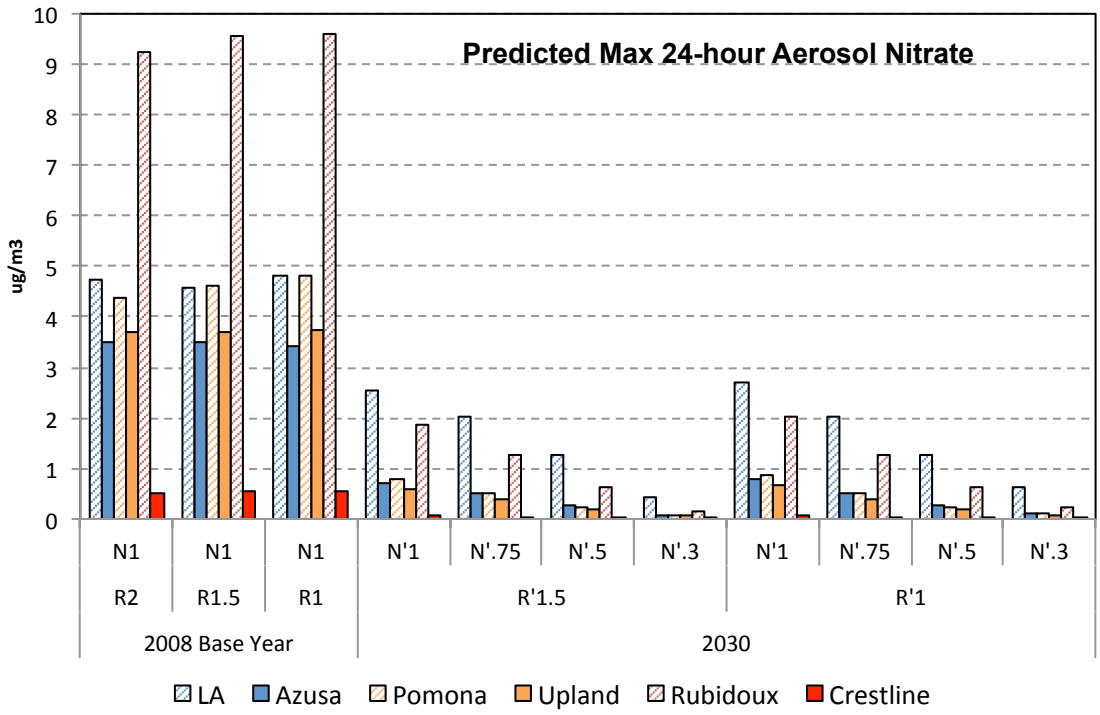

Figure 8-21. Simulated 2008 base-year and 2030 future-year maximum 24-hour aerosol nitrate concentrations (μg m^{-3}) for the July 2-8 episode. The x-axis shows the basin-wide NO_x and ROG emissions adjustment factors applied to the 2008 base-year NO_x (N) and ROG (R) emissions and 2030 baseline NO_x (N') and ROG (R') emissions.

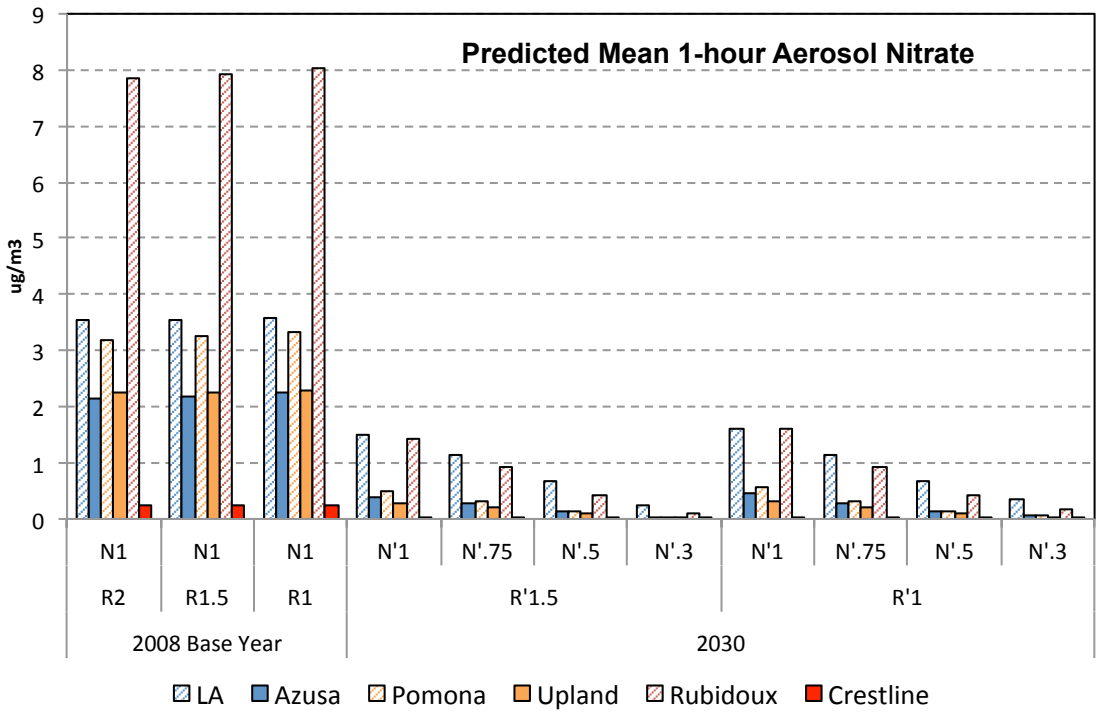

Figure 8-22. Simulated 2008 base-year and 2030 future-year mean 1-hour aerosol nitrate concentrations (μg m^{-3}) for the July 2-8 episode. The x-axis shows the basin-wide NO_x and ROG emissions adjustment factors applied to the 2008 base-year NO_x (N) and ROG (R) emissions and 2030 baseline NO_x (N') and ROG (R') emissions.

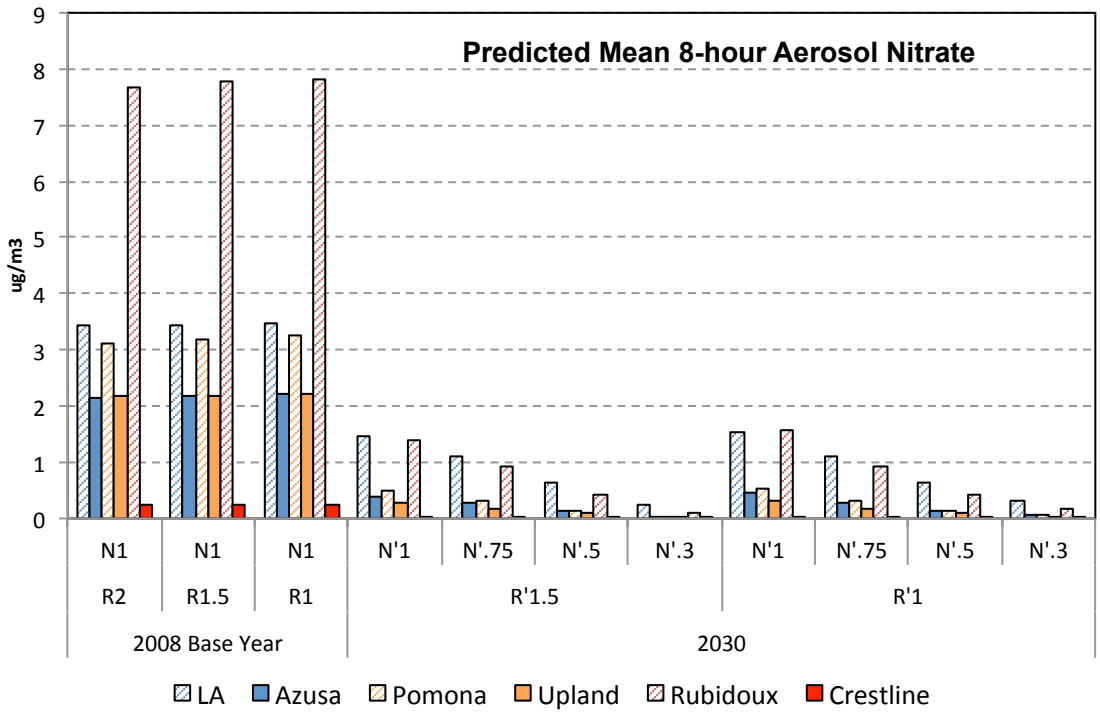

Figure 8-23. Simulated 2008 base-year and 2030 future-year mean 8-hour aerosol nitrate concentrations (μg m^{-3}) for the July 2-8 episode. The x-axis shows the basin-wide NO_x and ROG emissions adjustment factors applied to the 2008 base-year NO_x (N) and ROG (R) emissions and 2030 baseline NO_x (N') and ROG (R') emissions.

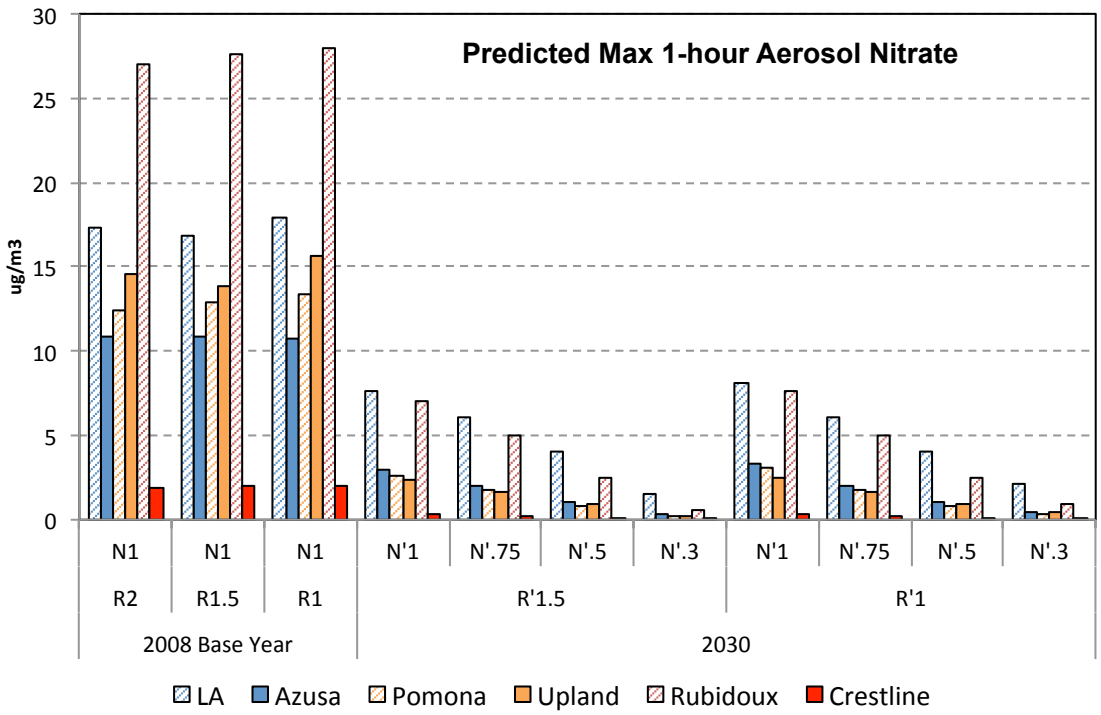

Figure 8-24. Simulated 2008 base-year and 2030 future-year maximum 1-hour aerosol nitrate concentrations (μg m^{-3}) for the July 2-8 episode. The x-axis shows the basin-wide NO_x and ROG emissions adjustment factors applied to the 2008 base-year NO_x (N) and ROG (R) emissions and 2030 baseline NO_x (N') and ROG (R') emissions.

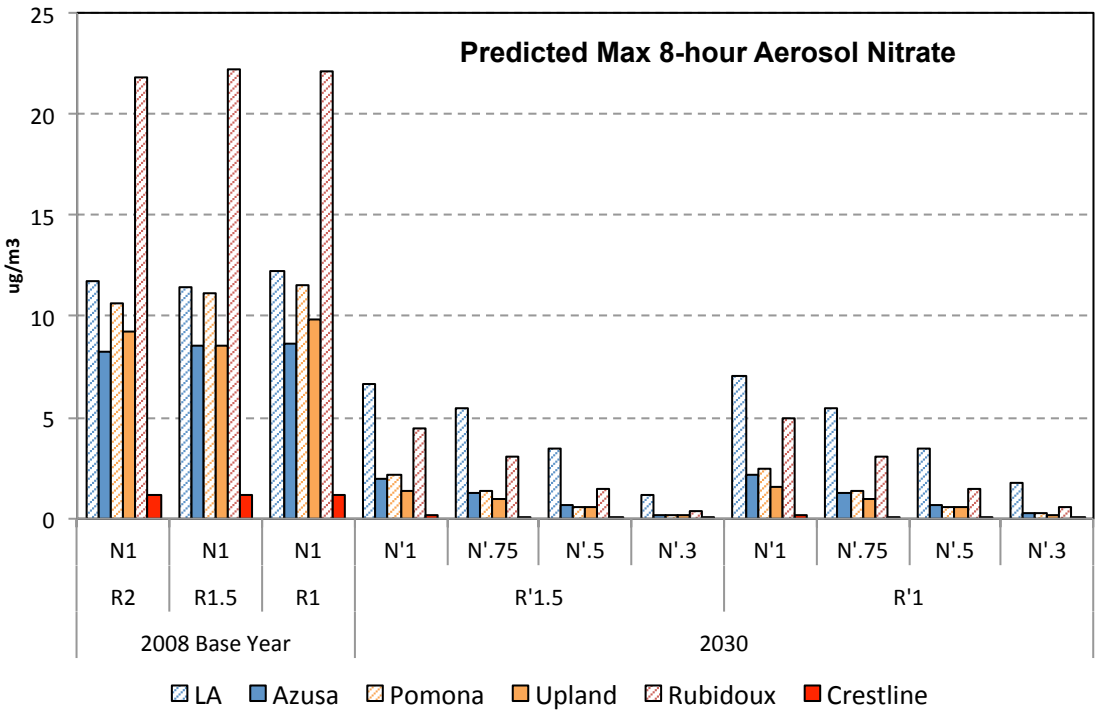

Figure 8-25. Simulated 2008 base-year and 2030 future-year maximum 8-hour aerosol nitrate concentrations (μg m^{-3}) for the July 2-8 episode. The x-axis shows the basin-wide NO_x and ROG emissions adjustment factors applied to the 2008 base-year NO_x (N) and ROG (R) emissions and 2030 baseline NO_x (N') and ROG (R') emissions.

The particulate ammonium nitrate concentration was estimated from the sum of CMAQ Aitken and accumulation mode aerosol nitrate, assuming it had all converted to NH_4NO_3 for the sensitivity simulations. Figure 8-26 shows the range of simulated daily average total ammonium nitrate mass concentrations during the two modeled PM episodes for various adjustments to the reactive organic gas (ROG) and NO_x emissions at Los Angeles, Long Beach, Anaheim, Azusa, Fontana and Rubidoux. For the base-year 2008, the daily average ammonium nitrate concentrations increased with increases in basin-wide ROG emissions with the greatest increases at Los Angeles, Long Beach and Anaheim. For the 2030 base-year emissions cases ammonium nitrate concentrations at Los Angeles, Long Beach, Anaheim and Rubidoux sites reached a maximum near the base-case basin-wide NO_x emissions and at these sites either higher or lower NO_x emissions tend to produce lower ammonium nitrate concentrations. Lower NO_x emissions at Azusa and Fontana uniformly lead to lower ammonium nitrate concentrations.

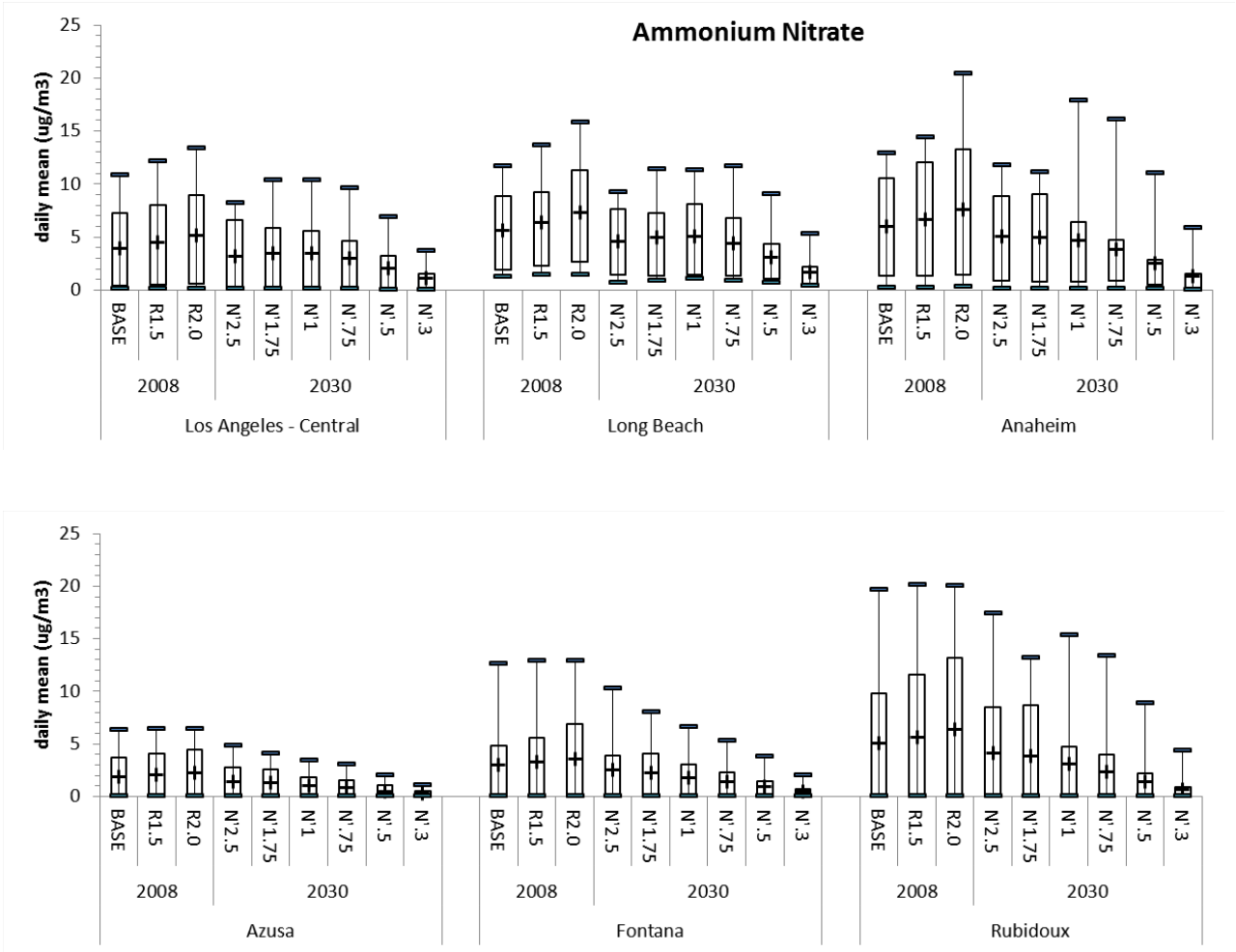

Figure 8-26. Range of simulated daily average total ammonium nitrate mass concentrations for various adjustments to ROG and NO_x emissions at six monitoring sites in the SoCAB. The adjustments to ROG emissions were made for 2008 and the adjustments to NO_x emissions were made for 2030. The box & whisker plots indicate the minimum, 1st and 3rd quantile, maximum, and mean (+) values during two high $PM_{2.5}$ episodes, September 12-15 and November 11-24. Ammonium nitrate was estimated from the sum of Aitken and accumulation mode aerosol nitrate, assuming it had all converted to NH_4NO_3.

Figure 8-27 shows a comparison of measured and simulated 24-hr average aerosol sulfate mass concentrations at two sites during the ozone season. The CMAQ simulated concentrations for 24-hr average aerosol sulfate mass were much lower than observations; possibly this is due to the holiday or an underestimation of the emissions of sulfur containing compounds. Comparison of the 2008 base-year 24-hr average aerosol sulfate with the 2030 forecasted values shows that the sulfate aerosol is expected to be lower by year 2030.

Figure 8-28 shows simulated maximum and average 24-hour aerosol sulfate concentrations for the 2008 base-year and the 2030 future-year. Variations in ROG and NO_x emissions show almost no effect on the sulfate aerosol concentrations.

Particulate ammonium sulfate was estimated from the sum of CMAQ simulated Aitken and accumulation mode aerosol sulfate, assuming it had all converted to $(NH_4)_2SO_4$, Figure 8-29. The daily average total ammonium sulfate mass concentrations were not strongly affected by the basin-wide ROG emissions for the base-year simulations. Relative to the 2008 base-year, the daily average total ammonium sulfate mass concentrations were substantially lower at Los Angeles, Long Beach and Anaheim, a little lower at Azusa and Fontana, and unchanged at Rubidoux for the 2030 future-year.

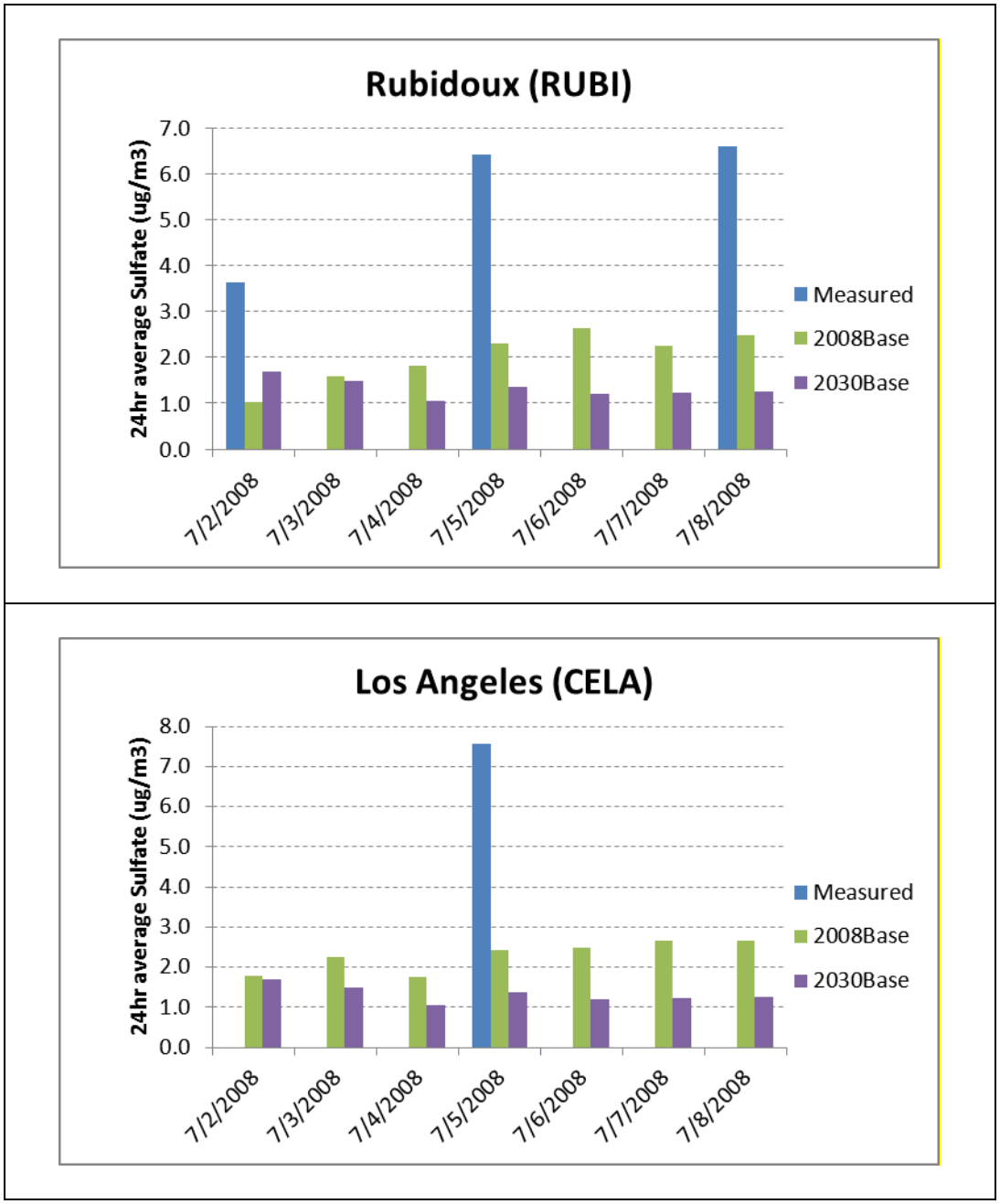

Figure 8-27. Comparison of measured (July 2, 2008, July 5, 2008, July 8, 2008 only for RUBI and July 5, 2008 only for CELA), 2008 base-year simulated and 2030 future-year 24-hr average aerosol sulfate mass concentrations at two sites. CMAQ estimates are the average $PM_{2.5}$ aerosol sulfate mass concentrations for the 9 grid cells surrounding the indicated sites.

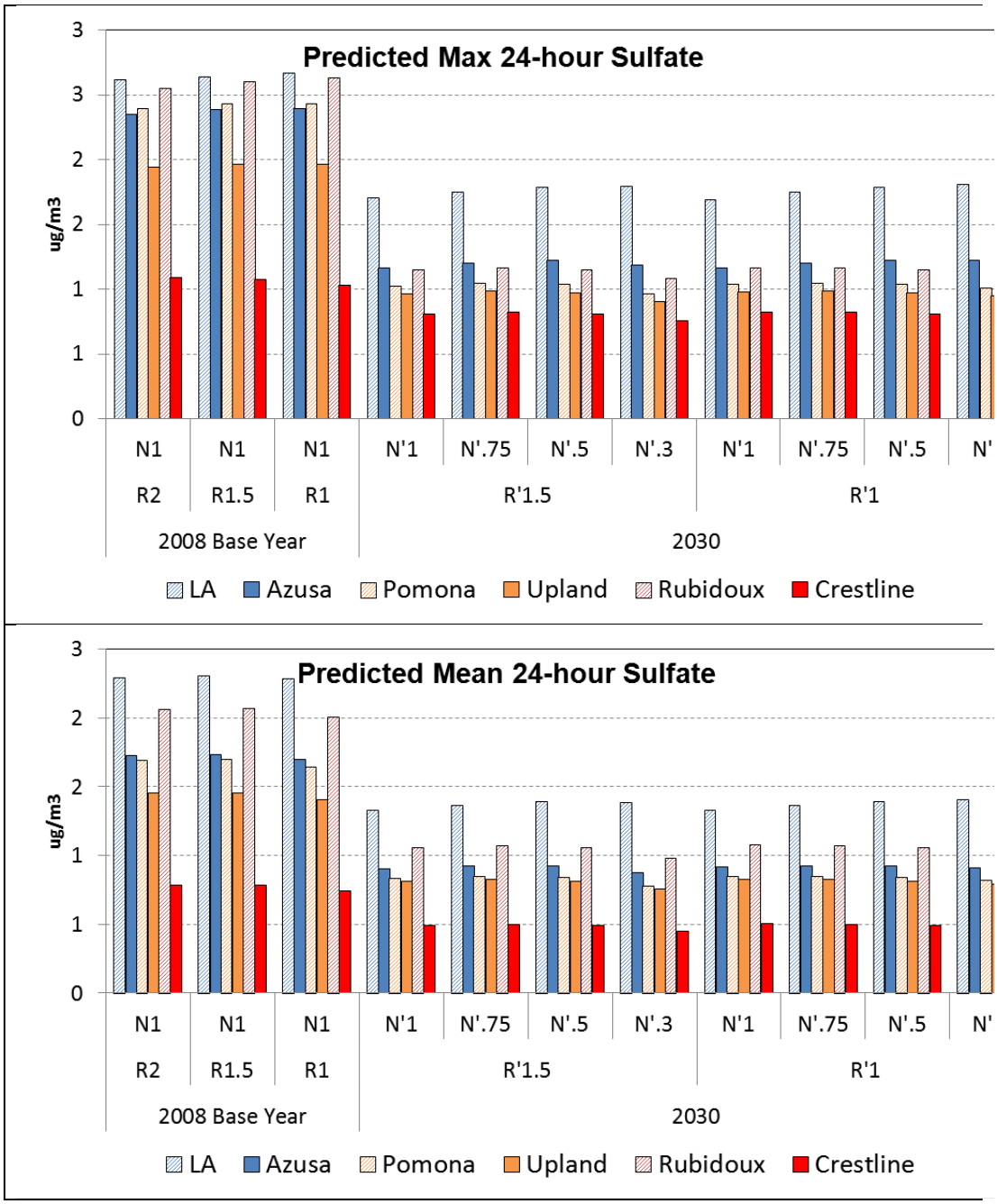

Figure 8-28. Simulated 2008 base-year and 2030 future-year maximum and average 24-hour aerosol sulfate concentrations (μg m^{-3}) for the July 2-8 episode. The x-axis shows the basin-wide NO_x and ROG emissions adjustment factors applied to the 2008 base-year NO_x (N) and ROG (R) emissions and 2030 baseline NO_x (N') and ROG (R') emissions.

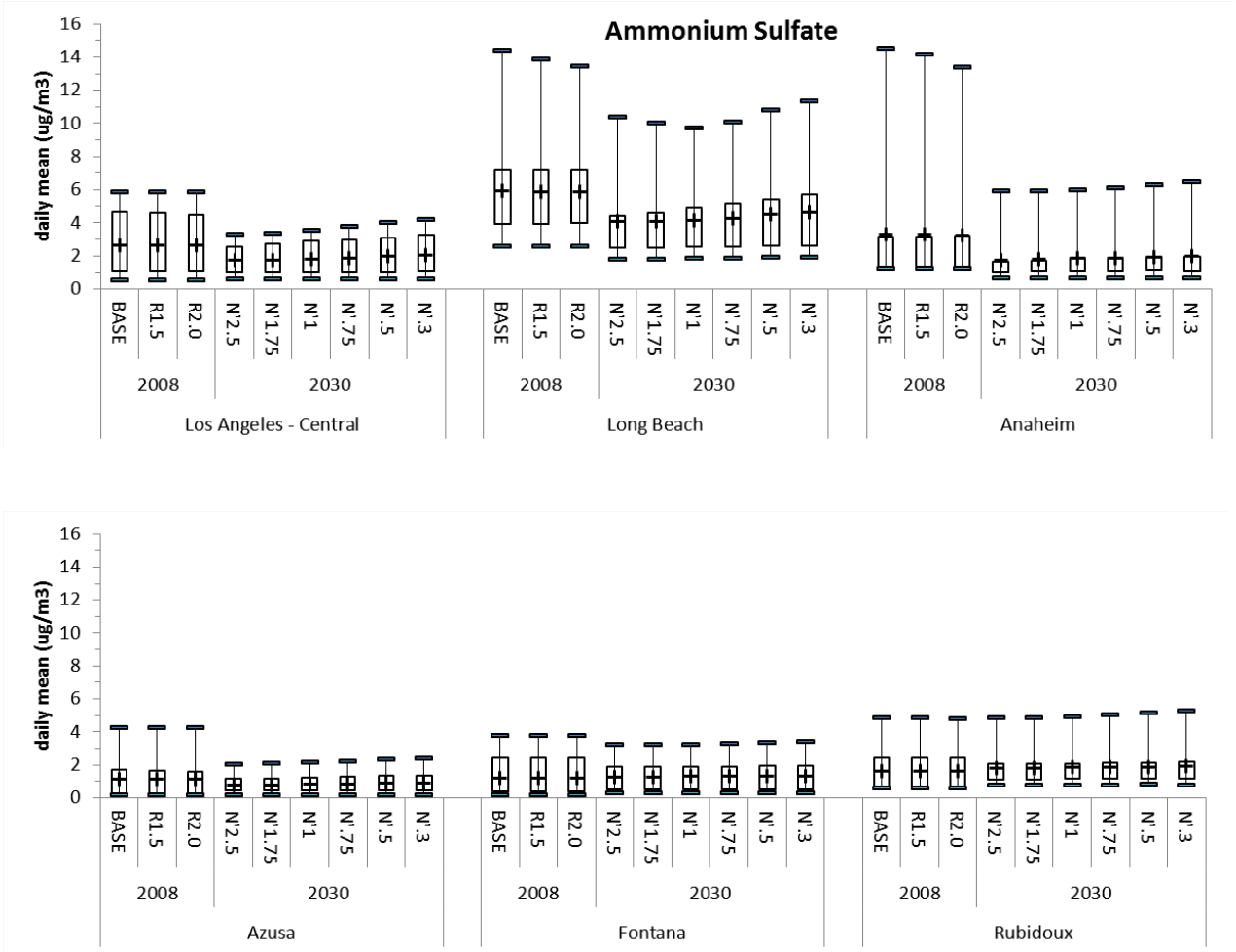

Figure 8-29. Range of simulated daily average total ammonium sulfate mass concentrations for various adjustments to ROG and NO_x emissions at six monitoring sites in the SoCAB. The adjustments to ROG emissions were made for 2008 and the adjustments to NO_x emissions were made for 2030. The box & whisker plots indicate the minimum, 1st and 3rd quantile, maximum, and mean (+) values during two high $PM_{2.5}$ episodes, September 12-15 and November 11-24. Ammonium sulfate was estimated from the sum of Aitken and accumulation mode aerosol sulfate, assuming it had all converted to $(NH_4)_2SO_4$).

8.7 Changes in Secondary PM Species: Anthropogenic Secondary Organic Aerosol and Biogenic Secondary Organic Aerosol Due to Changes in NO_x and ROG Emissions for Base and Future-Years

The daily average secondary organic aerosol concentrations show a strong positive dependence on the basin-wide ROG emissions for the base-year at all six stations, Figure 8-30. Higher basin-wide NO_x emissions are associated with lower daily average secondary organic aerosol concentrations for the future-year. In other words Figure 8-30 shows that greater reductions in NO_x emissions lead to higher daily average secondary organic aerosol concentrations. The same pattern occurs if only anthropogenic SOA is considered, Figure 8-31.

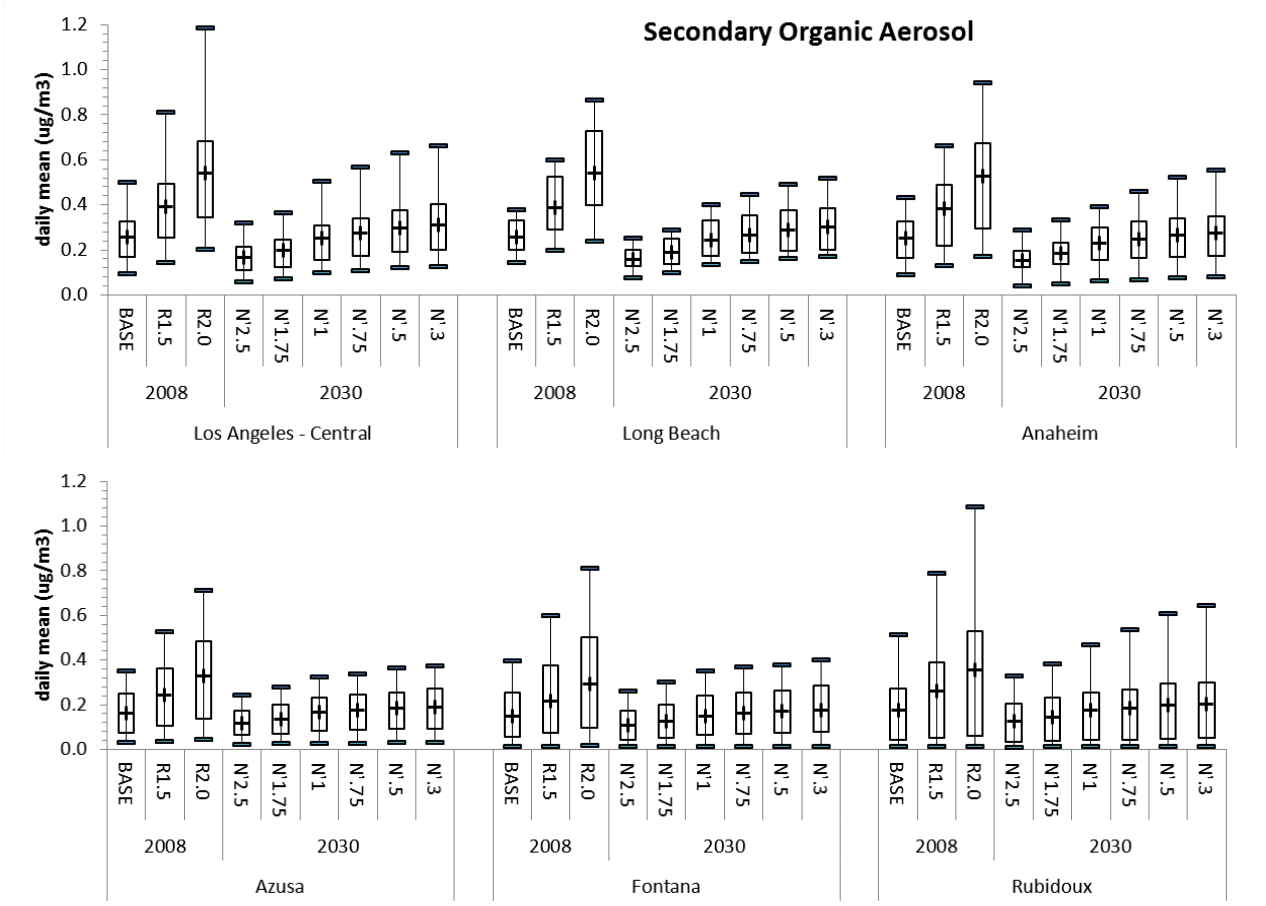

Figure 8-30. Range of simulated daily average secondary organic aerosol concentrations for various adjustments to ROG and NO_x emissions at six monitoring sites in the SoCAB. The adjustments to ROG emissions were made for 2008 and the adjustments to NO_x emissions were made for 2030. The box & whisker plots indicate the minimum, 1st and 3rd quantile, maximum, and mean (+) values during two high $PM_{2.5}$ episodes, September 12-15 and November 11-24.

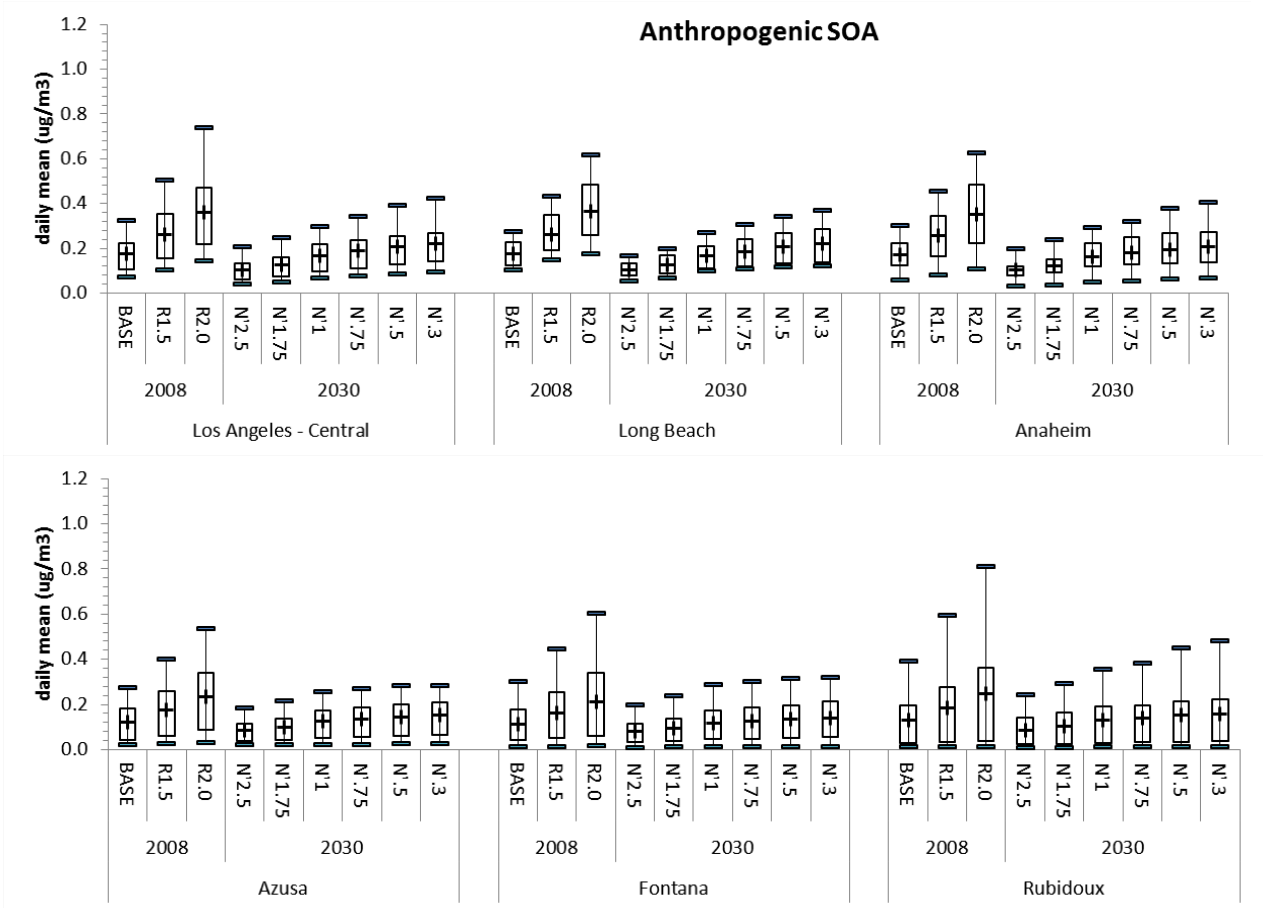

Figure 8-31. Range of simulated daily average anthropogenic secondary organic aerosol concentrations for various adjustments to ROG and NO_x emissions at six monitoring sites in the SoCAB. The adjustments to ROG emissions were made for 2008 and the adjustments to NO_x emissions were made for 2030. The box & whisker plots indicate the minimum, 1st and 3rd quantile, maximum, and mean (+) values during two high $PM_{2.5}$ episodes, September 12-15 and November 11-24.

8.8 Summary of Future-Year 2030 Sensitivity Studies

Primary PM species, elemental carbon and organic mass are not affected by changes to the NO_x and ROG emissions inventory. But coarse aerosol mass particle concentrations decrease slightly due to reductions in the NO_x emissions inventory. Ammonium nitrate particle concentrations show a strong dependence on the NO_x emissions inventory. The projected 2030 NO_x emission inventory results in lower ammonium nitrate concentrations in 2030 than in 2008. However the projected 2030 NO_x emission inventory is the least effective in reducing ammonium nitrate concentrations. Higher NO_x emissions (greater than the projected 2030 inventory) yield lower ammonium nitrate concentrations in 2030. And greater reductions in NO_x emissions from the projected NO_x emissions inventory eventually lead to reductions in ammonium nitrate concentrations. At Azusa and Fontana reductions in NO_x emissions decrease ammonium nitrate for all of the 2030 cases. Ammonium sulfate is not greatly affected by changes in the NO_x and ROG emissions inventory. Secondary organic aerosol increases with increases in the ROG emissions inventory. Decreases in NO_x emissions lead to increases in secondary organic aerosol concentrations.

9. EXAMINATION OF THE EFFECT OF CHEMISTRY ON NITRATE AEROSOL FORMATION

9.1 Chemical Box Model and SCAPE Simulations

A detailed chemical box model was used to make simulations of nitric acid concentrations for a wide range of initial NO_x and VOC concentrations under CRC Project A-91. The daily maximum HNO_3 production was calculated with the Regional Atmospheric Chemistry Mechanism, version 2 (RACM2, Goliff et al., 2013) which included detailed chemistry for HNO_3 production. The RACM2 is consistent with the SAPRC chemical mechanism used for the CMAQ modeling. The calculated nitric acid isopleth is shown in Figure 9-1. The main function of the chemical box model was to provide the links between an initial pair of NO_x and VOC concentrations and a daily maximum nitric acid concentration (Saunders, 2017).

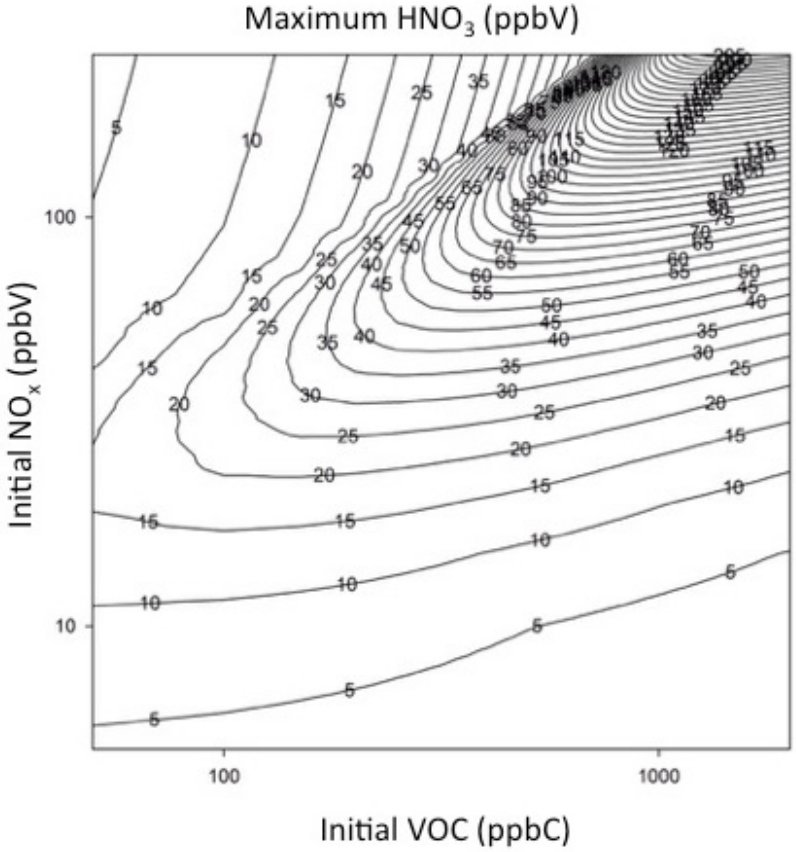

Figure 9-1. Daily maximum HNO_3 concentration as a function of initial NO_x and VOC. Simulations were made with a chemical box model employing the Regional Atmospheric Chemistry Mechanism, version 2 (Saunders, 2017).

Fujita et al. (2015) examined the trends of ROG and NO_x at several sites in the SoCAB over the years 1995-2011. The ranges of ROG and NO_x concentrations and the trends were similar among the different sites so Azusa is presented as a representative site, Figure 9-2. The projected range in ROG and NO_x concentration ranges for the future-year 2030 are shown in the figure. Notice that the average measurement points for the years 1995-2011 are lower but near the HNO_3 ridge-line but above the ozone ridge-line. This suggests that day-to-day variations in ROG and NO_x concentrations could yield daily HNO_3 production above and below the HNO_3 ridge-line. In other words current average ROG and NO_x concentrations may be near optimal for the daily production of HNO_3 at Azusa and across the SoCAB.

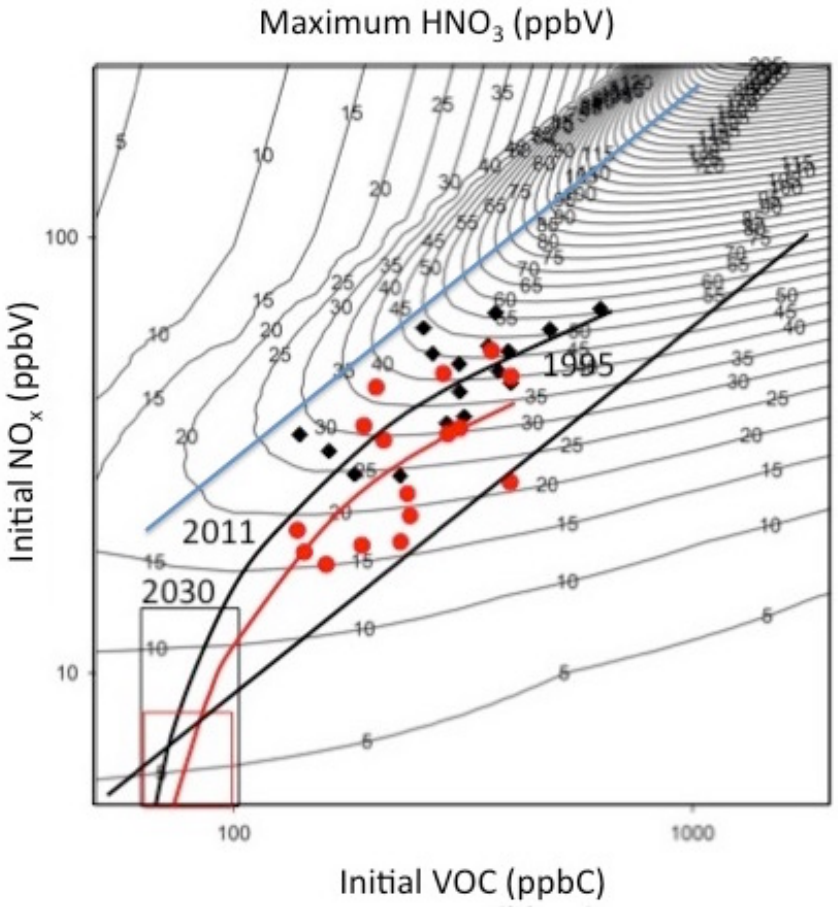

Figure 9-2. Isopleths for daily HNO_3 production at Azusa. Plotted on these isopleths are average values of ROG and NO_x for the years 1995-2011. The black diamonds are weekday averages and the red circles are weekends. Projections for 2030 are plotted as rectangles on the isopleths were the black rectangle represents weekdays and the red rectangle represents weekends. The trend lines for the ROG and NO_x weekday (black line) and weekend (red line) concentrations are plotted. The ozone ridge-line (black straight line) is plotted for reference to the ozone isopleth while the blue straight line is the HNO_3 ridge-line (Fujita et al., 2015).

The aerosol model, Simulating Composition of Atmospheric Particles at Equilibrium, version 2, (SCAPE2; Kim et al., 1993a,b; Kim and Seinfeld, 1995) was used to make simulations for the range of nitric acid produced for the same range of NO_x and VOC as shown in the nitric acid isopleth, Figure 9-1. SCAPE2 is a thermodynamic equilibrium model that can be used to predict multiphase components of inorganic aerosol based on initial gas phase conditions. We have used SCAPE2 in previous published studies of the American West (Kuhns et al., 2003; Stockwell et al., 2003). These studies were used to set estimates of the SCAPE inputs listed in Table 9-1. The relative humidity was varied from 0.50, 0.80 and 0.90. The box model simulated HNO_3 concentrations were used as input to the SCAPE model (Stewart, 2017).

Quantity	Value
Air Temperature	287.6 K
Relative humidity (between 0 and 1)	0.50, 0.80, 0.90
Total sodium concentration as Na^+	0.022 $\mu g\ m^{-3}$
Total sulfate concentration as H_2SO_4	2.000 $\mu g\ m^{-3}$
Total ammonia concentration as NH_3	7.394 $\mu g\ m^{-3}$
Total nitrate concentration as HNO_3	From Box Model
Total chloride concentration as HCl	0.100 $\mu g\ m^{-3}$
Total potassium concentration as K^+	0.069 $\mu g\ m^{-3}$
Total calcium concentration as Ca^{++}	0.005 $\mu g\ m^{-3}$
Total magnesium concentration as Mg^{++}	0.300 $\mu g\ m^{-3}$
Total carbonate concentration as H_2CO_3	885.0 $\mu g\ m^{-3}$

Table 9-1. SCAPE2 model initial conditions.

Figures 9-3 to 9-5 show that the overall response of particulate nitrate concentrations is not a strong function of the initial VOC and NO_x and that this result is not affected by variations in relative humidity. The SCAPE simulations show that the initial VOC and NO_x concentrations have little effect on the particulate nitrate concentrations until the VOC mixing ratio drops below 150 ppbC or the initial NO_x drops below about 10 to 20 ppbV. Reductions in the initial NO_x lead to increases in the particulate nitrate if the initial VOC is 100 ppbC or less. These effects are almost independent of relative humidity.

Figures 9-6 and 9-7 show the particulate nitrate concentrations simulated by SCAPE as a function of relative humidity and as functions of the initial VOC to NO_x ratio. The particulate nitrate is dependent on NO_x concentrations greater than 50 ppb only when the VOC is equal to 2000 ppbC and the effect is most apparent when the relative humidity equal to 0.90 but this is not a realistic condition for the SoCAB.

The SCAPE simulated particulate nitrate is directly related to the amount of initial nitric acid. Figure 9-1 and Figure 9-8 show that the available nitric acid depends strongly on the initial NO_x and ROG concentrations. Note that the

plots in Figure 9-8 are very similar to those shown in Figures 9-3, 9-4 and 9-5. This suggests a very direct relationship between the initial nitric acid and the production of particulate nitrate.

Figures 9-9 and 9-10 show a plot of the relationship between the initial nitric acid and the SCAPE simulated particulate nitrate. For initial HNO_3 concentrations less than about 16 ppbV the relationship is almost linear, Figure 9-9. There is nonlinearity between for initial nitric acid concentrations between 15 ppbV and 50 ppbV but the relationship returns to linear between 50 ppbV and 200 ppbV of nitric acid.

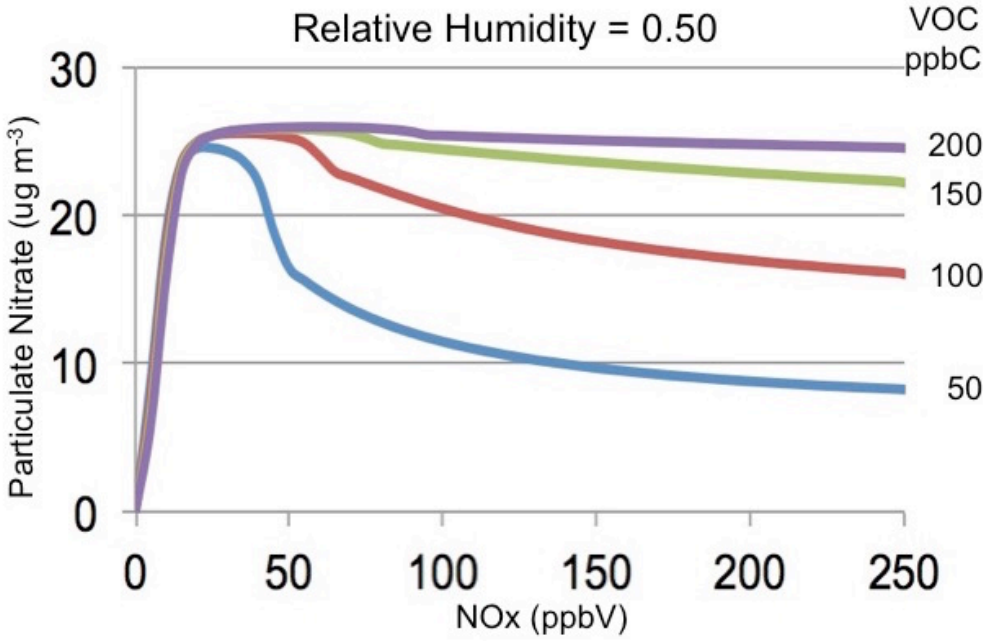

Figure 9-3. Plot shows the particulate nitrate concentrations as a function of the initial NO_x simulated by RACM2 and SCAPE2 from the input values given in Table 9-1 with the relative humidity equal to 0.5.

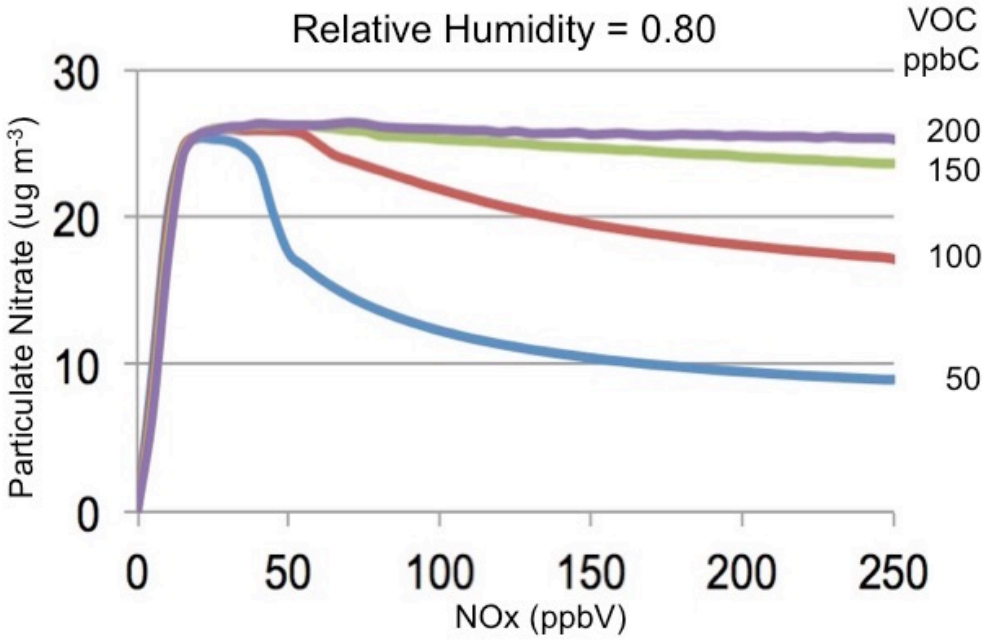

Figure 9-4. Plot shows the particulate nitrate concentrations simulated by as a function of the initial NO_x simulated by RACM2 and SCAPE2 from the input values given in Table 9-1 and the daily maximum HNO_3 with the relative humidity equal to 0.8.

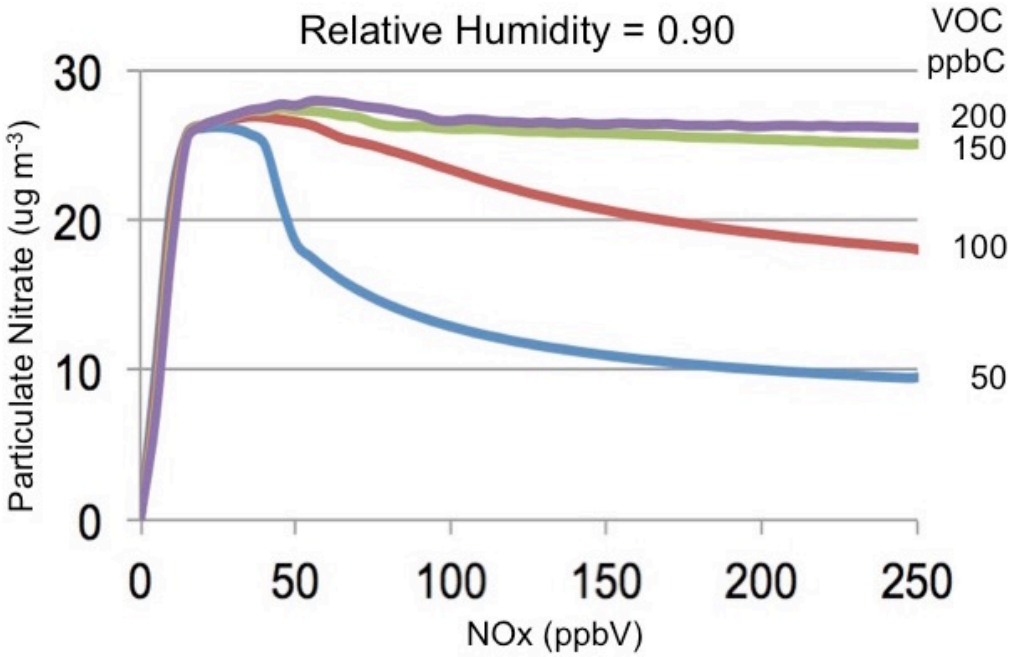

Figure 9-5. Plot shows the particulate nitrate concentrations as a function of the initial NO_x simulated by RACM2 and SCAPE2 from the input values given in Table 9-1 and the daily maximum HNO_3 with the relative humidity equal to 0.9.

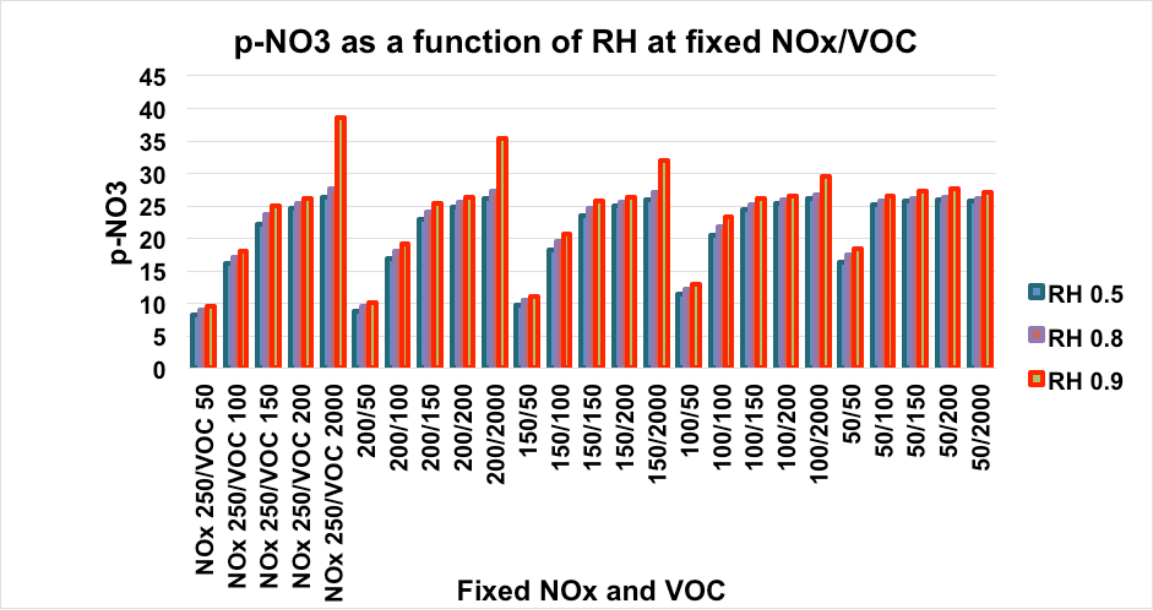

Figure 9-6. Plot shows the particulate nitrate concentrations simulated by RACM2 and SCAPE2 as a function of relative humidity.

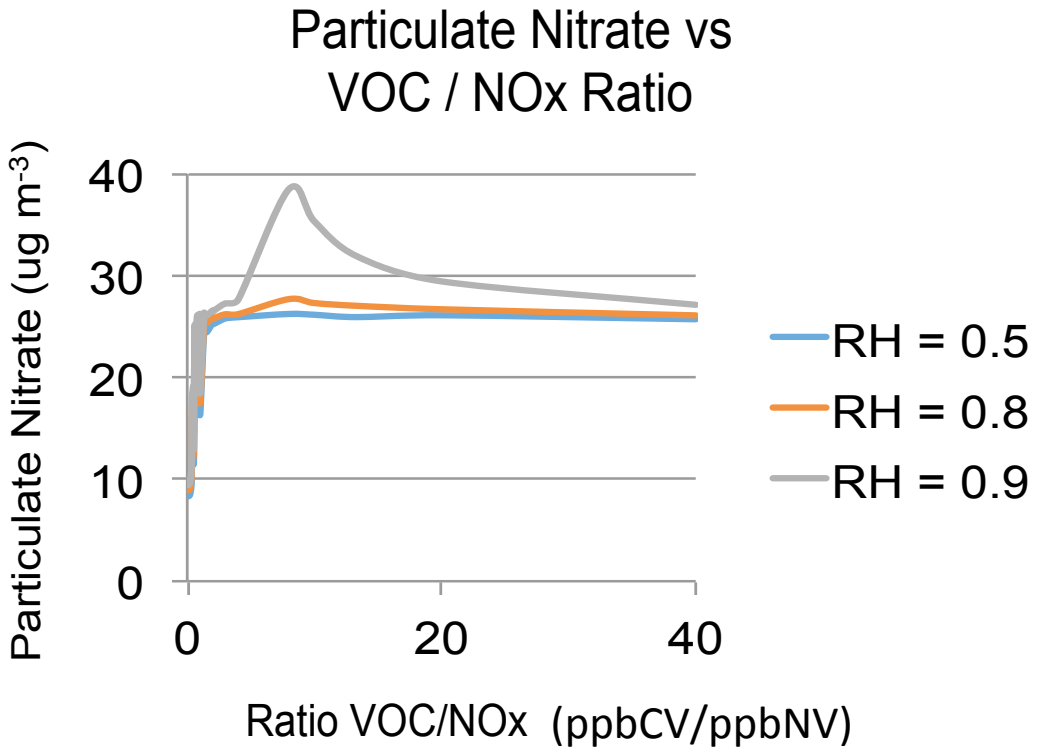

Figure 9-7. Plot shows the particulate nitrate concentrations simulated by RACM2 and SCAPE2 as a function of the initial VOC to NO_x ratio for three different relative humidities.

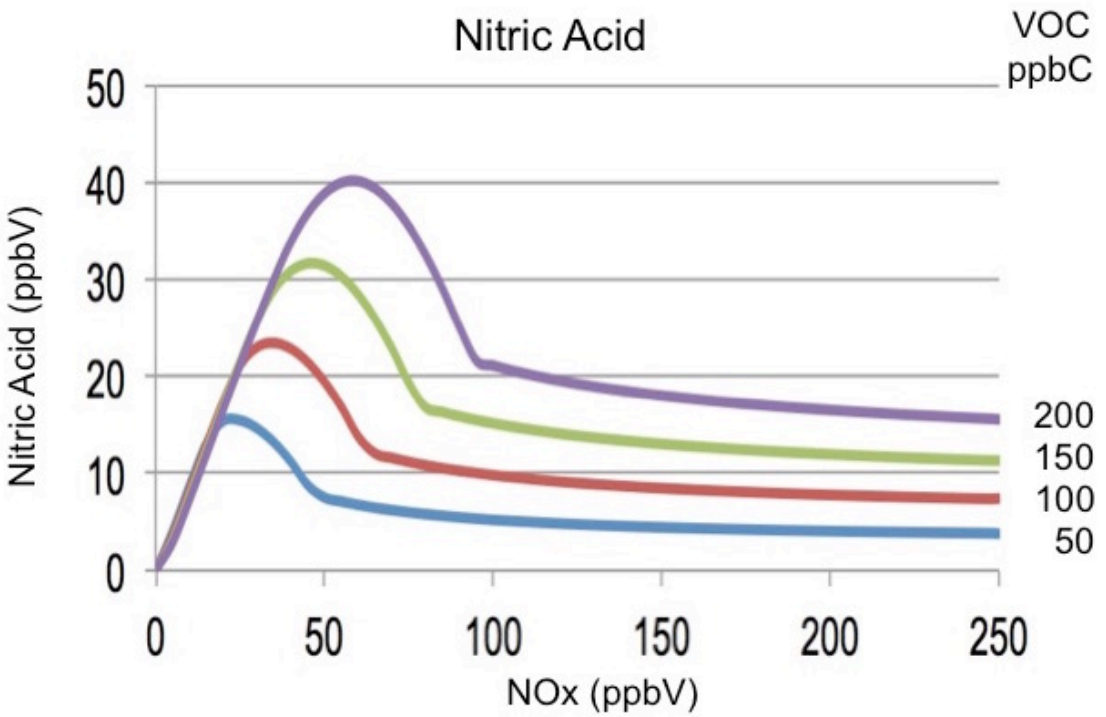

Figure 9-8. Plot shows the initial nitric acid concentrations used as input to SCAPE2 as a function of the initial VOC and NO_x. The nitric acid concentrations were taken from the RACM2 simulations made to prepare Figure 9-1 (Saunders, 2017).

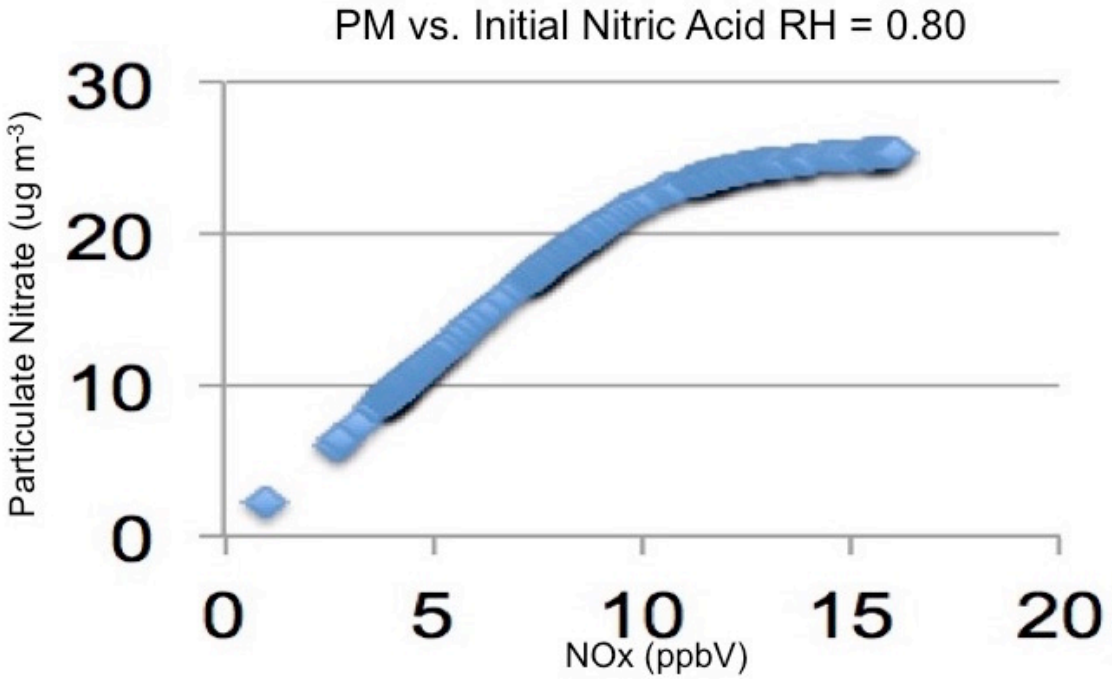

Figure 9-9. Plot shows the particulate nitrate simulated by SCAPE2 for the initial nitric acid concentrations less than 16 ppb.

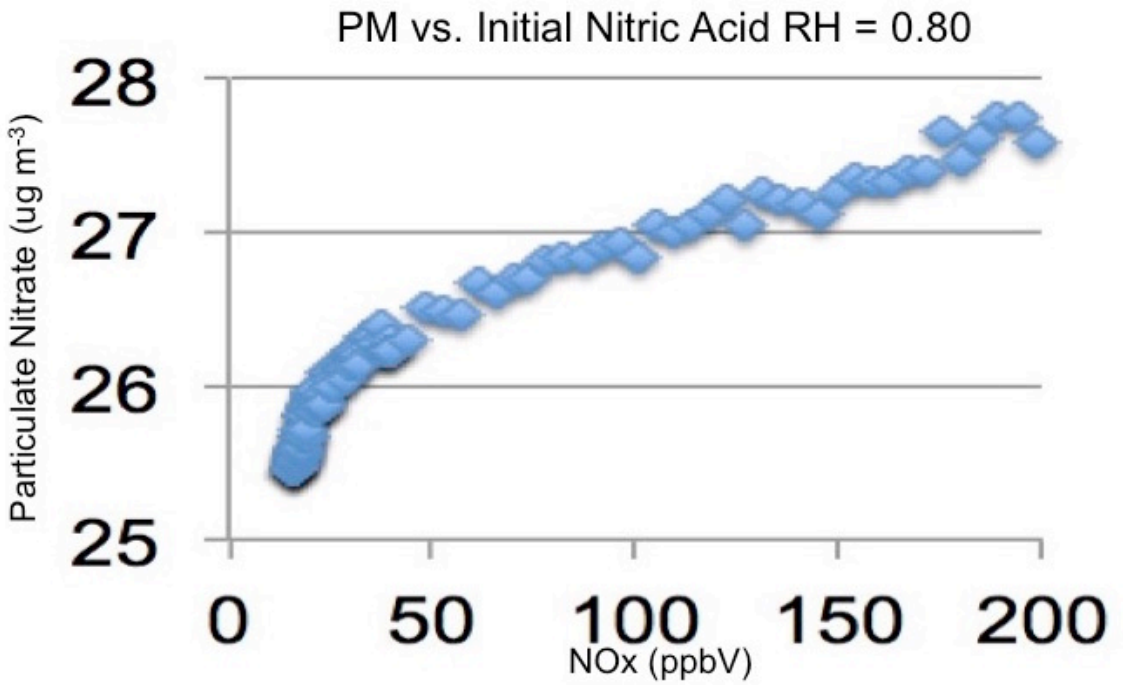

Figure 9-10. Plot shows the particulate nitrate simulated by SCAPE2 for the initial nitric acid concentrations greater than 16 ppb.

The main point that is made by Figures 9-1 through 9-10 and the discussion is that the particulate nitrate concentrations are a function of nitric acid. Nitric acid is a function of both NO_x and VOC. Therefore particulate nitrate is a function of both NO_x and ROG. Figure 9-8 shows that reductions in NO_x can increase the nitric acid available to form particulate nitrate. The lower the level of VOC, the lower the NO_x concentrations that lead to increases in nitric acid. This is important for understanding our CMAQ modeling results.

The SCAPE2 simulations appear to be reconcilable with the CMAQ simulations. Figure 8-9 showed that the $PM_{2.5}$ daily mean mass in the 2030 future-year is greatest at the six stations for the projected NO_x emission inventory (N'1). Increases or decreases from the projected NO_x emission inventory increase the $PM_{2.5}$ daily mean mass. A large fraction of the $PM_{2.5}$ is ammonium nitrate, Figure 8-10 and Figure 8-11. Figure 8-9 showed that the current NO_x emissions control strategy is the least effective in reducing $PM_{2.5}$ concentrations across the SoCAB. Either a control strategy with a lower level of NO_x emission reductions or one with much greater reductions in NO_x emissions would be more effective. The CMAQ and SCAPE modeling are consistent in their support of this conclusion.

Figure 8-24 shows that at Azusa and Fontana reductions in NO_x emissions led to lower simulated ammonium nitrate concentrations while for the Los Angeles, Long Beach, Anaheim and Rubidoux sites the CMAQ simulated ammonium nitrate concentrations were near a maximum with the projected 2030 NO_x emission inventory. Ammonium nitrate concentrations decreased

with increases from the 2030 NO_x emission inventory and also ammonium nitrate concentrations decreased if the NO_x emission reduction was greater than the projected 2030 emission inventory. This CMAQ modeling result is consistent with the SCAPE result shown in Figures 9-3, 9-4 and 9-5 where for a given level of ROG emissions there arises a maximum ammonium nitrate concentration as the initial NO_x concentration is varied.

9.2 Summary of the Effects of Chemistry on Nitrate Aerosol Formation

CMAQ modeling shows that ammonium nitrate is a large component of simulated $PM_{2.5}$ in the SoCAB. $PM_{2.5}$ is produced from nitric acid that is produced through the same chemistry that forms ozone. The production of nitric acid is not a function of NO_x ***alone*** rather its production is a function of ***both*** NO_x and ROG emissions. Since the production of particulate nitrate is a function of nitric acid the production of particulate nitrate is a function of both NO_x and ROG emissions. This dependence of particulate nitrate production and the production of ozone on NO_x and ROG is very similar. Therefore it should not be unexpected that reductions in NO_x alone have the possibility of being ineffective in reducing $PM_{2.5}$ and ozone concentrations depending upon conditions.

10. REFERENCES

Atkinson, R., D. L. Baulch, R. A. Cox, J. N. Crowley, R. F. Hampson, R. G. Hynes, M. E. Jenkin, M. J. Rossi, and J. Troe (2007), Evaluated kinetic and photochemical data for atmospheric chemistry: Volume III – gas phase reactions of inorganic halogens, *Atmos. Chem. Phys.,7*, 981; http://www.iupac-kinetic.ch.cam.ac.uk/, April 2012.

Aumont, B., S. Madronich, I. Bey, and G. S. Tyndall (2000), Contribution of secondary VOC to the composition of aqueous atmospheric particles: A modeling approach, *J. Atmos. Chem., 35*, 59-75, doi:10.1023/A:1006243509840.

Binkowski F.S. (1999), Chapter 10. Aerosols in MODELS-3 CMAQ, in Science Algorithms of the EPA Models-3 Community Multiscale Air Quality (CMAQ) Modeling System; Byun, Q.W., and J.K.S. Ching (ed.) EPA Report EPA-600/R-89-030; U.S. Environmental Protection Agency: Washington, DC, USA.

Binkowski F.S., and U. Shankar (1995), The regional particulate model 1. Model description and preliminary results. *J. Geophys. Res., 100*, 26,191-26,209.

Byun, Q.W., and J.K.S. Ching (1999), Science Algorithms of the EPA Models-3 Community Multiscale Air Quality (CMAQ) Modeling System; EPA Report EPA-600/R-89-030; U.S. Environmental Protection Agency: Washington, DC, USA.

Byun, D., and K.L. Schere (2006), Review of the governing equations, computational algorithms, and other components of the Models-3 Community Multiscale Air Quality (CMAQ) modeling system, *Appl. Mech. Rev., 59*, 51-77.

Chang J.S., R.A Brost, I.S.A. Isaksen, S. Madronich, P. Middleton, W.R. Stockwell and C.J. Walcek (1987), A Three-Dimensional Eulerian Acid Deposition Model: Physical Concepts and Formulation, *J. Geophys. Res.*, *92,* 14681-14700.

Calvert, J.G., J.J. Orlando, W.R. Stockwell and T.J. Wallington (2015), *The Mechanisms of Reactions Influencing Atmospheric Ozone*, Oxford University Press, Oxford.

Calvert, J.G., and W.R. Stockwell (1983), Acid generation in the troposphere by gas phase chemistry, *Environ. Sci. Technol., 17,* 428A-443A.

Claeys, M., B. Graham, G. Vas, W. Wang, R. Vermeylen, V. Pashynska, J. Cafmeyer, P. Guyon, M. O. Andreae, P. Artaxo, and W. Maenhut (2004), Formation of secondary organic aerosols through photooxidation of isoprene, Science, 303, 1173-1176, doi:10.1126/science.1092805.

Coe, H., J. D. Allan, M. R. Alfarra, K. N. Bower, M. J. Flynn, G. B. McFiggans, D. O. Topping, P. I. Williams, C. D. O'Dowd, M. Dall'Osto, D. C. S. Beddows, and R. M. Harrison (2006), Chemical and physical characteristics of aerosol particles at a remote coastal location, Mace Head, Ireland, during NAMBLEX, *Atmos. Chem. Phys., 6*, 3289-3301, doi:10.5194/acp-6-3289- 2006.

de Gouw, J. and J. L. Jimenez (2009), Organic aerosols in the Earth's atmosphere, *Environ. Sci. Technol., 43*, 7614-7618, doi:10.1021/es9006004.

de Gouw, J. A., C. A. Brock, E. L. Atlas, T. S. Bates, F. C. Fehsenfeld, P. D. Goldan, J. S. Holloway, W. C. Kuster, B. M. Lerner, B. M. Matthew, A. M. Middlebrook, T. B. Onasch, R. E. Peltier, P. K. Quinn, C. J. Senff, A. Stohl, A. P. Sullivan, M. Trainer, C. Warneke, R. J. Weber, and E. J. Williams (2008), Sources of particulate matter in the northeastern United States in summer: 1. Direct emissions and secondary formation of organic matter in urban plumes, *J. Geophys. Res.-Atmos., 113, D08301*, doi:10.1029/2007JD009243.

Goliff, W.S., W.R. Stockwell and C.V. Lawson (2013), The Regional Atmospheric Chemistry Mechanism, Version 2, *Atmos. Environ*., 68, 174-185.

Gurjar, B. R., T. M. Butler, M. G. Lawrence, and J. Lelieveld (2008), Evaluation of emissions and air quality in megacities, *Atmos. Environ., 42*, 1593-1606.

Donahue, N. M., A. L. Robinson, C. O. Stanier, and S. N. Pandis (2006), Coupled partitioning, dilution, and chemical aging of semivolatile organics, *Environ. Sci. Technol., 40*, 2635-2643, doi:10.1021/es052297c.

Eder, B. and S. Yu (2006), A performance evaluation of the 2004 release of Models-3 CMAQ, *Atmos. Environ., 40*, 4811-4824.

Fuentes, J.D., M. Lerdau, R. Atkinson, D. Baldocchi, J.W. Botteneheim, P. Ciccioli, B. Lamb, C. Geron, L. Gu, A. Guenther, T.D. Sharkey and W.R. Stockwell (2000), Biogenic Hydrocarbons in the Atmospheric Boundary Layer: A Review, *Bull. Amer. Meteor. Soc.*, *81*, 1537-1575.

Fujita, E.M., D.E. Campbell, R. Fitzgerald and R. Perea, W.R. Stockwell and E. Saunders (2015), *Projected Ozone Trends and Changes in the Ozone-Precursor Relationship in the South Coast Air Basin in Response to Varying Reductions of Precursor Emissions*, Final Report for CRC Project A-91, Coordinating Research Council, Atlanta, GA.

Goldstein, A. H. and I. E. Galbally (2007), Known and unexplored organic constituents in the earth's atmosphere, *Environ. Sci. Technol., 41*, 1514-1521, doi:10.1021/es072476p.

Griffin, R. J., D. R. Cocker, R. C. Flagan, and J.H. Seinfeld (1999), Organic aerosol formation from the oxidation of biogenic hydrocarbons, *J. Geophys. Res.-Atmos., 104*, 3555–3567, doi:10.1029/1998JD100049.

Grahame, T.J., R. Klemm and R.B. Schlesinger (2014), Public health and components of particulate matter: The changing assessment of black carbon, *Journal of the Air and Waste Management Association*, 64:6, 620-660, DOI: 10.1080/10962247.2014.912692

Gurjar, B. R., T. M. Butler, M. G. Lawrence, and J. Lelieveld (2008), Evaluation of emissions and air quality in megacities, *Atmos. Environ., 42*, 1593-1606.

Hallquist, M., J. C. Wenger, U. Baltensperger, Y. Rudich, D. Simpson, M. Claeys, J. Dommen, N. M. Donahue, C. George, A. H. Goldstein, J. F.

Hamilton, H. Herrmann, T. Hoffmann, Y. Iinuma, M. Jang, M. E. Jenkin, J. L. Jimenez, A. Kiendler-Scharr, W. Maenhaut, G. McFiggans, Th. F. Mentel, A. Monod, A. S. H. Prévôt, J. H. Seinfeld, J. D. Surratt, R. Szmigielski, and J. Wildt (2009), The formation, properties and impact of secondary organic aerosol: current and emerging issues, *Atmos. Chem. Phys., 9*, 5155–5236, doi:10.5194/acp-9-5155- 2009.

Hamilton, J. F., P. J. Webb, A. C. Lewis, J. R. Hopkins, S. Smith, and P. Davy (2004), Partially oxidised organic components in urban aerosol using GCXGC-TOF/MS, *Atmos. Chem. Phys., 4*, 1279-1290, doi:10.5194/acp-4-1279-2004.

Heald, C. L., D. J. Jacob, R. J. Park, L. M. Russell, B. J. Huebert, J. H. Seinfeld, H. Liao, and R. J. Weber (2005), A large organic aerosol source in the free troposphere missing from current models, *Geophys. Res. Lett., 32, L18809*, doi:10.1029/2005GL023831.

Heisler, S. L. and S. K. Friedlander (1977), Gas-to-particle conversion in photochemical smog: aerosol growth laws and mechanisms for organics, *Atmos. Environ., 11*, 157-168, doi:10.1016/0004-6981(77)90220-7.

Hodzic, A, J. L. Jimenez, A. S. H. Prévôt, S. Szidat, J. D. Fast and S. Madronich (2010a), Can 3-D models explain the observed fractions of fossil and non-fossil carbon in and near Mexico City? *Atmos. Chem. Phys., 10*, 10997-11016, doi:10.5194/acp-10-10997-2010.

Hodzic, A., J. L. Jimenez, S. Madronich, M. R. Canagaratna, P. F. DeCarlo, L. Kleinman, and J. Fast (2010b), Modeling organic aerosols in a megacity: potential contribution of semi-volatile and intermediate volatility primary organic compounds to secondary organic aerosol formation, *Atmos. Chem. Phys., 10*, 5491-5514, doi:10.5194/acp-10-5491-2010.

Jacobson, M.Z. (1999) Isolating nitrated and aromatic aerosols and nitrated aromatic gases as sources of ultraviolet light absorption, *J. Geophys. Res.-Atmos., 104*, 3527-3542, doi:10.1029/1998JD100054.

Jimenez, J.L., M.R. Canagaratna, N.M. Donahue, A.S.H. Prevot, Q. Zhang, J.H. Kroll, P.F. DeCarlo, J.D. Allan, H. Coe, N.L. Ng, A.C. Aiken, K.S. Docherty, I.M. Ulbrich, A.P. Grieshop, A.L. Robinson, J. Duplissy, J.D. Smith, K.R. Wilson, V.A. Lanz, C. Hueglin, Y.L. Sun, J. Tian, A. Laaksonen, T. Raatikainen, J. Rautiainen, P. Vaattovaara, M. Ehn, M. Kulmala, J. M. Tomlinson, D. R. Collins, M. J. Cubison, E. J. Dunlea, J.A. Huffman, T.B. Onasch, M.R. Alfarra, P.I. Williams, K. Bower, Y. Kondo, J. Schneider, F. Drewnick, S. Borrmann, S. Weimer, K. Demerjian, D. Salcedo, L. Cottrell, R. Griffin, A. Takami, T. Miyoshi, S. Hatakeyama, A. Shimono, J.Y. Sun, Y.M. Zhang, K. Dzepina, J.R. Kimmel, D. Sueper, J.T. Jayne, S.C. Herndon, A.M. Trimborn, L.R. Williams, E.C. Wood, A.M. Middlebrook, C.E. Kolb, U. Baltensperger, and D.R. Worsnop (2009), Evolution of organic aerosols in the atmosphere, *Science, 326*, 1525-1529, doi:10.1126/science.1180353.

Ketseridis, G., J. Hahn, R. Jaenicke, and C. Junge (1976), The organic constituents of atmospheric particulate matter, *Atmos. Environ., 10*, 603-610,

doi:10/1016/0004-6981(76)90045-7.

Kim, Y.P., and J.H., Seinfeld (1995), Atmospheric gas–aerosol equilibrium III. Thermodynamics of crustal elements Ca^{2+} ; K^{+} ; and Mg^{2+}, *Aerosol Science and Technology, 22*, 93-110.

Kim, Y.P., J.H. Seinfeld, P. Saxena (1993a), Atmospheric gas-aerosol equilibrium I. Thermodynamic model, *Aerosol Science and Technology, 19*, 157–181.

Kim, Y.P., J.H. Seinfeld, P. Saxena (1993b), Atmospheric gas-aerosol equilibrium II. Analysis of common approximations and activity coefficient calculation methods, *Aerosol Science and Technology 19*, 182–198.

Kuhns, H., V. Bohdan, J. Chow, V. Etyemezian, M. Green, D. Herlocker, S. Kohl, M. McGown, J. Ramsdell, W.R. Stockwell, M. Toole, J. Watson (2003), The treasure valley secondary aerosol study I: measurements and equilibrium modeling of inorganic secondary aerosols and precursors for southwestern Idaho, *Atmos. Environ., 37*, 511-524.

Lee-Taylor, J., S. Madronich, B. Aumont, A. Baker, M. Camredon, A. Hodzic, G. S. Tyndall, E. Apel and R. A. Zaveri (2011), Explicit modeling of organic chemistry and secondary organic aerosol partitioning for Mexico City and its outflow plume, *Atmos. Chem. Phys., 11*, 13219-13241, doi:10.5194/acp-11-13219-2011.

Middlebrook, A. M., D. M. Murphy, and D. S. Thomson (1998), Observations of organic material in individual marine particles at Cape Grim during the First Aerosol Characterization Experiment (ACE 1), *J. Geophys. Res.-Atmos., 103*, 16475-16483, doi:10.1029/97JD03719.

Pandis, S. N., S. E. Paulson, J. H. Seinfeld, and R. C. Flagan (1991), Aerosol formation in the photooxidation of isoprene and beta-pinene, *Atmos. Environ., 25A*, 997-1008, doi:10.1016/0960-1686(91)90141-S.

Pandis, S. N., R. A. Harley, G. R. Cass, and J. H. Seinfeld (1992), Secondary organic aerosol formation and transport, *Atmos. Environ., 26A*, 2269-2282, doi:10.1016/0960-1686(92)90358-R.

Sander, S.P., R.R. Friedl, J.R. Barker, D.M.Golden, M.J. Kurylo, P.H. Wine, J.P.D. Abbatt, J.B. Burkholder, C.E. Kolb, G.K. Moortgat, R.E.Huie, and B.L. Orkin (2011), Chemical kinetics and photochemical data for use in atmospheric studies, Evaluation Number 17, Jet Propulsion Laboratory, Pasadena, California, JPL Publication 10-6, http://jpldataeval.jpl.nasa.gov/pdf/JPL_10-6_Final_15June2011.pdf.

Saunders, E. (2017), *Modeling Regional & Global Atmospheric Chemistry Mechanisms: Observing Adverse Respiratory Health Effects due to Air Pollution from Modeling Output*, Ph.D. Dissertation, Howard University.

SCAQMD (2013), South Coast Air Quality Management District, *Final 2012 Air Quality Management Plan*, Diamond Bar, California.

Seinfeld, J. H. and S. N. Pandis (2006), Atmospheric Chemistry and Physics: From Air Pollution to Climate Change, John Wiley, Hoboken, NJ, USA, 350-434.

Sicard, P., Mangin, A., Hebel, P., and Mallea, P. (2011), Detection and estimation trends linked to air quality and mortality on French Riviera over the 1990–2005 period, *Sci. Total Environ., 408*, 1943-1950.

Solomon, P., D. Crumpler, J. Flanagan, R. Jayanty, E. Rickman, AND C. McDade, (2014), U.S. National $PM_{2.5}$ Chemical Speciation Monitoring Networks – CSN and IMPROVE: Description of Networks. *Journal of the Air and Waste Management Association*, *64*, 1410-1438.

Stewart, D. (2017), *Air Quality Modeling and Health and Economic Assessment of Projected Ozone and Particulate Matter Response to Varying Reductions of Oxides of Nitrogen and Volatile Organic Compound Emissions in the South Coast Air Basin*, Ph.D. Dissertation, Howard University.

Stockwell, W.R., and J.G. Calvert (1983), The mechanism of the HO-SO_2 reaction, *Atmos. Environ., 17*, 2231-2235.

Stockwell, W.R., H. Kuhns, V. Etyemezian, M.C. Green, J.C. Chow, J.G. Watson and N.F. Robinson (2003), The Treasure Valley Secondary Aerosol Study II: Modeling of the Formation of Inorganic Secondary Aerosols and Precursors for Southwestern Idaho, Atmos. Environ., 37, 525-534.

Stockwell, W.R., C.V. Lawson, E. Saunders and W.S. Goliff (2012), A Review of Tropospheric Atmospheric Chemistry and Gas-Phase Chemical Mechanisms for Air Quality Modeling, *Atmosphere*, *3*, 1-32.

(doi:10.3390/atmos30100012011)

Sun, J. Y., Q. Zhang, M. R. Canagaratna, Y. M. Zhang, N. L. Ng, Y. L. Sun, J. T. Jayne, X. C. Zhang, X. Y. Zhang, and D. R. Worsnop (2010), Highly time- and size-resolved characterization of submicron aerosol particles in Beijing using an Aerodyne Aerosol Mass Spectrometer, *Atmos. Environ., 44*, 131-140, doi:10.1016/j.atmosenv.2009.03.020.

Turpin, B. J., J. J. Huntzicker, S. M. Larson, and G. R. Cass (1991), Los-Angeles summer midday particulate carbon – primary and secondary aerosol, *Environ. Sci. Technol.*, 25, 1788-1793, doi:10.1021/es00022a017.

Virtanen, A., J. Joutsensaari, T. Koop, J. Kannosto, P. Yli-Pirila, J. Leskinen, J. M. Makela, J. K. Holopainen, U. Pöschl, M. Kulmala, D. R. Worsnop, and A. Laaksonen (2010), An amorphous solid state of biogenic secondary organic aerosol particles, *Nature, 467,* 824-827, doi:10.1038/nature09455.

Volkamer, R., J. L. Jimenez, F. S. Martini, K. Dzepina, Q. Zhang, D. Salcedo, L. T. Molina, D. R. Worsnop, and M. J. Molina (2006), Secondary organic aerosol formation from anthropogenic air pollution: Rapid and higher than expected, *Geophys. Res. Lett., 33, L17811*, doi:10.1029/2006GL026899.

Zhang, Q., J. L. Jimenez, M. R. Canagaratna, J. D. Allan, H. Coe, I. Ulbrich, M.

R. Alfarra, A. Takami, A. M. Middlebrook, Y. L. Sun, K. Dzepina, E. Dunlea, K. Docherty, P. F. DeCarlo, D. Salcedo, T. Onasch, J. T. Jayne, T. Miyoshi, A. Shimono, S. Hatakeyama, N. Takegawa, Y. Kondo, J. Schneider, F. Drewnick, S. Borrmann, S. Weimer, K. Demerjian, P. Williams, K. Bower, R. Bahreini, L. Cottrell, R. J. Griffin, J. Rautiainen, J. Y. Sun, Y. M. Zhang, and D. R. Worsnop (2007), Ubiquity and dominance of oxygenated species in organic aerosols in anthropogenically-influenced Northern Hemisphere midlatitudes, *Geophys. Res. Lett., 34, L13801*, doi:10.1029/2007GL029979.

Zhang, Q.J., M. Beekmann, F. Drewnick, F. Freutel, J. Schneider, M. Crippa, A.S.H. Prévôt, U. Baltensperger, L. Poulain, A. Wiedensohler, J. Sciare, V. Gros, A. Borbon, A. Colomb, V. Michoud, J.-F. Doussin, H.A.C. DeniervanderGon, M. Haeffelin, J.-C. Dupont, G. Siour, H. Petetin, B. Bessagnet, S.N. Pandis, A. Hodzic, O. Sanchez, C. Honoré and O. Perrussel (2013). Formation of organic aerosol in the Paris region during the MEGAPOLI summer campaign: evaluation of the volatility-basis-set approach within the CHIMERE model, *Atmos. Chem. Phys., 13*, 5767–5790, doi:10.5194/acp-13-5767-2013.